Tissue-specific effects of ICOS signaling on regulatory T cell maintenance and function

Kristen Leigh Mittelsteadt

A dissertation
submitted in partial fulfillment of the
requirements for the degree of

Doctor of Philosophy

University of Washington

2020

Reading Committee:

Daniel J. Campbell, Chair

Marion Pepper

Michael Y. Gerner

Program Authorized to Offer Degree:
Molecular and Cellular Biology

University of Washington

Abstract:

Tissue-specific effects of ICOS signaling on regulatory T cell maintenance and function

Kristen Leigh Mittelsteadt

Chair of the Supervisory Committee:

Daniel J. Campbell
Department of Immunology

Foxp3$^+$ regulatory T cells (T_R) are a population of CD4$^+$ T cells with a well-recognized ability to restrain inappropriate or overreactive immune responses against both self- and foreign-antigens. T_R are vitally important in maintaining immune tolerance and act at different tissue sites to prevent the development of autoimmunity, lymphoproliferative disease, and pathological tissue damage. Our lab and others have demonstrated considerable phenotypic and functional heterogeneity among T_R localized in lymphoid versus nonlymphoid tissues. Broadly, central T_R (cT_R) found in lymphoid tissues rely on paracrine IL-2 signals for their maintenance and prevent priming of autoreactive T cells, whereas effector T_R (eT_R) residing in nonlymphoid organs are dependent on T cell receptor (TCR)/costimulatory ICOS signals and modulate ongoing inflammatory responses. Adding another layer to this complexity, there is growing evidence that T_R found across nonlymphoid tissues are distinct from one another and respond to unique cues within their respective microenvironments. Although they display hallmarks of eT_R, tissue-specific T_R exhibit unique transcriptional and epigenetic profiles, express distinct chemokine receptors and TCR repertoires, and exert functions that go beyond classical modulation of immune responses, including tissue repair and maintaining organismal metabolic homeostasis.

The costimulatory molecule ICOS is highly expressed on eT_R that migrate to nonlymphoid tissues and contributes to their maintenance and function in models of autoimmunity. In this dissertation, we report an unexpected cell-intrinsic role for ICOS

expression and downstream PI3K signaling in limiting the maintenance, phenotype, and function of T_R specifically in visceral adipose tissue (VAT). *Icos*$^{-/-}$ mice and mice expressing a knock-in form of ICOS with the inability to activate PI3K demonstrated increased VAT-T_R abundance and expression of canonical VAT-T_R markers. Loss of ICOS signaling facilitated enhanced accumulation of T_R to VAT associated with increased CCR3 expression and resulted in reduced adipose inflammation and retained insulin sensitivity in the context of high-fat diet. In contrast, preliminary studies utilizing models of autoimmune central nervous system (CNS) inflammation indicated a requirement for ICOS signaling in disease resolution mediated by CNS-T_R. Collectively, these findings suggest that eT_R residing within different tissues and immune environments differentially rely on ICOS signaling, highlighting new and surprising mechanisms that regulate eT_R development, accumulation, and function.

TABLE OF CONTENTS

LIST OF FIGURES

LIST OF ABBREVIATIONS

(Alphabetically)

APC	Antigen-presenting cell
ATM	Adipose tissue macrophage
BGL	Blood glucose level
CFA	Complete Freund's adjuvant
CNS	Central nervous system
cT_R	Central regulatory T cell
EAE	Experimental autoimmune encephalomyelitis
eT_R	Effector regulatory T cell
gMFI	Geometric mean fluorescence intensity
GTT	Glucose tolerance test
HFD	High-fat diet
IEL	Intraepithelial lymphocytes
ILC2	Group-2 innate lymphoid cell
ITT	Insulin tolerance test
KO	*Icos*$^{-/-}$
LPL	Lamina propria lymphocytes
MHC	Major histocompatibility complex
MOG_{35-55}	Myelin oligodendrocyte glycoprotein peptide
MS	Multiple sclerosis
PI3K	Phosphoinositide 3-kinase
PPARγ	Peroxisome proliferator-activated receptor gamma
RFP	Red fluorescent protein
SLO	Secondary lymphoid organ
SQAT	Subcutaneous adipose tissue
T_{conv}	Conventional T cell
TCR	T cell receptor
T_{eff}	Effector T cell
T_R	Regulatory T cell
VAT	Visceral adipose tissue
YF	*Icos*^{Y181F}

ACKNOWLEDGEMENTS

We would like to thank Adam Wojno, K. Arumuganathan, and Tuan Nguyen for help with flow cytometry and maintaining the BRI Flow Cytometry Core; Pamela Johnson in the BRI Histology/Imaging Core; and Daryl Hackney and Sakeneh Zraika from the UW Diabetes Research Center Cell Function Analysis Core for help with metabolic profiling tests. Dr. Marion Pepper generously provided *Icos*^{Y181F} mice with kind permission from Woong-Kyung Suh. Dr. Andrew Burich, Carlos Toledano, and the BRI vivarium helped maintain mouse colonies. We thank members of the Campbell lab for helpful discussion and laboratory support. Drs. Marion Pepper, Michael Gerner, Kevin Urdahl, Jessica Hamerman, and Oliver Harrison provided comments and suggestions regarding the experiments and data herein.

This work was supported by grants to D.J.C. from the National Institutes of Health (NIH) (R01AI124693, R01AI136475). K.L.M. was supported by NIH National Institute of Allergy and Infectious Diseases T32 Grant AI106677, National Institute of General Medical Sciences T32 Grant GM007270, and the UW Diabetes Research Center Samuel and Althea Stroum Endowed Graduate Fellowship (2P30 DK17047).

DEDICATION

For my dad, Wade Lee.

CHAPTER 1: Introduction

Immune tolerance

The vertebrate immune system plays a critical role in protecting the host from a wide range of pathogenic microorganisms. This is primarily accomplished through the ability of an organism to distinguish its own cells and tissues, as well as innocuous environmental antigens and commensal microbiota, from those of pathogenic origin. Two overlapping arms of immunity, the innate and adaptive immune systems, work in concert to selectively eliminate and provide immunological memory against pathogens. Sentinel cells of the innate immune system reside at environmental barrier surfaces. Recognition of conserved molecular patterns on infectious microbes by a small set of invariant receptors expressed on these cells results in rapid anti-microbial effector responses. However, in the case that the invading pathogen evade control by innate responses, engagement of the adaptive immune system can contribute to pathogen clearance and long-term immunological memory. Lymphocytes of the adaptive immune system, including T cells, express surface receptors which are generated by somatic gene rearrangement and are capable of recognizing an enormous diversity of antigens. T cell receptor (TCR) specificity drives highly targeted and potent responses. Thus, misidentification of self- or harmless environmental antigens as pathogenic can result in tissue damage, autoimmunity, or allergy.

Development of self-tolerance is crucial for preventing inappropriate immune responses. Central tolerance processes occur in the thymus, where during development, T cells are assessed for their ability to recognize peptide bound to major histocompatibility complex (MHC) with appropriate affinity (positive selection) without strong reactivity to self-antigens expressed on MHC molecules (negative selection) (Xing and Hogquist, 2012). Clonal deletion of self-reactive cells is thought to be an efficient process. However, because not all self-antigens are expressed in the thymus, and because of the sheer number and diversity of TCRs that are

tested during development, a small number of autoreactive T cell clones inevitably escape into the periphery. Those that do circumvent clonal deletion are kept in check by additional tolerance mechanisms in the periphery, including elimination by apoptotic cell death (deletion) and functional hyporesponsiveness (anergy) upon recognition of self-antigen/MHC complexes in the absence of costimulatory signals (Xing and Hogquist, 2012). Additionally, T cell development results in a complementary population of self-reactive T cells that are specialized for immune suppression. These regulatory T cells (T_R) are critical for establishing tolerance and use various mechanisms to prevent aberrant immune responses (Schmidt et al., 2012).

Regulatory T cells

In 1995, a population of $CD4^+CD25^+$ cells that could suppress autoreactive T cells and prevent autoimmunity in mice was discovered (Sakaguchi et al., 1995). The critical suppressive function of these "regulatory" cells was fully realized after the discovery that the fatal multi-organ lymphoproliferative disease observed in *scurfy* mice and humans with IPEX syndrome developed due to non-functional or hypomorphic alleles of the *Foxp3* gene (Bennett et al., 2001; Brunkow et al., 2001). In 2003, three seminal papers demonstrated that Foxp3 indeed was a key transcription factor essential for the development and function of $CD4^+CD25^+$ T_R (Fontenot et al., 2003; Hori et al., 2003; Khattri et al., 2003). Since their discovery, studies have revealed that T_R not only function to suppress autoimmunity, but also modulate immune responses in the setting of transplantation, cancer, and chronic infection, highlighting the extraordinary potential for therapeutic manipulation of T_R in a variety of clinical settings.

$CD4^+$ natural T_R develop in the thymus and express a TCR repertoire with high affinity to self-peptides, though Foxp3 can also be induced in peripheral conventional $CD4^+$ T cells (T_{conv}) under specific antigen and cytokine conditions (Hsieh et al., 2012; Yadev et al., 2013). T_R are capable of modulating immune responses through a variety of mechanisms. CTLA-4 on T_R can bind and trans-endocytose the costimulatory molecules CD80 and CD86 on antigen presenting

cells (APC), rendering these cells unable to efficiently activate self-reactive T cells (Qureshi et al., 2011). T_R can produce immunosuppressive cytokines like IL-10, IL-35, and TGFβ, or the cytolytic enzyme granzyme B, which results in the inhibition or death of autoreactive T cells (Gondek et al., 2005; Josefowicz et al., 2012). Additionally, T_R can metabolically inhibit T cell proliferation via generation of adenosine or by acting as a sink for available IL-2 (Deaglio et al., 2007; Josefowicz et al., 2012).

Functional diversity of T_R is supported by their ability to co-opt expression of transcription factors and activation profiles that match the class of effector immune response being suppressed. For example, IRF4 forms complexes with Foxp3 and together these transcription factors regulate expression of genes that enable T_R to restrain T_H2 responses (Zheng et al., 2009). Similarly, T-bet, a critical transcription factor in T_H1 lineage commitment, expressed in T_R results in expression of CXCR3, allowing migration and accumulation at sites of T_H1 responses (Koch et al., 2009). Expression of T helper transcription factors in T_R is beneficial in part because these programs drive expression of chemokine receptors to allow for colocalization of effector cell targets. Indeed, the proper distribution of T_R across tissues, even in the absence of any overt inflammation, is essential for their ability to maintain tolerance (Sather et al., 2007).

Factors impacting T_R homeostasis

T_R phenotypic and functional diversity

Similar to T_{conv}, T_R can be broadly subsetted based on the expression of the adhesion molecules CD44 and CD62L. $CD44^{lo}CD62L^{hi}$ central T_R (cT_R) emerge from the thymus and home preferentially to secondary lymphoid organs (SLO). Given their autoreactivity, entry into the periphery and engagement with self-antigen or inflammatory signals drives the differentiation of cT_R to $CD44^{hi}CD62L^{lo}$ effector T_R (eT_R), which access nonlymphoid tissues based on expression of specific homing receptors (Campbell and Koch, 2011; Fisson et al., 2003; Lee et al., 2007; Smigiel et al., 2014a). This distribution of T_R allows for a “division of

labor" to control effector responses in different tissues. cT_R are poised to prevent priming of naive T cells in SLO via deprivation of activation signals including CD80/86 and IL-2, whereas eT_R in the periphery can dampen immune responses by producing immunosuppressive cytokines like IL-10 (Yamaguchi et al., 2011). Our lab and others have found that cT_R and eT_R have unique homeostatic properties, with increased proliferation and cellular turnover in eT_R compared to cT_R (Fisson et al., 2003; Smigiel et al., 2014a). These homeostatic differences in cT_R and eT_R are not simply a reflection of differential TCR stimulation as both populations engage TCR to a similar extent based on GFP expression in *Nur77* reporter mice, suggesting that additional cues account for the distinct properties of cT_R and eT_R.

IL-2 signaling in cT_R homeostasis

Interleukin-2 (IL-2) is a cytokine that signals via a receptor complex which contains the common gamma (γc) chain, IL2/15Rβ (CD122) and IL2Rα (CD25). The original identification of T_R was based on their constitutive expression of CD25, which serves to increase the affinity of the IL-2R for IL-2 binding (Sakaguchi et al., 1995). IL-2 primarily supports T_R through phosphorylation of the transcription factor STAT5 and subsequent regulation of genes involved in proliferation, survival, and metabolism (Fontenot et al., 2005). Because Foxp3 cooperates with NFAT and Runx to repress *Il2* transcription (Ono et al., 2007; Wu et al., 2006), T_R must rely on paracrine sources of IL-2, primarily from autoreactive $CD4^+$ T cells (Setoguchi et al., 2005; Stolley and Campbell, 2016).

Work from our lab indicates that *ex vivo* STAT5 phosphorylation, a proxy for *in vivo* IL-2 signaling, in splenic T_R is restricted to $Ki67^-$ cT_R. In line with this observation, genetic or antibody-mediated blockade of IL-2 signaling *in vivo* results in the selective loss of cT_R. Although both cT_R and eT_R are sensitive to exogenous IL-2 *in vitro* and *in vivo*, differential responses to IL-2 signaling blockade *in vivo* are explained by differences in localization of these T_R subsets. Indeed, selective expression of CCR7 on cT_R allows them to migrate into organized

T cell zones within SLO. Here, cT_R are able to access paracrine IL-2 signals which drives their homeostatic maintenance via activation of pro-survival genes (Liu et al., 2015; Smigiel et al., 2014a).

TCR and costimulatory signals in eT_R maintenance

In contrast to the selective maintenance of cT_R by IL-2, $CD44^{hi}$ eT_R that populate nonlymphoid tissues do not access IL-2-rich regions *in vivo*, and thus must be supported by other mechanisms. Specificity for self directs the selection of T_R in the thymus, shaping a unique TCR repertoire against self-antigens (Hsieh et al., 2004; Jordan et al., 2001). Accordingly, self-reactivity results in accumulation of T_R in tissues containing these self-antigens for which they are specific, and this is critical for preventing tissue-specific autoimmunity (Killebrew et al., 2011; Seddon and Mason, 1999). In addition to ensuring appropriate tissue distribution, T_R-specific deletion of the TCRα constant chain revealed a critical role for TCR expression and signaling in the maintenance of $CD44^{hi}$ eT_R abundance and transcriptional identity, independent of IL-2 signaling (Levine et al., 2014).

In addition to continuous TCR signaling, proper eT_R maintenance and function is dependent on costimulatory molecules, which provide a secondary signal to propagate proliferation and survival of T cells which have engaged peptide-MHC complexes through TCR interactions. Mice deficient in expression of the costimulatory molecules CD28 or ICOS harbor a reduced frequency of T_R due to defects in proliferation and survival (Burmeister et al., 2008; Zhang et al., 2013). Whereas CD28-deficient animals demonstrate altered development of T_R in the thymus, loss of ICOS appears to specifically drive defective peripheral maintenance as thymic T_R are by-and-large normal in *Icos*$^{-/-}$ mice (Burmeister et al., 2008). Indeed, antibody-mediated blockade of ICOS signaling *in vivo* results in the selective loss of eT_R in both lymphoid and nonlymphoid sites without impacting cT_R numbers or phenotype (Smigiel et al., 2014a). In addition to supporting T_R abundance, ICOS signaling can also impact T_R function. The

immunosuppressive cytokine IL-10 is produced primarily by $ICOS^+$ eT_R (Cretney et al., 2011). *In vitro*, ICOS costimulation induces production of IL-10 (Arimura et al., 2002; Hutloff et al., 1999). Although mice deficient in ICOS or ICOS ligand (ICOSL) do not develop spontaneous inflammatory or autoimmune disease, genetic or antibody-mediated blockade of ICOS signaling promotes inflammatory immune responses in mouse models of diabetes, allergic airway inflammation, experimental autoimmune encephalomyelitis, and colitis as a result of dysregulated T_R abundance and/or IL-10 production at effector tissue sites (Busse et al., 2012; Dong et al., 2001; Herman et al., 2004; Kornete et al., 2012; Landuyt et al., 2019).

ICOS and PI3K signaling

ICOS binds exclusively to ICOSL, which is expressed on a variety of antigen-presenting cells including B cells, macrophages, and dendritic cells, as well as some endothelial and epithelial cells (Wikenheiser and Stumhofer, 2016). Signaling downstream of ICOS resembles that of the related molecule CD28. However, although ICOS ligation can enhance activation of MAP kinases like ERK, JNK, and p38, it does so less effectively than upon CD28 costimulation (Arimura et al., 2002; Feito et al., 2003). Additionally, ICOS is a potent activator of phosphoinositide 3-kinase (PI3K) signaling due to the presence of a unique YMFM motif in its cytoplasmic tail.

PI3Ks in general act by phosphorylating the 3-position hydroxyl group of membrane-associated inositol lipids. Mammalian PI3Ks include eight enzymes that can be grouped into three classes based on their structures and substrates. Class I PI3Ks can be further subdivided into class IA and IB and are the most comprehensively studied in T cells. In T cells, class IA PI3Ks are activated by antigen receptors, costimulatory molecules, and other tyrosine kinase receptors, whereas class IB PI3Ks are recruited to and signal downstream of G-protein-coupled receptors, like chemokine receptors (Huang and Sauer, 2010). In response to tyrosine kinase receptor signals, the SH2 domains on the regulatory subunit of class IA PI3Ks bind to

phosphorylated tyrosine residues, bringing the catalytic subunit into close proximity to its lipid substrates **[Fig. 1.1]**. PI3Ks catalyze the phosphorylation of membrane-associated phosphatidylinositol (PI)P_2 to generate the second messenger PIP_3. This results in the recruitment and activation of downstream signaling molecules such as PDK1/AKT and mTOR. Activation of AKT occurs through phosphorylation of two essential residues: Thr308 by PDK1 and Ser473 by mTORC2 (Bhaskar and Hay, 2007). Once activated, AKT can exert downstream functions by phosphorylation and nuclear exclusion of Foxo transcription factors, which results in modulation of genes involved in proliferation, survival, metabolic reprogramming, and migration/tissue tropism (So and Fruman, 2012). Additionally, AKT kinase activity can activate mTORC1, which integrates metabolic signals to drive cell growth. Negative regulation of PI3K signaling occurs through lipid phosphatases like PTEN and SHIP, which dephosphorylate PIP_3 back to PIP_2 (Harris et al., 2008). Additionally, the protein phosphatase PHLPP is able to dephosphorylate activated AKT (Gao et al., 2005).

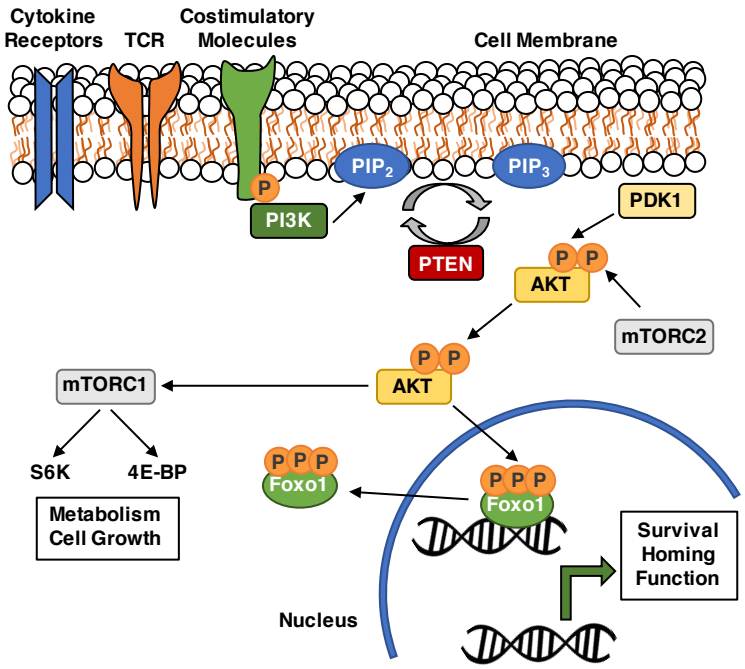

Figure 1.1: Class IA PI3K signaling in T cells. PI3K signaling in T cells can occur downstream of TCR, costimulatory molecules, and cytokine receptors. Receptor engagement results in recruitment and activation of PI3K. Generation of the second messenger PIP_3 brings substrates in close proximity near the cell membrane, which catalyzes downstream signaling cascades that drive changes in many cellular processes.

Inactivation of Foxo1 by AKT is essential for the differentiation of eT_R and regulation of genes including those required for migration to nonlymphoid tissues (Luo et al., 2016). In line with this, mice expressing a kinase-dead form of the p110δ catalytic subunit of PI3K have fewer functional peripheral T_R (Patton et al., 2006). Despite this requirement for PI3K signaling, TCR or IL-2R engagement does not elicit strong PI3K activation in T_R, at least in part due to elevated expression of the negative regulator PTEN (Bensinger et al., 2004; Ouyang et al., 2012). The YMFM cytoplasmic motif of ICOS is uniquely associated with strong lipid kinase activity, and ICOS ligation results in enhanced production of PIP_3 and phosphorylation of AKT (Arimura et al., 2002; Fos et al., 2008). Therefore, engagement of ICOS may facilitate eT_R development and/or maintenance via activation of PI3K.

Specialized tissue T_R

Several recent studies underscore the importance of specialized, tissue-specific T_R phenotypes and functions that go beyond the broad cT_R/eT_R dichotomy. T_R within tissues exhibit hallmarks of eT_R, including expression of the activation markers CD44, GITR, and ICOS, TCR repertoires that recognize tissue antigens, and chemokine receptors that allow for migration and access to specific organs. Tissue T_R additionally integrate cues from distinct tissue microenvironments, driving unique transcriptional and epigenetic landscapes and cellular functions. These include prototypical roles in suppressing inflammatory responses as well as non-canonical functions in maintaining organ and organismal homeostasis and contributing to tissue repair. This recent focus on understanding T_R within distinct tissue environments unveils considerably more complexity and diversity in T_R biology than once appreciated. Below are just a few of many examples of T_R heterogeneity.

Skin-resident T_R support hair growth and wound healing

T_R in skin preferentially localize to hair follicles and abundance is correlated with hair growth cycles (Ali et al., 2017). Indeed, loss of T_R using the *Foxp3*^{DTR} model results in failure of depilated hair to regenerate. Production of the Notch ligand, Jagged-1, by T_R within hair follicles results in stem cell proliferation and differentiation, thus initiating hair follicle cycling (Ali et al., 2017). Skin T_R also promote barrier function by facilitating cutaneous wound healing and suppressing dermal fibrosis. In a model of full thickness wounding, ICOS$^+$CTLA-4$^+$EGFR$^+$ T_R accumulated in wounded skin, peaking at ~70% of the total CD4$^+$ T cell compartment. These highly activated T_R suppressed IFNγ production and pro-inflammatory macrophage accumulation, and depletion of T_R resulted in delayed wound closure and re-epithelialization (Nosbaum et al., 2016). A separate study from the same group identified T_R as important regulators of fibroblast activity in skin. RNAseq experiments revealed a T_H2 signature in skin T_R, including high expression of *Gata3* and the IL-33 receptor, *Il1rl1*. Loss of T_R in *Foxp3*^{DTR} mice led to profibrotic gene activation and dermal fibrosis, which was augmented in a bleomycin-induced model of skin sclerosis (Kalekar et al., 2019). Together, specialized subsets of T_R in the skin coordinate processes critical for hair growth, maintenance of epidermal barrier function, and fibroblast activation.

T_R accumulate in the central nervous system to promote tissue repair

Although there are very few T_R present in the brain and spinal cord under normal conditions, tissue injury and inflammation results in T_R infiltration from the periphery. In a murine model of focal brain ischemia, tissue damage resulted in the recruitment of T_R to the brain, which prevented astrogliosis and neural cell apoptosis via secretion of the epidermal growth factor receptor ligand, AREG. These cells expressed several overlapping TCR clones and high levels of CD44, IL-10, CTLA-4, and ST2 (Ito et al., 2019). Whereas the transcriptional profile of brain T_R shared many features of T_R in other nonlymphoid organs like skeletal muscle and

adipose, several genes related to the nervous system were expressed exclusively in brain T_R, including the serotonin receptor *Htr7*. T_R from the brain were capable of responding to 5-HT *in vitro*, resulting in proliferation and upregulation of suppressive molecules. *In vivo*, pharmacologically enhancing serotonin levels led to improved recruitment of T_R and neurological readouts (Ito et al., 2019*)*. T_R in the central nervous system have also be reported to promote axonal remyelination. Using a model of pharmacologically-induced focal demyelination, Dombrowski *et al*. identified a critical role for T_R in promoting both brain and spinal cord oligodendrocyte differentiation and remyelination through production of the growth regulatory protein CCN3 (Dombrowski et al., 2017). Overall, these studies confirm additional roles for T_R in regenerative functions.

Visceral adipose tissue T_R control adipose inflammation and metabolic homeostasis

Adipose tissue architecture and biology

Visceral adipose tissue (VAT) is primarily a storage site for excess energy in the form of triglycerides. VAT, which is found in proximity to internal organs, is distinct from both thermogenic brown adipose tissue and subcutaneous adipose tissue. VAT is comprised of adipocytes and a stromal vascular fraction that contains pre-adipocytes, fibroblasts, endothelial cells, and a plethora of immune cells. In addition to its storage function, adipocytes from VAT are capable of secreting hundreds of different adipokines, which can act on distal organs to produce profound effects on organismal metabolic homeostasis (Fasshauer and Blüher, 2015). In lean individuals, VAT is maintained in an anti-inflammatory state. This is coordinated by a variety of immune cells, including anti-inflammatory adipose tissue macrophages (ATM), T_H2 cells, eosinophils, group-2 innate lymphoid cells (ILC2), and T_R and is critical for maintenance of metabolic health (Burhans et al., 2018; Feuerer et al., 2009; Molofsky et al., 2013). However, expansion of adipocytes due to chronic caloric excess can promote adipose inflammation and hypoxia and drive accumulation of inflammatory monocytes/macrophages, activate cytotoxic T

cells and neutrophils, and result in insulin resistance and glucose intolerance due to changes in circulation of pro-inflammatory cytokines and adipokines (comprehensively reviewed in Burhans et al., 2018) **[Fig. 1.2]**. VAT plays a central role in metabolic processes, thus keeping adipose tissue inflammation in check is critical for maintaining organismal metabolic health.

VAT-T_R phenotype and function

VAT-T_R are the most extensively studied subpopulation of tissue T_R. A study in 2009 identified the presence of a unique population of T_R in VAT, comprising upwards of 50-80% of the $CD4^+$ T cell fraction in lean, aged male mice (Feuerer et al., 2009). A similar population is found in human omental fat, though at a reduced frequency compared to mice. VAT-T_R are bona fide Foxp3-expressing T_R and are likely thymically derived based on dual expression of Nrp-1 and Helios (Kolodin et al., 2015). Compared to T_R from SLO, VAT-T_R have a much more restricted and clonally expanded TCR repertoire, suggesting that these cells respond to one or more adipose tissue antigens expressed on MHCII (Feuerer et al., 2009; Kolodin et al., 2015). VAT-T_R have distinct transcriptomic and epigenetic signatures associated with both eT_R-related gene expression as well as unique tissue-specific genes (DiSpirito et al., 2018; Feuerer et al., 2009). These include expression of the chemokine receptors *Ccr2*, *Ccr3*, and *Ccr9*, *Il1rl1*, *Il10*, the transcription factors *Pparγ, Batf, Irf4, Blimp1*, *Id2*, and *Gata3* and a host of genes involved in lipid metabolism (Cipolletta et al., 2012; Feuerer et al., 2009; Sullivan et al., 2019; Vasanthakumar et al., 2015).

Several studies have demonstrated a correlation between loss of VAT-T_R abundance and reduction in insulin sensitivity in genetically- or diet-induced murine models of obesity (Deiuliis et al., 2011; Feuerer et al., 2009). Loss- or gain-of-function experiments that manipulate VAT-T_R frequency have corroborated this. For example, depletion of T_R in *Foxp3*^{DTR} mice or by αCD25 depleting antibody administration precipitates increased measures of VAT inflammation and worsened metabolic readouts (Eller et al., 2011; Feuerer et al., 2009).

Expansion of T_R however by, for example, injection of IL-2 immune complexes, improves metabolic parameters and reduces inflammatory measures in VAT (Feuerer et al., 2009, Ilan et al., 2010).

How T_R function within the VAT is still poorly understood, however the presence of VAT-T_R is correlated with anti-inflammatory cell types and reduced indices of inflammation. VAT-T_R express the enzyme hydroxyprostaglandin dehydrogenase (HPGD), which generates the metabolite 15-keto PGE_2 from prostaglandin E_2 (PGE_2) to suppress T_{conv} proliferation (Schmidleithner et al., 2019). Compared to lymphoid T_R, VAT-T_R are poised to produce large amounts of IL-10. *In vitro* treatment of differentiated 3T3-L1 IL-10R-expressing preadipocyte cell line cells with IL-10 impeded responses to TNFα and reduced secretion of CCL2, which promotes inflammatory monocyte recruitment. Additionally, IL-10 signaling in 3T3-L1 cells led to reduced expression of GLUT4, through which excess glucose uptake and fat mass storage in adipocytes occurs (Lumeng et al., 2007). Together, T_R mechanisms of maintaining an anti-inflammatory VAT environment likely involve regulation of both immune and nonhematopoietic cell types.

Maintenance of VAT-T_R

Several factors that contribute to the homeostasis and function of VAT-T_R have been identified. As mentioned previously, VAT-T_R exhibit a restricted TCR repertoire and are comprised of clonally expanded populations (Feuerer et al., 2009). Studies using a transgenic mouse line carrying TCR chains of an expanded VAT-T_R clone (termed vTreg53 TCR-tg) demonstrated a preferential enrichment of clonotype$^+$ T_R in VAT compared to other lymphoid and nonlymphoid tissues (Li et al., 2018). This study suggests that TCR specificity for currently unspecified VAT antigens is important for T_R accumulation in VAT.

Peroxisome proliferator-activated receptor gamma (PPARγ) is the master transcriptional regulator of adipocyte differentiation and is expressed in a large fraction of T_R from VAT

(Cipolletta et al., 2012). Mice with deletion of PPARγ specifically in T_R had reduced T_R abundance in VAT, but not in SLO, and had reduced expression of transcripts consistent with a prototypical VAT-T_R phenotype (Cipolletta et al., 2012). PPARγ upregulates expression of the molecules *Dgat1* and *Pcyt1a*, regulators of triglyceride biosynthesis and phosphatidylcholine metabolism, respectively. Accordingly, expression of PPARγ in VAT-T_R may allow these cells to utilize lipid metabolism for fuel and thrive in an otherwise lipotoxic environment.

Although variable depending on the age of mice, a substantial fraction of VAT-T_R express the IL-33 receptor, ST2. Signaling through ST2 is chiefly known to coordinate production of IL-4, IL-5, and IL-13 by T_H2 effector cells, and thus has been studied in the context of allergic disease (Schmitz et al., 2005). IL-33 is also highly expressed in VAT adipose progenitor cells and mesenchymal stromal cells (Mahlakõiv et al., 2019; Spallanzani et al. 2019), and is capable of promoting the production of IL-5 and IL-13 in ILC2s in VAT, leading to increases in eosinophils and anti-inflammatory ATM (Molofsky et al., 2013). Global loss of IL-33 or ST2 expression in mice results in a dearth of VAT-T_R, whereas administration of exogenous IL-33 boosts VAT-T_R without significant impacts on lymphoid T_R (Han et al., 2015; Vasanthakumar et al., 2015). Expression of ST2 in T_R is thought to be induced downstream of TCR engagement, and potentially IL-33 signaling itself, through the transcriptional regulators BATF and IRF4 (Vasanthakumar et al., 2015). The effects of ST2 expression and IL-33 signaling on VAT-T_R are thought to be at least in part cell-intrinsic. In mixed bone marrow chimeric mice generated from WT and ST2-deficient hematopoietic donor cells, T_R lacking ST2 expression displayed a severe competitive disadvantage in repopulating VAT compared to ST2-sufficient T_R, suggesting a critical role for this cytokine in VAT-T_R maintenance (Vasanthakumar et al., 2015).

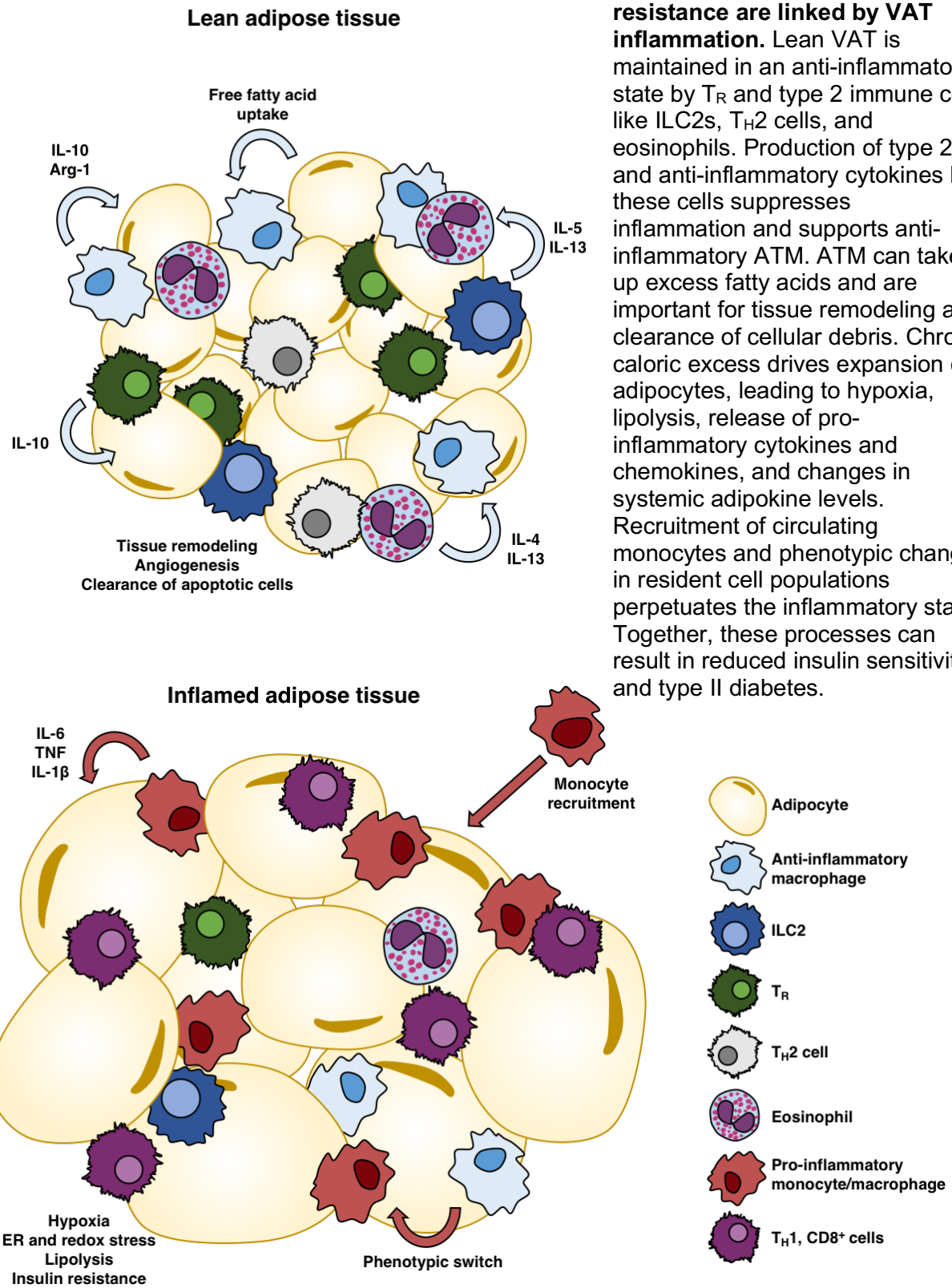

Figure 1.2: Obesity and insulin resistance are linked by VAT inflammation. Lean VAT is maintained in an anti-inflammatory state by T_R and type 2 immune cells like ILC2s, T_H2 cells, and eosinophils. Production of type 2- and anti-inflammatory cytokines by these cells suppresses inflammation and supports anti-inflammatory ATM. ATM can take up excess fatty acids and are important for tissue remodeling and clearance of cellular debris. Chronic caloric excess drives expansion of adipocytes, leading to hypoxia, lipolysis, release of pro-inflammatory cytokines and chemokines, and changes in systemic adipokine levels. Recruitment of circulating monocytes and phenotypic changes in resident cell populations perpetuates the inflammatory state. Together, these processes can result in reduced insulin sensitivity and type II diabetes.

Outstanding questions

Despite exhibiting a general eT_R phenotype, T_R that populate specific tissues are subject to specific environmental cues that drive considerable phenotypic and functional diversity. The ability of T_R to adapt to and be maintained in distinct biological niches is critical for preventing tissue-specific inflammation and for coordinating organismal homeostasis. Although recent work has focused on understanding the development, recruitment, phenotype, and function of tissue-specific T_R, there is still much to discover.

ICOS expression and signaling are critical for the maintenance of eT_R. However the tissue-specific impacts of ICOS signaling in T_R have not been well-characterized. Additionally, although ICOS is a potent driver of PI3K signaling, whether this is the primary signal by which ICOS engagement exerts its effects on subsets of T_R has not been formally investigated.

In the following body of work, we identify divergent roles for ICOS-mediated PI3K signaling in supporting T_R in distinct nonlymphoid tissues. In **Chapter 3**, we determine a surprising role for ICOS-dependent PI3K signaling in antagonizing the abundance and function of VAT-T_R and subsequent protective impacts on VAT inflammation and metabolic homeostasis. **Chapter 4** summarizes preliminary work elucidating a role for ICOS-PI3K in promoting T_R accumulation and function in a murine model of central nervous system autoimmunity/inflammation.

CHAPTER 2: Materials and Methods

Mice

CD45.1$^+$ B6.SJL (B6.SJL-*Ptprc*^{a}*Pepc*^{b}/BoyJ), B6.*Icos*$^{-/-}$ (B6.129P2-*Icos*^{tm1Mak}/J), B6.*Foxp3*^{mRFP} (C57BL/6-*Foxp3*^{tm1Flv}/J), and 2D2 (C57BL/6 Tg(Tcra2D2,Tcrb2D2)1Kuch/J) mice were purchased from The Jackson Laboratory. B6.*Icos*^{Y181F} mice were provided by M. Pepper (University of Washington, Seattle, WA). CD45.1$^+$ B6.SJL mice were crossed to B6.*Foxp3*^{mRFP} mice to generate *Foxp3*^{mRFP} mice expressing CD45.1, CD45.2, and CD45.1/.2 allelic variants. B6.*Icos*$^{-/-}$ and B6.*Icos*^{Y181F} mice were crossed to B6.*Foxp3*^{mRFP} mice to generate B6.*Icos*$^{-/-}$ and B6.*Icos*^{Y181F} mice expressing *Foxp3*^{mRFP}. All animals were bred and housed in specific pathogen-free conditions under the approval of the Institutional Animal Care and Use Committee of the Benaroya Research Institute. Males were used unless specified otherwise. Age of mice is indicated per experiment.

Mixed bone marrow chimeras

Bone marrow cells were prepared from donor mice by flushing femurs and tibias with PBS. Red blood cells (RBC) from filtered cells were lysed in ACK lysis buffer (Life Technologies) for 5 min at room temperature (RT). Recipient mice were lethally irradiated (2 x 600 rad separated by ≥4 hr). Mixed bone marrow chimeras were generated by retro-orbitally (r.o.) injecting a 1:1 ratio (≥2 x10^6 million cells total) of bone marrow cells of the appropriate genotypes into anesthetized recipient mice. Chimeric mice were rested for ≥10 wk.

Intravascular labeling

Mice were anesthetized with 4% isoflurane and 3 µg BV510- or BV650-conjugated CD45 (30-F11) was injected into mice r.o. in 200 µL PBS 5 min prior to sacrifice. Single cell suspensions

were prepared for flow cytometry as described below, and localization of cells was determined by positive (blood-exposed) and negative (tissue-restricted) staining.

Cell isolation

Single-cell suspensions were prepared from spleen and peripheral LNs (pooled inguinal, axillary, brachial, and superficial cervical nodes) by tissue disruption with frosted glass slides into RPMI with 10% bovine calf serum (R-10, BCS) and filtered through nitex mesh. Blood was collected via cardiac puncture into PBS containing 2 mM EDTA. Epididymal visceral adipose (VAT) and inguinal subcutaneous adipose (SQAT) were excised, finely minced with scissors, and digested in RPMI basal medium with 0.14 U/mL Liberase TM (Roche) and 10 U/mL DNase I (Roche) for 30 min at 37°C with shaking (200 rpm). Supernatants were filtered through 100 μM cell strainers and washed several times to remove mature adipocytes from the stromal vascular fraction. Ears were harvested for skin-infiltrating cells. Dorsal and ventral sides were separated using forceps and digested as described for VAT/SQAT for 45 min. Lungs were digested as described for skin. Large intestines were cleaned, stripped of fatty tissue, and inverted. Tissue was placed into extraction media (RPMI basal medium, 2 mM DTT, 1 mM EDTA, 2% BCS) and shaken at 37°C for 20 min to release intraepithelial lymphocytes (IEL). IEL-containing supernatant was removed and filtered into 50 mL conical tubes. For lamina propria lymphocyte (LPL) isolation, immediately following incubation with extraction media, tissue was finely minced and placed into digestion media (RPMI basal media, 300 U/mL collagenase I [Worthington Biochemical Corporation], 1% BCS), shaken for 30 min at 37°C, and filtered into 50 mL conical tubes. To isolate CNS mononuclear cells from EAE mice, brains were dissected out and spinal cords were flushed from the spinal column with PBS using an 18G needle. Brain and spinal cord were finely minced and digested in plain RPMI containing 2.5 mg/mL Collagenase D (Roche) and 1 mg/mL DNase I (Roche) for 30 min at 37°C with vigorous shaking. Cells were filtered and

isolated over a 35%/70% Percoll gradient (VWR) and washed twice before staining for flow cytometry.

Flow cytometry & intracellular cytokine staining

Single-cell suspensions were stained with Fixable Viability Dye eFluor 780 (eBioscience) in PBS for 10 min at RT. For surface staining, cells were incubated at 4°C for 30 min in FACS buffer (PBS, 2% BCS) with directly conjugated antibodies (Abs) for murine proteins. Abs purchased from BioLegend unless noted: CD4 (RM4-5), CD8 (53-6.7), CD11b (M1/70), CD11c (N418), CD25 (PC61), CD44 (IM7), CD45 (30-F11), CD45.1 (A20), CD45.2 (104), CD45RB (C363-16A), CD62L (MEL-14), CD69 (H1.2F3), CD206 (C068C2), CXCR3 (CXCR3-173), F4/80 (BM8), Gr1 (RB6-8C5), ICOS (15F9), KLRG1 (2F1/KLRG1), Siglec-F (E50-2440; BD Biosciences), ST2 (U29-93; BD Biosciences), TCRβ (H57-597). For intracellular staining, cells were stained for surface antigens as described above, washed, and permeabilized for 20 min with eBioscience Fix/Perm buffer at 4°C. Cells were washed and stained in PermWash buffer (eBioscience) for 30 min at 4°C with Abs (purchased from BioLegend unless noted) against Bcl2 (BCL/10C4), CTLA-4 (UC10-4B9), Foxp3 (FJK-16s; Invitrogen), IFNγ (XMG1.2; BD Biosciences), IL-10 (JES5-16E3), IL-17A (TC11-18H10.1), Ki67 (11F6), TNFα (MP6-XT22). For intracellular cytokine staining following restimulation, cells were incubated in FACS tubes with PMA (50 ng/mL) and ionomycin (1 μg/mL) plus monensin (2 μM) in 0.3 mL complete RPMI medium (RPMI-C) [RPMI with 10% (vol/vol) fetal bovine serum, 100 U/mL penicillin, 100 μg/mL streptomycin, 25 μg/mL gentamycin, 1 mM sodium pyruvate, 10 mM HEPES, 2 mM L-glutamine, 55 μM β-ME] for 4 hr at 37°C, 5% CO_2 prior to staining as described above. Loss of mRFP expression occurred with our fixation/permeabilization protocols, requiring intracellular Foxp3 staining. Data were acquired on LSR II or FACSCanto flow cytometers (BD Biosciences) and analyzed using FlowJo software (TreeStar). Due to intraexperimental variability, geometric MFI was normalized as fold change compared to average expression in WT samples per

experiment. Polybead polystyrene nonfluorescent microspheres (15 mm, Polysciences) were used to determine absolute cell numbers in flow cytometry samples. 100 µL of a fixed concentration (C_B) of beads was mixed with 100 µL cells to be counted. Samples were acquired on a flow cytometer, with gates drawn on lymphocyte and bead populations based on their forward- and side-scatter properties. The ratio of lymphocyte gate events (N_L) to bead gate events (N_B) was determined and used to calculate the concentration (C_L) of the original cell suspension as follows: $C_L = (N_L / N_B) \times C_B$

Phospho-flow cytometry staining

~1/4 of each spleen was immediately disrupted between frosted glass slides into BD Fix/Perm buffer (BD Biosciences). Cells were incubated for 20 min at RT, washed in FACS buffer, and resuspended in 90% ice cold methanol for ≥30 min. Cells were washed with BD Perm/Wash buffer (BD Biosciences) and stained for surface and intracellular antigens, including p-S6 (D57.2.2E; Cell Signaling Technology) for 45 min at RT.

Chemokine receptor staining

Freshly isolated cells were incubated for 2.5 hr at 37°C, 5% CO_2 in RPMI-C. For CCR7 expression, cells were incubated with CCL19-human IgGFc fusion protein for 20 min at 4°C, washed, then incubated with PE-conjugated goat anti-human IgGFc (Jackson ImmunoResearch Laboratories) for 20 min at 4°C. To detect CCR2 (475301; R&D Systems) and CCR3 (J073E5; BioLegend), cells were incubated for 30 min at 37°C with directly conjugated antibodies diluted in FACS buffer. Cells were washed twice with FACS buffer before being acquired on the flow cytometer.

Histology

VAT was excised, immediately fixed in 10% formalin for 24 hr, then paraffin-embedded. Hematoxylin and eosin (H&E) staining was performed on 6 µm tissue sections by the Benaroya Research Institute Histology Core. Images were acquired using a Leica DM E compound microscope.

RNA extraction and quantitative PCR

VAT was dissected, immediately stabilized in RNAlater (Thermo Fisher), and frozen at -20°C until ready for processing. ~100 mg tissue was homogenized in 1 mL Qiazol and RNA was extracted using RNeasy Lipid Tissue Mini Kit (Qiagen) according to the manufacturer's instructions. RNA quality and quantity were determined using an ND-1000 spectrophotometer (NanoDrop, Thermo Fisher). 500 ng template RNA was reverse transcribed with random hexamer primers in 20 µL using RevertAid First Strand cDNA Synthesis Kit (Thermo Fisher) and subsequently diluted 1:3.3 with nuclease-free water. qPCR was performed using 2 µL diluted cDNA and presynthesized TaqMan Gene Expression assays in TaqMan Gene Expression Master Mix (Applied Biosystems) for amplification of the following transcripts in a final volume of 20 µL: *Ccl5* (Mm01302427_m1), *Ccl7* (Mm00443113_m1), *Ccl11* (Mm0441238_m1), *Ccl24* (Mm00444701_m1), and *Ccl26* (Mm02763057_u1). Samples were run in technical triplicates using the QuantStudio 5 Real-Time PCR System (Thermo Fisher) with 10 min initial activation at 95°C followed by 40 cycles of 15 sec at 95°C, 60 sec at 60°C. Mean target mRNA levels were calculated by $\Delta\Delta$CT method and normalized to *Tbp* (Mm01277042_m1) expression using QuantStudio Design and Analysis Software (Thermo Fisher).

In vitro stimulation of VAT T cells

VAT was pooled from 2-3 mice of the same genotype to ensure adequate cell number for culture. Cells were isolated as described above, and $CD4^+$ T cells were enriched by incubating

cells with CD4 MicroBeads and positively selecting with MACS cell separation MS columns (Miltenyi Biotec). Purified cells were resuspended in RPMI-C with 500 U/mL recombinant IL-2 (eBioscience). Cells were cultured for 48 hr in 96-well flat-bottom plates with plate-bound αCD3 (2C11) and αCD28 (37.51) from Bio X Cell at 1 μg/μL, with or without the addition of plate-bound αICOS (C398.4A; BioLegend) at 2 μg/μL. Expression of CCR3 was assessed by flow cytometry as described above.

In vivo antibody blockade

Mice aged 8-10 weeks were given 0.75 μg/g body weight αCCL11 and αCCL24 (R&D Systems; MAB420 and MAB528) or an equivalent amount of rat IgG (Sigma) diluted in PBS by intraperitoneal (i.p.) injection on days 0, 5, and 10 and sacrificed for analysis on day 13.

High-fat diet

Mice were placed on 18-week HFD (60% kcal fat diet, Research Diets D124928, *ad libitum*) beginning at 5-7 weeks of age. Weights and blood glucose (BGL) by tail prick (Contour Next One glucose meter; Ascensia Diabetes Care) were taken weekly after 6 hr of fasting.

Insulin and glucose tolerance tests

Insulin tolerance tests were performed in conscious mice fasted for 6 hr. 1 U/kg human insulin (Sigma) was given i.p. and blood was collected by tail prick for BGL at 0, 15, 30, 45, and 60 min post insulin administration. Three days later, glucose tolerance tests were performed in conscious mice fasted for 6 hr. 1 g/kg glucose (Sigma) was administered i.p. Blood was collected by tail prick for BGL at 0, 15, 30, 60, 90, and 120 min post-glucose bolus .

Active induction of EAE

EAE was induced by subcutaneous injection above inguinal lymph nodes of 150 µg MOG_{35-55} (ChinaPeptides) emulsified in CFA (Sigma) supplemented with 40 mg *Mycobacterium tuberculosis* H37Ra (Difco), 100 µL per flank. Animals received 200 ng pertussis toxin intraperitoneally on day 0 and 2 after MOG_{35-55} immunization. Animals were monitored daily for development of EAE with a 0- to 5-point scoring system as follows: 0 – no clinical signs; 1 – limp tail; 2 – impaired righting reflex; 2.5 – partial hind limb paralysis; 3 – total hind limb paralysis; 3.5 – total hind limb paralysis/partial forelimb paralysis; 4 – forelimb paralysis; 5 – moribund

Passive transfer of EAE

$CD4^+$ T cells were isolated from pooled spleen and lymph nodes of 2D2 mice by incubating cells with CD4 MicroBeads and positively selecting with MACS cell separation LS columns (Mitenyi Biotec). The flow-through fraction was irradiated with 4000 rad for antigen-presenting cells (APC). A 1:5 ratio of $CD4^+$ T cell:APC was cultured in 6-well plates in RPMI-C containing 2.5 µg/mL soluble αCD3 (2C11; Bio X Cell) and 10 ng/mL IL-12 (eBioscience). Cells were split on day 2 into media containing 10 U/mL mIL-2 (eBioscience) and cultured for an additional 4 d. After several washes, 7.5×10^6 cells were transferred retro-orbitally into sublethally irradiated (500 rad) host mice. 200 ng pertussis toxin was given intraperitoneally on day 0 and 2 post-transfer. Animals were monitored for disease as described in “Active induction of EAE.”

Statistical analysis

All data are presented as mean values ± SD and graphs were created and analyzed using Prism Software (GraphPad). Comparisons between genotypes were analyzed using one- or two-way ANOVA where appropriate, adjusted for multiple comparisons using Tukey’s post-test. For mixed bone marrow chimeras, statistical significance was determined using two-tailed paired Student’s *t* tests when comparing cells within the same chimeric mouse.

CHAPTER 3: ICOS-dependent PI3K signaling limits regulatory T cell accumulation and function in visceral adipose tissue

Introduction

$CD4^+Foxp3^+$ regulatory T cells (T_R) are critical for the development and maintenance of immune tolerance, the inhibition of immune responses to innocuous environmental antigens, and the resolution of ongoing inflammation after infection (Dominguez-Villar and Hafler, 2018; Rivas and Chatila, 2016; Smigiel et al., 2014b). More recent work highlights additional roles for specialized subsets of tissue-specific T_R in tissue repair and homeostasis. For example, $AREG^+$ T_R expand in skeletal muscle and the lungs in response to injury and are required for proper tissue repair (Arpaia et al., 2015; Burzyn et al., 2013), whereas T_R within hair follicles and skin are essential for hair generation and keeping profibrotic processes in check, respectively (Ali et al., 2017; Kalekar et al., 2019). A transcriptionally unique population of T_R are found in the visceral adipose tissue (VAT) of both mice and humans, and these T_R regulate adipose inflammation and preserve metabolic homeostasis as demonstrated by loss- and gain-of-function experiments (Deiuliis et al., 2011; Eller et al., 2011; Feuerer et al., 2009; Ilan et al., 2010). For example, T_R ablation in diphtheria toxin-treated *Foxp3*^{DTR} mice results in increased inflammatory mediators in VAT and reduced insulin sensitivity, whereas augmentation of T_R by administration of IL-2 immune complexes or IL-33 results in improved metabolic readouts in mice on high-fat diet (HFD) (Feuerer et al., 2009; Han et al., 2015; Vasanthakumar et al., 2015).

Given that T_R modulate diverse responses in different anatomical and inflammatory settings, it is not surprising that they exhibit considerable phenotypic and functional heterogeneity. Expression of CD62L and CD44 broadly divides T_R into distinct subsets that are enriched in lymphoid and nonlymphoid tissues (Campbell, 2015; Smigiel et al., 2014a). We term these populations central T_R (cT_R) and effector T_R (eT_R), respectively. Differential activation of

PI3K, unique epigenetic landscapes, and distinct transcriptional programs drive functional diversification of T_R, and selective expression of chemokine receptors and cell adhesion molecules give subsets of T_R access to specific tissues (Delacher et al., 2017; DiSpirito et al., 2018; Luo et al., 2016). The proper distribution and function of T_R across tissues is crucial for maintaining immune tolerance and tissue homeostasis (Sather et al., 2007; Yamaguchi et al., 2011). Hence, understanding the signals that control the development, maintenance, and function of tissue-specific T_R is vital to fully harnessing their therapeutic potential.

T_R occupancy in lymphoid versus nonlymphoid tissues is met with unique homeostatic maintenance requirements. Generally, IL-2 signaling maintains cT_R within T cell zones of secondary lymphoid tissues by driving pro-survival signals, whereas maintenance of eT_R in nonlymphoid tissues can be IL-2 independent and instead relies on TCR and costimulatory molecule engagement (Levine et al., 2014; Smigiel et al., 2014a; Tang et al., 2003). ICOS is expressed on highly suppressive T_R and can control T_R abundance by inhibiting apoptosis and stimulating proliferation (Burmeister et al., 2008; Redpath et al., 2013). ICOS can also impact T_R function. T_R production of the immunosuppressive cytokine IL-10 is essential for control of local immune responses, and is primarily expressed by Blimp-$1^+$$ICOS^+$ eT_R (Cretney et al., 2011). ICOS costimulation *in vitro* super-induces IL-10 expression (Arimura et al., 2002; Hutloff et al., 1999), and this depends on its ability to activate phosphoinositide 3-kinase (PI3K) (Feito et al., 2003; Okamoto et al., 2003). Although mice deficient in ICOS or ICOS ligand do not develop spontaneous inflammatory or autoimmune disease, genetic or antibody-mediated blockade of ICOS signaling promotes inflammatory immune responses in mouse models of autoimmunity and infection as a result of reduced T_R abundance and/or IL-10 production (Busse et al., 2012; Dong et al., 2001; Herman et al., 2004; Kohyama et al., 2004; Kornete et al., 2012; Landuyt et al., 2019; Miyamoto et al., 2005; Redpath et al., 2013).

ICOS potently activates PI3K and downstream AKT due to the presence of a unique YMFM motif in its cytoplasmic tail (Arimura et al., 2002*;* Fos et al., 2008). AKT can act on

several different substrates, including the transcription factor Foxo1, to modulate transcription of genes involved in proliferation, survival, metabolic reprogramming, and migration/tissue tropism (So and Fruman, 2012). Indeed, inactivation of Foxo1 by AKT is essential for the differentiation of eT_R and their migration to nonlymphoid tissues (Luo et al., 2016). Thus, engagement of ICOS may facilitate the development and/or maintenance of eT_R via PI3K-dependent signaling pathways.

Accumulation of T_R in VAT is dependent on several signals. Local TCR:MHCII interactions are likely important, as VAT-T_R consist of clonally expanded populations, suggesting recognition of one or more adipose tissue antigens (Feuerer et al., 2009; Kolodin et al., 2015). A fraction of VAT-T_R express the IL-33 receptor, ST2. Indeed, mice lacking expression of IL-33 or ST2 are deficient in VAT-T_R, whereas injection of exogenous IL-33 results in increased VAT-T_R abundance with little impact on lymphoid T_R (Han et al., 2015; Vasanthakumar et al., 2015). Recent work assessing WT:*Ccr2*$^{-/-}$ mixed bone marrow chimeric mice also identified a cell-intrinsic role for CCR2 in the ability of donor T_R to repopulate VAT (Vasanthakumar et al., 2020). Finally, T_R expression of PPARγ, the master regulator of adipocyte differentiation, supports VAT-T_R phenotype and accumulation and drives expression of factors important for lipid metabolism (Cipolletta et al., 2012; Cipolletta et al., 2015). However, despite having an eT_R phenotype, the role of costimulatory molecule signaling in VAT-T_R is poorly understood.

In this study, we demonstrate an unexpected role for cell-intrinsic ICOS-dependent PI3K signaling in restricting VAT-T_R accumulation and activated phenotype. Moreover, we implicate the CCL11/24-CCR3 axis in driving recruitment of T_R to VAT, which is enhanced in the absence of ICOS signaling. These surprising findings challenge the current model regarding signals that support diverse T_R subsets, and highlights the cell- and tissue-specific effects of ICOS expression and signaling on T_R development, accumulation, and function.

Results

Mice lacking ICOS signaling have reduced T_R in lymphoid tissues and altered expression of PI3K targets

To determine how ICOS signaling impacts T_R abundance in different tissues, we crossed *Foxp3*^{mRFP} mice to *Icos*$^{-/-}$ (KO) mice and to *Icos*^{Y181F} (YF) mice, which carry a tyrosine-to-phenylalanine knock-in mutation in the YMFM motif in the cytoplasmic tail of ICOS, thereby specifically abolishing ICOS-mediated PI3K activation (Gigoux et al., 2009). Thus we had WT, YF, and KO mice whose T_R expressed monomeric red fluorescent protein (RFP) under control of the *Foxp3* locus, faithfully marking T_R without the need for intracellular Foxp3 staining (Wan and Flavell, 2005). In line with published data, we found a ~30% reduction in the frequency and number of T_R in the spleens of KO compared to WT mice (Burmeister et al., 2008; Landuyt et al., 2019) **[Fig. 3.1A]**. This was even more pronounced in older animals, as T_R accumulate with age (Nishioka et al., 2006) **[Fig. 3.1B]**. Despite normal ICOS expression on the cell surface **[Fig. S3.1A]** and intact MAPK signaling (Gigoux et al., 2009), we saw a similar reduction in splenic T_R abundance in YF mice, indicating that activation of PI3K signaling is the critical pathway by which ICOS regulates T_R abundance **[Fig. 3.1A, B]**. ICOS is expressed on both cT_R and eT_R, however its expression is upregulated on eT_R **[Fig. S3.1B]**. The loss of T_R we observed in YF and KO spleens was associated with a disproportionate reduction in the frequency and number of eT_R, whereas the number of cT_R was unchanged, consistent with results from our lab using *in vivo* antibody blockade of ICOS signaling (Smigiel et al., 2014a) **[Fig. 3.1C]**. Loss of T_R was also observed in the peripheral lymph nodes of YF and KO mice, indicating that ICOS signaling is important for eT_R maintenance in multiple secondary lymphoid organs **[Fig. S3.1C]**. Both YF and KO T_R in the spleen had altered expression of targets controlled by PI3K signaling, including elevated expression of the lymphoid homing molecules CD62L and CCR7 which are downregulated upon PI3K activation via phosphorylation and sequestration of Foxo1 (Kerdiles et al., 2009) **[Fig. 3.2A]**. When examined directly *ex vivo*, YF

and KO splenic T_R also exhibited reduced phosphorylation of the mTORC1 target, ribosomal protein S6, consistent with diminished activation of PI3K **[Fig. 3.2B]**. This further indicates that absence of ICOS-mediated PI3K activation drives the altered lymphoid T_R frequency and phenotype we see in YF and KO mice.

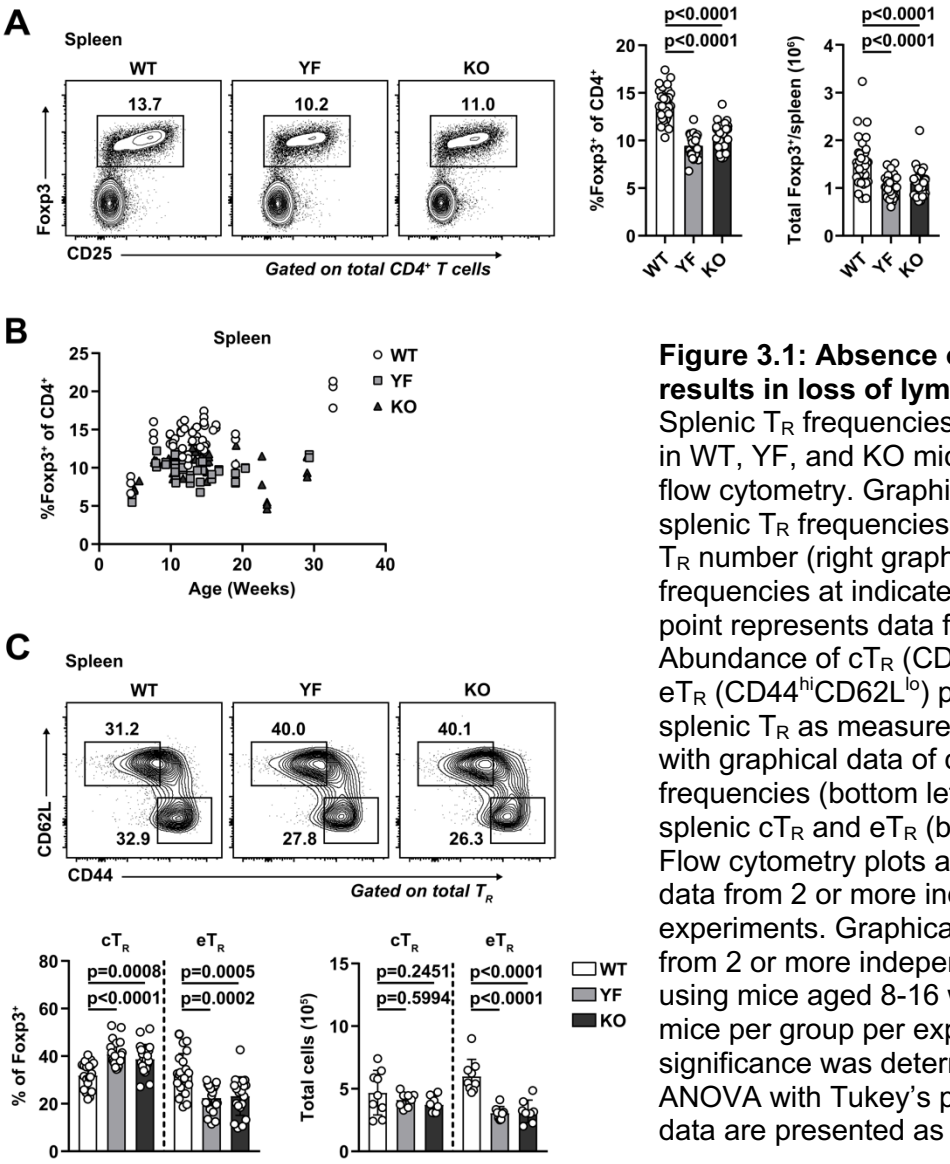

Figure 3.1: Absence of ICOS signaling results in loss of lymphoid T_R. (A) Splenic T_R frequencies of total $CD4^+$ T cells in WT, YF, and KO mice as measured by flow cytometry. Graphical data shows splenic T_R frequencies (left graph) and total T_R number (right graph). **(B)** Splenic T_R frequencies at indicated mouse ages. Each point represents data from one mouse. **(C)** Abundance of cT_R ($CD44^{lo}CD62L^{hi}$) and eT_R ($CD44^{hi}CD62L^{lo}$) populations of total splenic T_R as measured by flow cytometry with graphical data of cT_R and eT_R frequencies (bottom left graph) and total splenic cT_R and eT_R (bottom right graph). Flow cytometry plots are representative of data from 2 or more independent experiments. Graphical data are compiled from 2 or more independent experiments using mice aged 8-16 weeks, with n = 3-5 mice per group per experiment. Statistical significance was determined using one-way ANOVA with Tukey's post-test. All graphical data are presented as mean values ± SD.

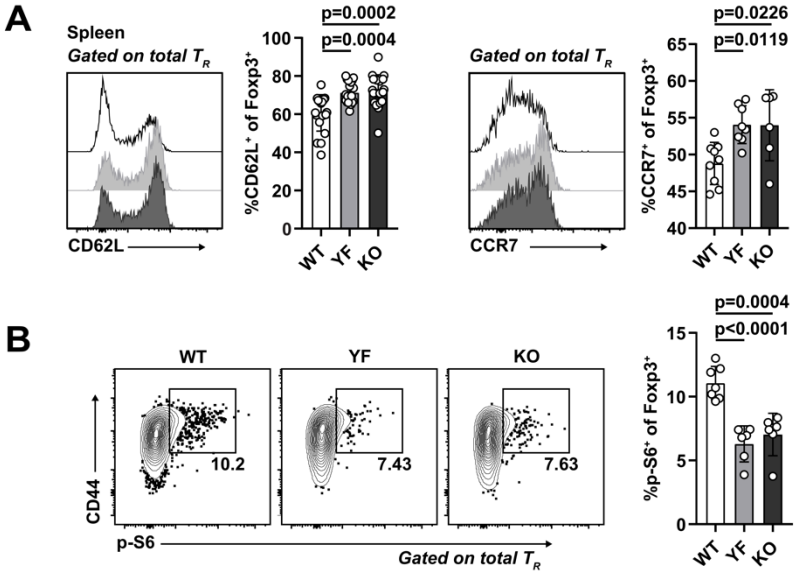

Figure 3.2: Loss of ICOS signaling results in altered expression of PI3K targets. (A) Expression of CD62L and CCR7 in gated splenic T_R. **(B)** S6 phosphorylation measured directly *ex vivo* in splenic T_R by flow cytometry. Flow cytometry plots are representative of data from 2 or more independent experiments. Graphical data are compiled from 2 or more independent experiments using mice aged 8-16 weeks, with *n* = 3-5 mice per group per experiment. Statistical significance was determined using one-way ANOVA with Tukey's post-test. All graphical data are presented as mean values ± SD.

T_R are enriched in VAT in the absence of ICOS signaling

As eT_R are highly enriched in nonlymphoid sites (Lee et al., 2007; Smigiel et al., 2014a), we next assessed whether maintenance of T_R in peripheral tissues was diminished in YF and KO mice. Using intravascular labeling to identify tissue-localized T_R (Anderson et al., 2014), we observed a reduction in the frequency and number of T_R in the skin and decrease in the absolute number of T_R in the lungs of YF and KO mice **[Fig. 3.3A, B]**. However, T_R frequency and total number were actually elevated in the VAT of both strains **[Fig. 3.3C]**. This was specific to VAT, as frequency and total number of T_R in subcutaneous adipose tissue (SQAT) remained similar between genotypes **[Fig. S3.2A]**. The increased abundance of VAT-T_R in YF and KO mice was present in both males and females, although the frequency and number of VAT-T_R was significantly reduced in females **[Fig. 3.3D, E]**. Consistent with previous studies, we observed age-dependent accumulation of VAT-T_R across all three genotypes (Feuerer et al.,

2009), but despite considerable mouse-to-mouse variability, VAT-T_R remained elevated in YF and KO mice across all age groups analyzed **[Fig. 3.3F].**

We utilized male mice for the remainder of our studies as we found female mice harbor ~4-5-fold fewer T_R/gram VAT than age-matched males, and female mice are protected from the development of diet-induced metabolic syndrome (Ahnstedt et al., 2018; Pettersson et al., 2012; Vasanthakumar et al., 2020). The frequency of VAT-T_R expressing KLRG1 and CD69 was significantly elevated in YF and KO mice compared to WT controls **[Fig. 3.4A]**. This is in contrast to what we found in the spleen, where a reduced frequency of YF and KO T_R expressed CD69, and very few T_R expressed KLRG1 **[Fig. S3.3A]**. We assessed VAT-T_R Foxp3 and CD44 expression, and found no difference in the absence of ICOS **[Fig. S3.3B]**. We did however observe a modest increase in the expression of CTLA-4 and a slight reduction in the frequency of $CD25^+$ T_R in YF and KO VAT **[Fig. 3.4A]**. Therefore, T_R in the VAT of YF and KO mice are enriched in expression of markers indicative of an eT_R and VAT-T_R phenotype (Feuerer et al., 2009; Smigiel et al., 2014a).

In addition to prototypical eT_R markers, a fraction of VAT-T_R express the IL-33 receptor, ST2 (Kolodin et al., 2015; Vasanthakumar et al., 2015). Signaling downstream of ST2 is required for the establishment and maintenance of VAT-T_R, and expansion of VAT-T_R through administration of IL-33 can reduce VAT inflammation and improve metabolic indices in models of diet-induced obesity (Han et al., 2015; Kolodin et al., 2015; Vasanthakumar et al., 2015). In addition to ST2-expressing T_R, we found a substantial population of $CXCR3^+$ T_R in the VAT of lean mice, confirming previously reported findings **[Fig. 3.4B]** (Li et al., 2018). Although there were no significant differences in the frequency of WT, YF, or KO VAT-T_R singly-expressing ST2 or CXCR3, we found a unique population of double-expressing $ST2^+CXCR3^+$ T_R in YF and KO VAT which resembled canonical VAT-T_R in their expression of KLRG1 and CD69 **[Fig. 3.4B, C]**.

ICOS signaling is implicated in IL-10 production both *in vitro* and *in vivo* (Busse et al., 2012; Dong et al., 2001; Herman et al., 2004; Hutloff et al., 1999; Kohyama et al., 2004; Kornete

et al., 2012; Landuyt et al., 2019; Miyamoto et al., 2005; Redpath et al., 2013). Surprisingly, compared to VAT-T_R from WT mice, a substantially higher frequency of YF and KO VAT-T_R were poised to produce IL-10 upon *ex vivo* stimulation with PMA/I, with no appreciable differences in IL-10 expression by splenic T_R **[Fig. 3.4D]**. Thus, absence of ICOS-dependent PI3K signaling supports both the accumulation and suppressive phenotype of T_R in VAT.

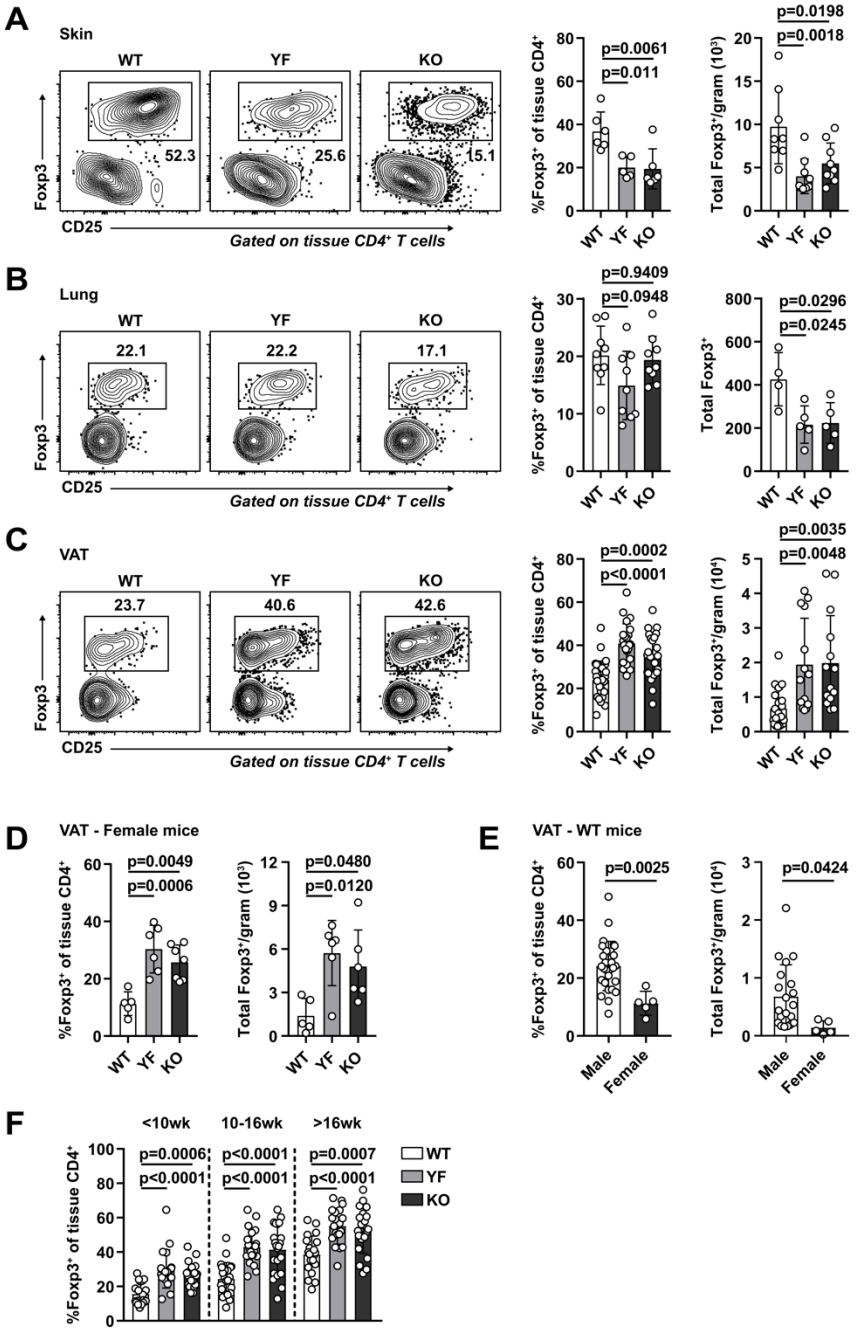

Figure 3.3: T_R frequency and number are increased in VAT in the absence of ICOS signaling. (A-C) Representative flow cytometry plots showing frequency of T_R among tissue-localized TCRβ$^+$CD4$^+$ cells in WT, YF, and KO ear skin **(A)**, lung **(B)**, and VAT **(C)**. Pooled data from mice 8-16 weeks old with T_R frequencies (left graphs) and total T_R number (right graphs) of aforementioned tissues. **(D)** T_R frequency of tissue-localized CD4$^+$ T cells (left) and total T_R number (right) in VAT of female WT, YF, and KO mice. **(E)** T_R frequency (left) and total T_R number (right) in VAT of 8-16 week old male and female WT mice. **(F)** VAT-T_R frequencies by noted age bins as measured by flow cytometry. Flow cytometry plots are representative of data from 2 or more independent experiments. Graphical data are compiled from 2 or more independent experiments with *n* = 2-5 mice per group per experiment. Statistical significance was determined using one-way ANOVA with Tukey's post-test or two-tailed Student's *t* test where appropriate. All data are presented as mean values ± SD.

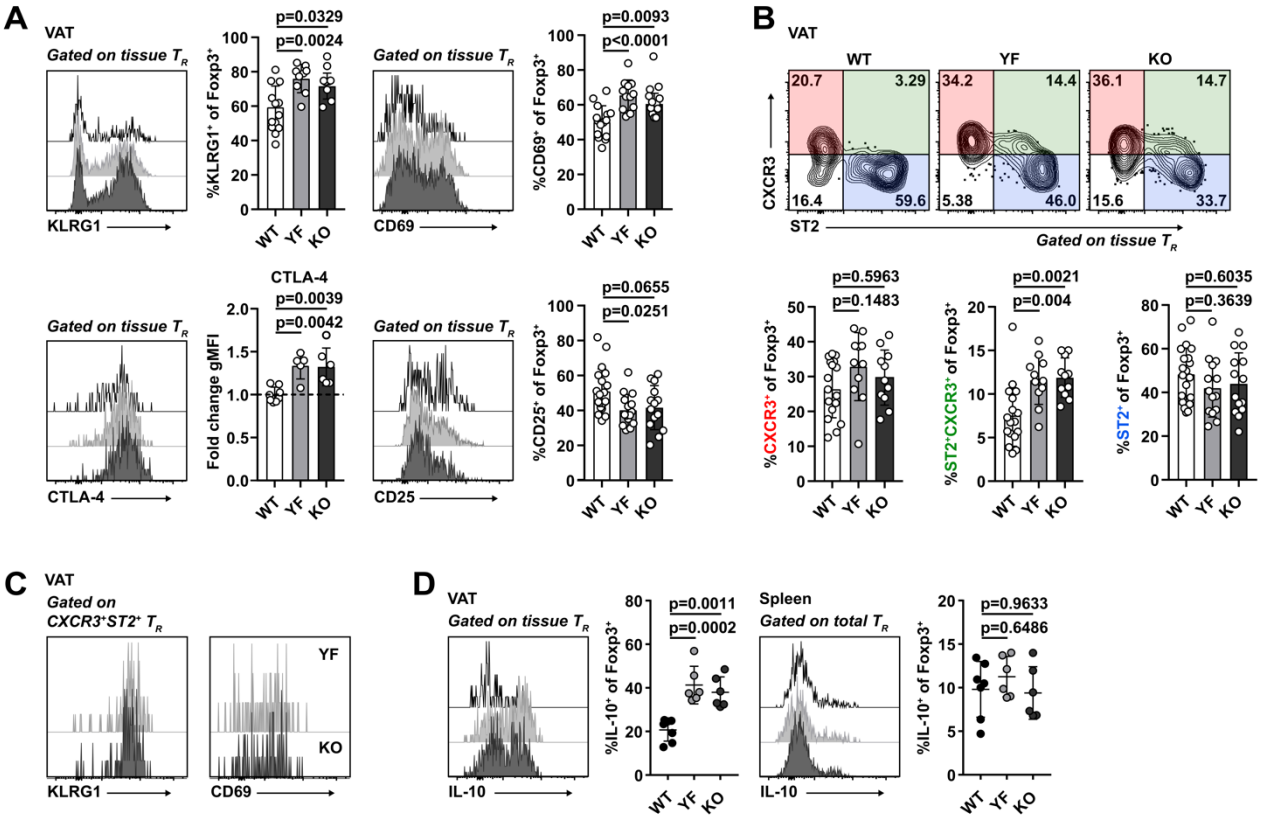

Figure 3.4: Loss of ICOS signaling supports an eT_R phenotype in VAT. (A) KLRG1, CD69, CTLA-4, and CD25 expression in tissue-localized VAT-T_R. CTLA-4 geometric MFI was calculated as fold change compared to average expression in WT T_R for each individual experiment. **(B)** Representative gating of VAT-T_R on CXCR3 and ST2 expression. Graphs summarize the frequency of WT, YF, and KO VAT-T_R positive for CXCR3 (left) or ST2 (right) alone, or double-expressers of CXCR3 and ST2 (middle). **(C)** Histograms showing expression of KLRG1 and CD69 in CXCR3$^+$ST2$^+$ YF and KO VAT-T_R as measured by flow cytometry. **(D)** Representative flow cytometry plots and summarized graphical data showing IL-10 expression in T_R from VAT and spleen after 4h PMA/I+monensin stimulation *ex vivo*. Flow cytometry plots are representative of data from 2 or more independent experiments. Graphical data are compiled from 2 or more independent experiments using 8-16 week old mice, with *n* = 3-5 mice per group per experiment. Statistical significance was determined using one-way ANOVA with Tukey's post-test. All data are presented as mean values ± SD.

Baseline adipose inflammation is reduced in YF and KO mice

T_R regulate inflammatory responses in VAT, so we next assessed whether the loss of ICOS signaling resulted in changes in VAT inflammation. VAT inflammation is modulated through a balance of different immune cells. T_R, eosinophils, alternatively activated anti-inflammatory adipose tissue macrophages (ATM), and group-2 innate lymphoid cells (ILC2) maintain a type-2 immune environment that supports metabolic homeostasis in lean animals. Inflammation however drives recruitment of neutrophils and cytotoxic T cells, differentiation of inflammatory ATM, and production of pro-inflammatory cytokines like TNFα (Burhans et al., 2018; Molofsky et al., 2013). Although there was no difference in mouse weights between WT, YF, and KO mouse across different ages, we did observe a trend toward increased VAT weight in YF mice, and a significant increase in KO mice **[Fig. 3.5A]**. By histology, we did not observe any overt morphological differences in VAT from WT, YF, and KO mice, including no observable differences in adipocyte size **[Fig. S3.4A].** This increase in VAT weight however did correlate with a modest increase in the total number of $CD4^+$ T_{eff} per gram of tissue **[Fig. 3.5B]**. Despite this increase in VAT-T_{eff} number, there was a substantially lower frequency of YF and KO VAT-T_{eff} expressing features of inflammatory T_H1 cells, including CXCR3, IFNγ, and TNFα **[Fig. 3.5C]**. Rather, ST2-expressing T_{eff} were enriched in YF and KO VAT **[Fig. 3.5C]**. Similar to VAT-T_R, YF and KO VAT-T_{eff} were superior at producing IL-10 upon stimulation, suggesting that absence of ICOS signaling in effector cells supports a self-regulatory function **[Fig. 3.5C]**. IL-33 signaling induces production of T_H2 cytokines (Schmitz et al., 2005), which maintain ATM in an anti-inflammatory state. While we didn't find any significant changes in ATM or ILC2 populations **[Fig. S3.4B, C]**, we did note an increased frequency of eosinophils in YF and KO VAT **[Fig. 3.5D]**, which produce IL-4 to maintain anti-inflammatory ATM (Molofsky et al., 2013; Wu et al., 2011). Overall, global loss of ICOS expression and signaling impacts T_R along with other adipose-resident immune cells to maintain an anti-inflammatory state in VAT.

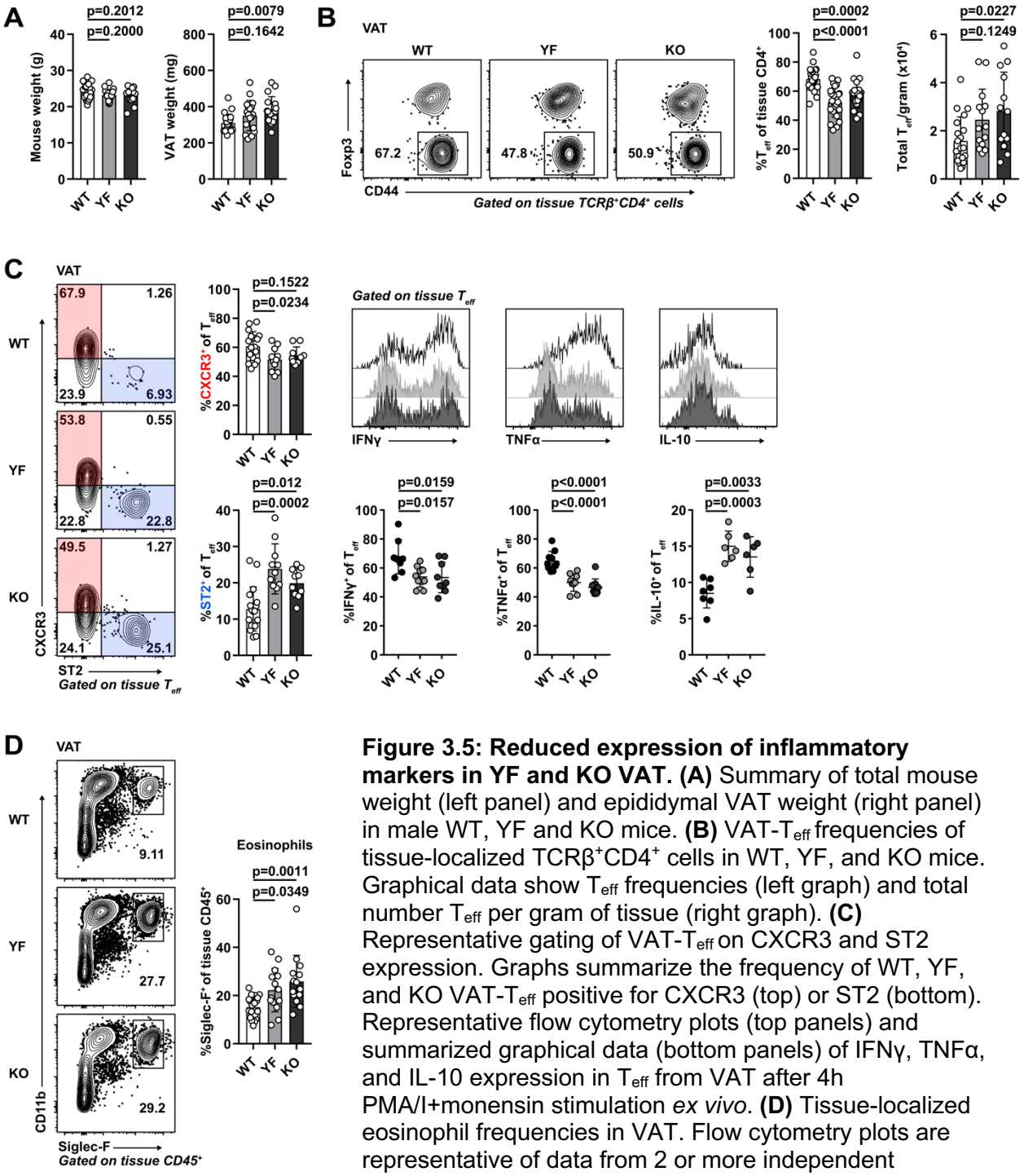

Figure 3.5: Reduced expression of inflammatory markers in YF and KO VAT. (A) Summary of total mouse weight (left panel) and epididymal VAT weight (right panel) in male WT, YF and KO mice. **(B)** VAT-T_{eff} frequencies of tissue-localized TCRβ$^+$CD4$^+$ cells in WT, YF, and KO mice. Graphical data show T_{eff} frequencies (left graph) and total number T_{eff} per gram of tissue (right graph). **(C)** Representative gating of VAT-T_{eff} on CXCR3 and ST2 expression. Graphs summarize the frequency of WT, YF, and KO VAT-T_{eff} positive for CXCR3 (top) or ST2 (bottom). Representative flow cytometry plots (top panels) and summarized graphical data (bottom panels) of IFNγ, TNFα, and IL-10 expression in T_{eff} from VAT after 4h PMA/I+monensin stimulation *ex vivo*. **(D)** Tissue-localized eosinophil frequencies in VAT. Flow cytometry plots are representative of data from 2 or more independent experiments. Graphical data are compiled from 2 or more independent experiments using mice aged 8-16 weeks, with *n* = 3-5 mice per group per experiment. Statistical significance was determined using one-way ANOVA with Tukey's post-test. All graphical data are presented as mean values ± SD.

YF and KO mice are protected from high-fat diet-induced insulin resistance, correlating with maintenance of VAT-T_R

Given the abundance and suppressive phenotype of T_R and other anti-inflammatory immune cells in VAT in the absence of ICOS signaling, we wondered if this would render YF and KO mice more resistant to developing HFD-induced inflammation and metabolic changes. Mice placed on an 18-week HFD steadily gained body mass, with a modest reduction in weight gained by KO mice compared to WT **[Fig. 3.6A]**. After 18 weeks on HFD, YF and KO mice sustained elevated T_R frequencies in VAT compared to WT mice, with an increased fraction of cells expressing the canonical VAT-T_R markers ST2 and KLRG1, and a smaller proportion of T_R expressing CXCR3 **[Fig. 3.6B, C]**. Additionally, YF and KO mice placed on HFD retained a greater frequency of eosinophils and T_{eff} skewed toward a type-2, ST2-expressing phenotype **[Fig. 3.6D, E]**. Fasting blood glucose levels (BGL) were similar among genotypes after 18-weeks, and WT, YF, and KO mice were able to clear glucose to the same extent, as measured by glucose tolerance test (GTT) **[Fig. 3.6F]**. However, in an insulin tolerance test (ITT), YF and KO mice demonstrated improved insulin sensitivity compared to WT mice **[Fig. 3.6G]**. Thus, loss of ICOS supports T_R and other anti-inflammatory cells in VAT during HFD, and this has functional consequences in maintaining metabolic homeostasis.

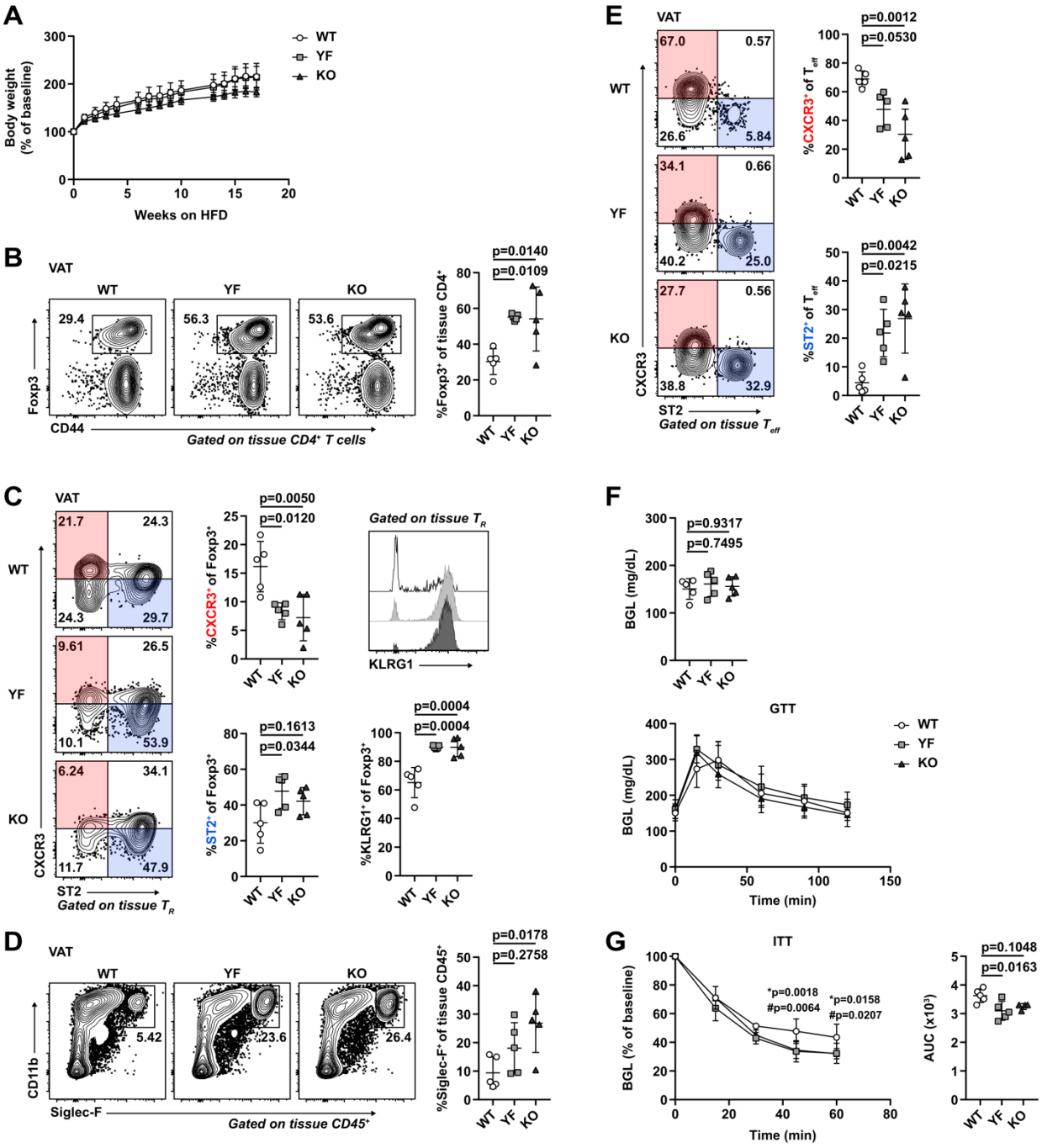
A
Body weight (% of baseline)
Weeks on HFD
WT
YF
KO
B
VAT
WT
YF
KO
Foxp3
CD44
Gated on tissue CD4+ T cells
%Foxp3+ of tissue CD4+
p=0.0140
p=0.0109
C
VAT
WT
YF
KO
CXCR3
ST2
Gated on tissue T_R
%CXCR3+ of Foxp3+
p=0.0050
p=0.0120
%ST2+ of Foxp3+
p=0.1613
p=0.0344
KLRG1
%KLRG1+ of Foxp3+
p=0.0004
p=0.0004
D
VAT
CD11b
Siglec-F
Gated on tissue CD45+
%Siglec-F+ of tissue CD45+
p=0.0178
p=0.2758
E
VAT
WT
YF
KO
CXCR3
ST2
Gated on tissue T_eff
%CXCR3+ of T_eff
p=0.0012
p=0.0530
%ST2+ of T_eff
p=0.0042
p=0.0215
F
BGL (mg/dL)
p=0.9317
p=0.7495
GTT
Time (min)
G
ITT
BGL (% of baseline)
Time (min)
*p=0.0018
#p=0.0064
*p=0.0158
#p=0.0207
AUC (x10³)
p=0.1048
p=0.0163

Figure 3.6: Mice deficient in ICOS signaling maintain anti-inflammatory immune cell abundance and phenotype in VAT after long-term HFD, correlating with improved insulin sensitivity. Groups of WT, YF, and KO mice were placed on HFD for 18 wk. **(A)** Fasted body weights taken at indicated timepoints and graphed as percentage of baseline body weight at start of HFD. **(B)** Tissue-localized VAT-T_R frequency at the end of the HFD treatment. **(C)** VAT-T_R phenotypic data as measured by flow cytometry showing expression of CXCR3, ST2, and KLRG1. **(D)** Frequency of tissue-localized eosinophils in VAT. **(E)** Representative gating of VAT-T_{eff} on CXCR3 and ST2 with summarized graphical data. **(F)** Fasting BGL (top) and GTT (bottom) in HFD-fed mice. **(G)** ITT in HFD-fed mice. * indicates significant difference between WT and YF; # indicates significant difference between WT and KO. ITT area under the curve (AUC) was calculated for each individual mouse. Flow cytometry plots are representative of data from 2 experiments. Graphical data are compiled from 2 experiments with *n* = 4-5 mice per group per experiment. For weight **(A)**, GTT, and ITT **(F, G)** graphs, statistical significance was determined using two-way repeated measures ANOVA with Tukey's post-test for multiple comparisons. For fasted BGL **(F)**, ITT AUC **(G)**, and all flow cytometry summary graphs, statistical significance was determined using one-way ANOVA with Tukey's post-test. All graphs are presented as mean values ± SD.

Absence of ICOS supports the accumulation and phenotype of VAT-T_R in a cell-intrinsic manner

ICOS signaling supports a wide array of cellular processes in the context of adaptive immunity, including induction and localization of T follicular helper cells, T-dependent antibody production, and $CD4^+$ T_{eff} polarization and function (Panneton et al., 2019). To assess which of the T cell phenotypes we observed in intact YF and KO mice were the result of intrinsic ICOS expression and signaling, we generated mixed bone marrow chimeras using congenically marked $CD45.1^+$ WT and $CD45.2^+$ WT, YF, or KO donors **[Fig. 3.7]**. Body and adipose depot weights were similar between groups of chimeric mice **[Fig. S3.5A]**. Consistent with the increased abundance of VAT-T_R we observed at baseline in intact YF and KO mice, both $CD45.2^+$ YF and KO T_R displayed a competitive advantage compared to $CD45.1^+$ WT T_R in repopulating VAT in our chimeric mice. While WT:WT chimeras reconstituted VAT-T_R at a ~1:1 ratio, YF and KO T_R exhibited a significantly higher reconstitution ratio of ~5.5:1 **[Fig. 3.8A]**. In addition to supporting VAT-T_R abundance, absence of cell-intrinsic ICOS signaling also promoted a canonical VAT-T_R phenotype. Within the same chimeras, a higher frequency of YF and KO VAT-T_R expressed CD69 and ST2 **[Fig. 3.8B]**. Aligned with data from intact mice, more YF and KO VAT-T_R within chimeras were double-expressers of CXCR3 and ST2 **[Fig. 3.8B]**.

Functionally, a larger proportion of YF and KO VAT-T_R were poised to produce IL-10 after *ex vivo* stimulation **[Fig. 3.8B]**. Mixed bone marrow chimeras retain a population of radioresistant host T_R, which proliferate to replenish a portion of the available niche after irradiation (Komatsu and Hori, 2007), and this is particularly evident in many nonlymphoid tissues. Remarkably, in addition to preferentially reconstituting VAT compared to WT donor T_R, YF and KO VAT-T_R were able to outcompete endogenous WT VAT-T_R as well, nearly replacing the entire T_R compartment in some chimeras **[Fig. 3.8C]**.

Contrary to our findings in VAT, YF and KO T_R were at a selective disadvantage in the skin, spleen, and large intestine, with no difference in reconstitution in the lungs **[Fig. 3.8D, Fig. S3.5B]**. T_R found in SQAT are phenotypically distinct from VAT-T_R and do not appear to accumulate with age (Feuerer et al., 2009; Li et al., 2018). However, unlike in intact mice, we did note that YF and KO donor T_R displayed a competitive advantage in repopulating SQAT in chimeric mice at a ratio of ~3:1 **[Fig. 3.8D]**. This could be due to low level inflammation following irradiation of the recipient mice that drives reconstitution of the SQAT niche with T_R exhibiting a more VAT-T_R phenotype.

Although $CD8^+$ T cells and ILC2s of either genotype were similarly represented **[Fig. S3.5C]**, we did find that YF and KO T_{eff} were modestly, but significantly, enriched in VAT, at a ~2:1 ratio compared to WT T_{eff} with no difference in reconstitution of other tissues **[Fig. 3.9A]**. A higher frequency of YF and KO VAT-T_{eff} were $ST2^+$ within the same chimeras, with a reduction in CXCR3-expressing T_{eff} **[Fig. 3.9B]**. Functionally, YF and KO VAT-T_{eff} were comprised of fewer $IFN\gamma^+$ and $TNF\alpha^+$ and more $IL\text{-}10^+$ cells when stimulated *ex vivo* **[Fig. 3.9B]**, indicating that in addition to driving increased T_R abundance, the absence of ICOS signaling also promotes a regulatory phenotype in VAT-T_{eff}. Taken together, loss of ICOS signaling supports VAT-T_R, and to a lesser extent, T_{eff} accumulation and phenotype through cell-intrinsic mechanisms.

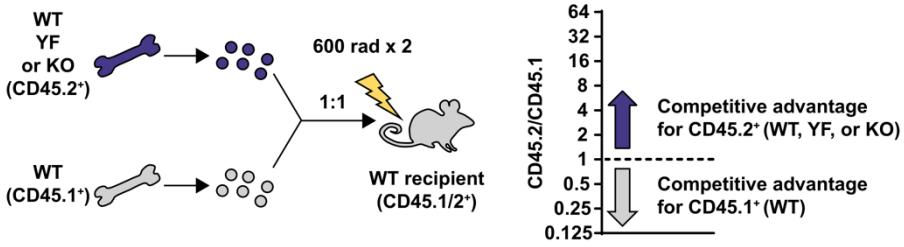

Figure 3.7: Schematic of mixed bone marrow chimera set-up. (Left) CD45.1$^+$ (WT) and CD45.2$^+$ (WT, YF, or KO) hematopoietic cells were transferred at a 1:1 ratio into lethally irradiated WT hosts. (Right) Representative graph depicting the method for visualizing donor cell reconstitution as a ratio of CD45.2$^+$:CD45.1$^+$ cells, with the dashed line indicating 1:1 reconstitution.

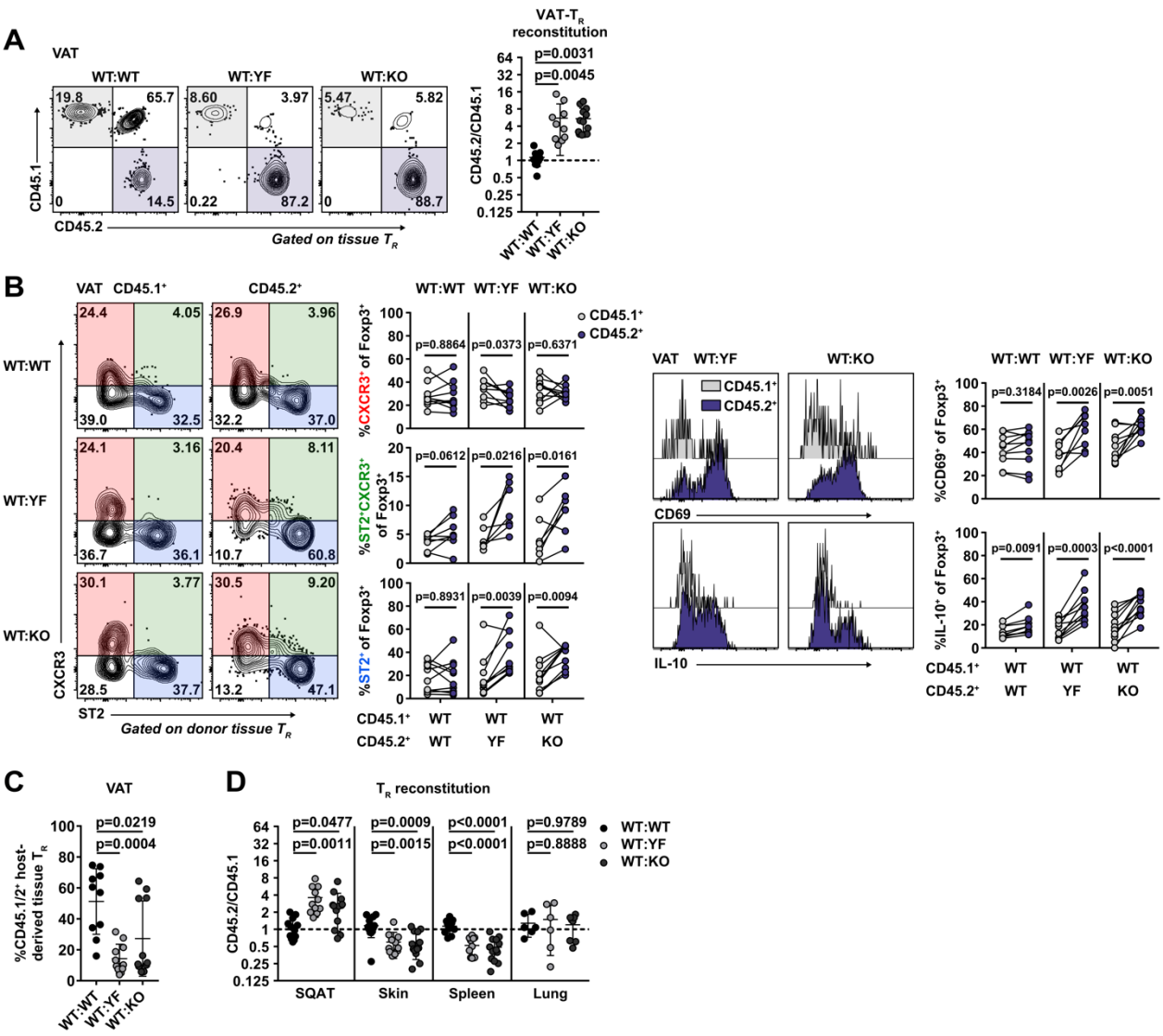

Figure 3.8: Cell-intrinsic ICOS signaling limits T_R abundance and phenotype specifically in VAT. (A) Representative gating of CD45.1 vs. CD45.2 expression in chimeric mice on tissue-localized T_R in VAT and graphical analysis of donor T_R reconstitution in VAT. **(B)** (Left) Representative gating on CXCR3- and ST2-expressing CD45.1$^+$ and CD45.2$^+$ donor VAT-T_R in chimeric mice. Line connects points indicating CD45.1$^+$ and CD45.2$^+$ cells within the same chimeric mouse. (Right) Histogram and graphical summary of donor VAT-T_R expression of CD69. Histogram and graphical summary of donor VAT-T_R expression of IL-10 after 4hr PMA/I+monensin stimulation *ex vivo*. **(C)** Frequency of endogenous CD45.1/2$^+$ VAT-T_R in chimeric mice. **(D)** Reconstitution of donor T_R in the indicated tissues. Flow cytometry plots are representative of data of 3 independent mixed bone marrow chimera experiments. Graphical data are compiled from 3 independent experiments with *n* = 3-5 mice per group per experiment. Statistical significance for cell population reconstitution was determined using one-way ANOVA with Tukey's post-test for each tissue analyzed. Data are presented as mean values ± SD. A two-tailed, paired Student's *t* test was used to assess statistical significance when comparing expression in donor cells within the same chimeric mouse.

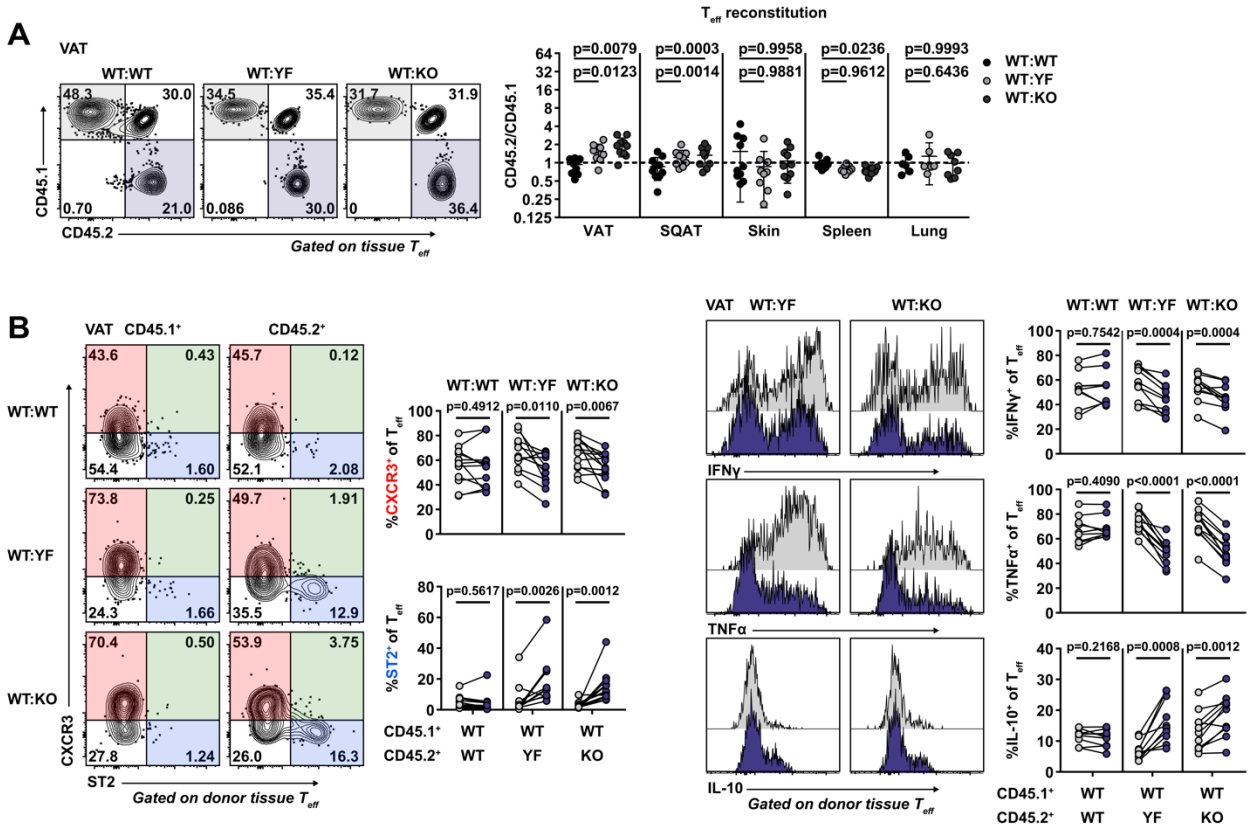

Figure 3.9: Cell-intrinsic ICOS signaling drives an anti-inflammatory T_{eff} phenotype in VAT. (A) Summary of donor T_{eff} reconstitution in the indicated tissues. **(B)** (Left) CXCR3 and ST2 expression by gated VAT-T_{eff}. (Right) Histograms and summary of donor VAT-T_{eff} expression of IFNγ, TNFα, and IL-10 after 4hr PMA/I+monensin stimulation *ex vivo*. Flow cytometry plots are representative of data of 3 independent mixed bone marrow chimera experiments. Graphical data are compiled from 3 independent experiments with *n* = 3-5 mice per group per experiment. Statistical significance for cell population reconstitution was determined using one-way ANOVA with Tukey's post-test for each tissue analyzed. Data are presented as mean values ± SD. A two-tailed, paired Student's *t* test was used to assess statistical significance when comparing expression in donor cells within the same chimeric mouse.

ICOS signaling impacts expression of homing receptors in T_R that allow access to VAT

The increased abundance of VAT-T_R from YF and KO mice could be the result of three non-mutually exclusive processes: increased proliferation; increased survival; or increased migration to the VAT. The proliferation marker Ki67 was generally expressed by ~10-20% of VAT-T_R, and we found no significant difference in the frequency of Ki67$^+$ VAT-T_R between WT, YF, and KO mice **[Fig. 3.10A]**. Similarly, WT, YF, and KO VAT-T_R expressed similar levels of the pro-survival protein Bcl2 **[Fig. 3.10B]**, and together these results suggest that differences in cellular turnover are not responsible for the accumulation of YF and KO T_R seen in VAT.

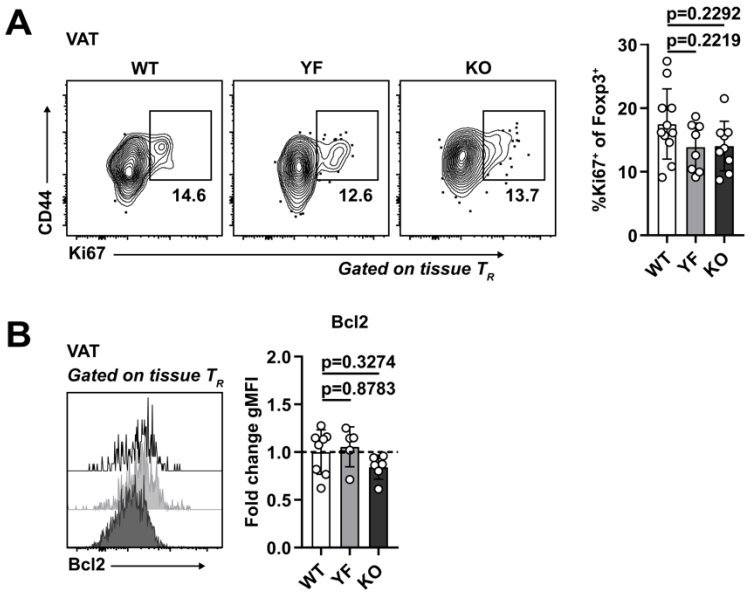

Figure 3.10: Increased abundance of YF and KO VAT-T_R is not due to enhanced cellular turnover or survival. (A, B) Ki67 **(A)** and Bcl2 expression **(B)** in tissue-localized VAT-T_R as measured by flow cytometry directly *ex vivo*. Bcl2 geometric MFI was calculated as fold change compared to average expression in WT T_R for each individual experiment. Flow cytometry plots are representative of data from 2 or more independent experiments. Graphical data are compiled from 2 or more independent experiments using mice aged 8-16 weeks, with *n* = 2-5 mice per group per experiment. Statistical significance was determined using one-way ANOVA with Tukey's post-test. All data are presented as mean values ± SD.

In both intact and mixed bone marrow chimeric mice, YF and KO splenic T_R contained a small but significantly increased population of $ST2^+$ T_R **[Fig. 3.11A, B]**, a subset of T_R that is both transcriptionally and epigenetically poised to take up residence in peripheral tissues (Delacher et al., 2017; Delacher et al., 2020). Given this, we hypothesized that superior migration and accumulation could account for the increased frequency of VAT-T_R in YF and KO mice. Although CCR2 facilitates recruitment of T_R to VAT (Vasanthakumar et al., 2020), we detected no difference in CCR2 expression among genotypes, and a modest decrease in $CCR2^+$ T_R in KO spleens **[Fig. S3.6A]**, arguing against enhanced CCR2-mediated recruitment of YF and KO T_R to VAT.

Previous studies identified both an open chromatin landscape around the *Ccr3* locus as well as high transcript levels in VAT-T_R (Cipolletta et al., 2012; Li et al., 2018). The frequency of CCR3-expressing splenic T_R was slightly elevated in both young (≤8 weeks) and older (>8 weeks) YF and KO mice **[Fig. S3.6B]**, indicating the presence of a T_R population primed for both potential early seeding and continuous repopulation of peripheral tissues. In line with this, YF and KO VAT contained more $CCR3^+$ T_R compared to WT mice and this population increased with age **[Fig. 3.12A]**. In mixed bone marrow chimeras, a significantly greater frequency of YF and KO donor T_R were $CCR3^+$ in spleen and VAT **[Fig. S3.6C]**. Additionally, YF and KO VAT contained a unique population of T_R that expressed CCR3 alone, while WT VAT-T_R expressing CCR3 were also positive for CCR2 **[Fig. 3.12B]**. CCR3 expression was unique to VAT-T_R, unlike CCR2, which we found to be also highly expressed on VAT-T_{eff} **[Fig. 3.12A, Fig. S3.6A]**. Additionally, the accumulation of $CCR3^+$ T_R was unique to VAT, as we detected very little CCR3 expression in skin, lungs, and large intestine T_R and no differences across genotypes **[Fig. S3.6D, E].** Within the VAT, we detected substantial expression of the CCR3 ligands *Ccl11* and *Ccl24* with no differences detected either by age or genotype and little expression of *Ccl5*, *Ccl7*, and *Ccl26* **[Fig. 3.12C]**.

We next assessed whether ICOS signaling could directly impact expression of CCR3 on T_R. WT, YF, and KO VAT-$CD4^+$ cells were cultured with αCD3/αCD28 and IL-2 in the presence or absence of an agonistic αICOS antibody **[Fig. 3.13A]**. After 48 hr in culture, T_R frequency remained unchanged in both groups. However, the frequency of $CCR3^+$ T_R in WT cultures significantly decreased after 2 days with addition of an ICOS agonist, whereas no changes were observed in YF or KO cultures, indicating that ICOS-dependent PI3K signaling can directly antagonize CCR3 expression in T_R **[Fig. 3.13B]**.

To address the impact of CCR3 signaling on continuous T_R seeding of VAT *in vivo*, we administered blocking antibodies to the CCR3 ligands CCL11 and CCL24 to 8-10 week old WT and YF mice. Blockade of CCL11/24 for ~2 weeks resulted in a modest although not statistically significant decrease in the frequency of VAT-T_R specifically in YF mice, with no differences in T_R abundance in spleen or lungs between treated and untreated mice **[Fig. 3.14A]**. We additionally noted a slight reduction in VAT-eosinophils in YF mice treated with αCCL11/24 **[Fig. S3.6F]**. Together, these results suggest a potential mechanism by which loss of ICOS-dependent PI3K signaling can drive increased recruitment of T_R to VAT by CCR3-CCL11/24 interactions.

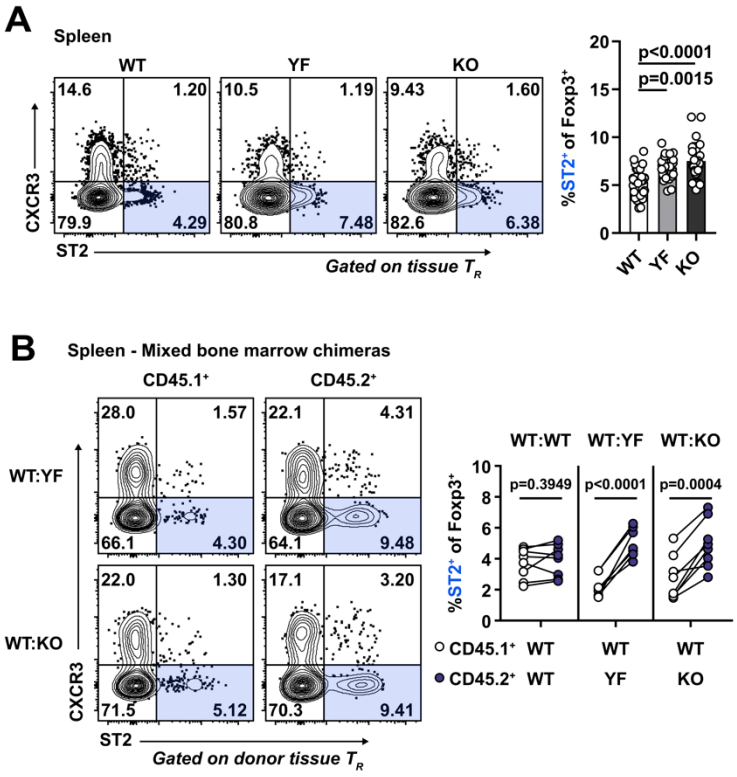

Figure 3.11: ST2-expressing tissue precursor T_R are enriched in the spleens of YF and KO mice. (A) ST2 expression in splenic T_R in mice aged 8-16 weeks. **(B)** ST2 expression in CD45.1$^+$ and CD45.2$^+$ donor splenic T_R in WT:YF and WT:KO chimeric mice. Line in graph connects CD45.1$^+$ and CD45.2$^+$ donor splenic T_R within the same chimera. Flow cytometry plots are representative of data from 2 or more independent experiments. Graphical data are compiled from 2 or more independent experiments with *n* = 3-4 per group per experiment. Statistical significance was determined using one-way ANOVA with Tukey's post-test **(A)** or two-tailed, paired Student's *t* test for expression in donor cells within the same chimeric mouse **(B)**. All data are presented as mean values ± SD.

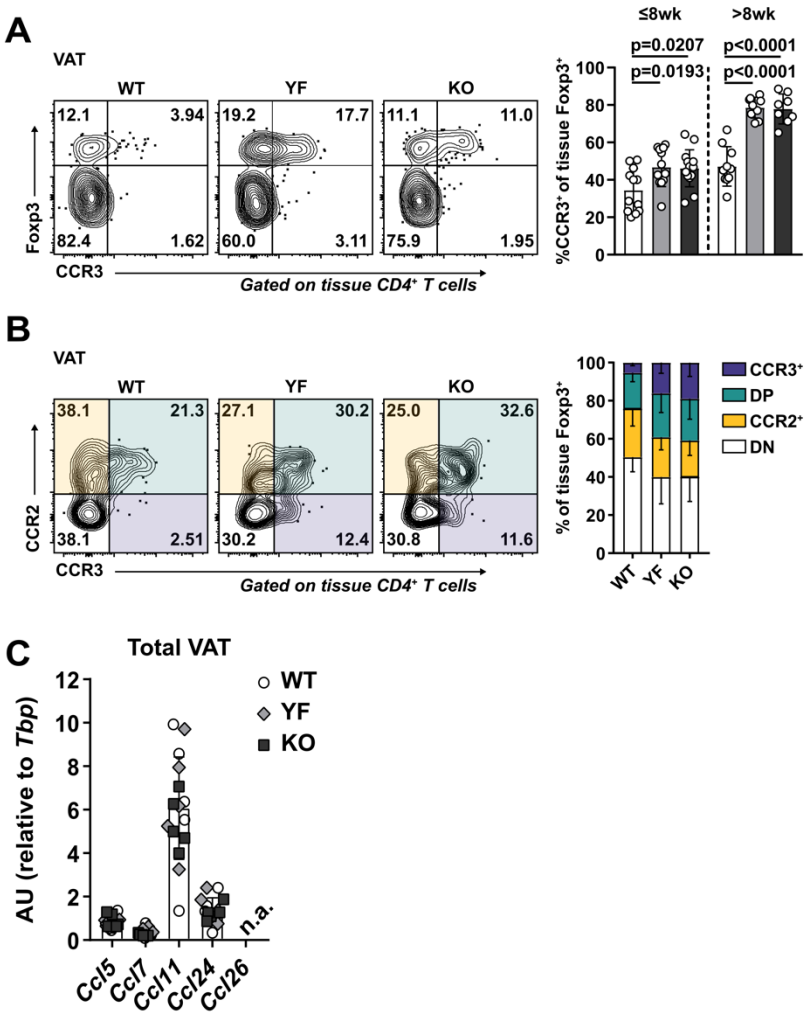

Figure 3.12: CCR3-expressing T_R accumulate in YF and KO VAT with age. (A) Expression of CCR3 in VAT-T_R in mice ≤8 wk and >8 wk of age. **(B)** Expression of CCR2 and CCR3 by VAT-T_R. **(C)** Expression of indicated CCR3 ligands in total VAT normalized to *Tbp* as measured by qPCR. Flow cytometry plots are representative of data from 2 or more independent experiments. Graphical data are compiled from 2 or more independent experiments with n = 3-4 per group per experiment. Statistical significance was determined using one-way ANOVA with Tukey's post-test. All data are presented as mean values ± SD.

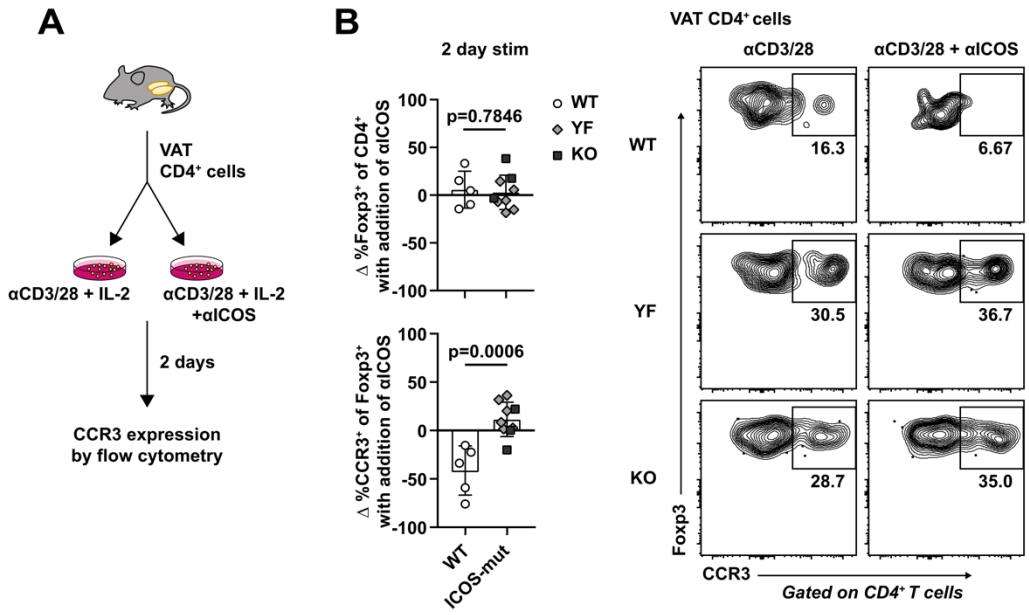

Figure 3.13: ICOS signaling antagonizes expression of CCR3. (A) Schematic of *in vitro* culture experiments examining the impact of ICOS signaling on CCR3 expression. **(B)** (Left) Graphs indicating fold change in T_R frequency of $CD4^+$ cells (top) and $\%CCR3^+$ of T_R (bottom) between individual culture samples stimulated with or without αICOS for 2 d. (Right) Representative flow cytometry plots with frequency of $CCR3^+$ T_R after 2 d in specified culture conditions. Flow cytometry plots are representative of data from 2 or more independent experiments. Graphical data are compiled from 2 or more independent experiments with *n* = 3-4 per group per experiment. Statistical significance was determined using a two-tailed Student's *t* test. All data are presented as mean values ± SD.

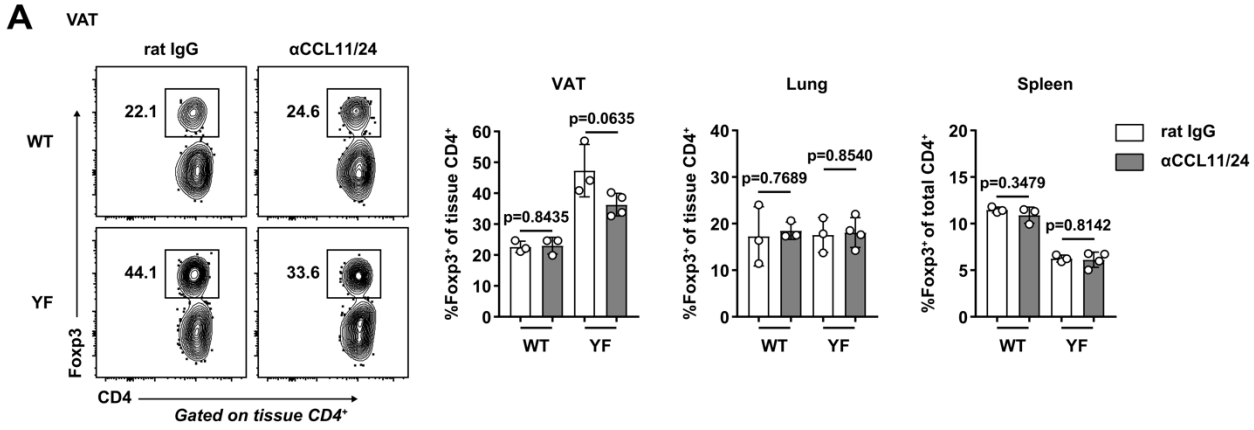

Figure 3.14: 2-week *in vivo* blockade of CCL11/24 results in a modest reduction of T_R in YF VAT. Groups of WT and YF mice were treated intraperitoneally with blocking antibodies against CCL11 and CCL24 every 5 days for 2 wk. **(A)** (Left) Representative flow cytometry plots indicating VAT-T_R frequency with or without CCL11/24 blockade. Graphs summarize T_R frequencies in indicated tissues after 2 wk. Data in **(A)** are from 1 experiment with *n* = 3-4 mice per group. Statistical significance was determined a two-tailed Student's *t* test. Data are presented as mean values ± SD.

Discussion

We have identified surprising tissue-specific effects of ICOS signaling on T_R abundance and phenotype. Although there was a significant loss of $CD44^+$ eT_R in the spleen, pLN, skin, and lungs of YF and KO mice compared to WT, we unexpectedly observed a substantial increase in T_R abundance in VAT. T_R frequency and phenotype were similar in YF and KO mice, including comparably altered readouts of PI3K signaling, suggesting that ICOS primarily impacts T_R abundance and homeostasis via PI3K-dependent mechanisms.

In addition to supporting VAT-T_R abundance, loss of ICOS signaling promoted a highly suppressive VAT-T_R phenotype, including an increased proportion of T_R expressing KLRG1, CD69, and IL-10. *In vitro*, addition of ICOS stimulation augments IL-10 production in $CD4^+$ T cells while loss of ICOS signaling *in vivo* results in reduced T_R abundance and IL-10 expression in models of autoimmunity, allergy, and infection (Busse et al., 2012; Hutloff et al., 1999; Kohyama et al., 2004; Kornete et al., 2012; Landuyt et al., 2019; Redpath et al., 2013). Although ICOS expression is associated with IL-10-producing T_R, ICOS signaling does not appear to be intrinsically required for IL-10 production. $CD4^+$ T cells from KO mice are capable of producing WT levels of IL-10 *in vitro*, and interestingly, appear to produce more IL-10 than WT counterparts under T_H2-polarizing conditions (Dong et al., 2001). Furthermore, recent studies assessing T_R in the brain during chronic *Toxoplasma gondii* infection and lamina propria T_R at baseline report no changes in IL-10 production in the presence or absence of ICOS signaling (Landuyt et al., 2019; O'Brien et al., 2019). Therefore, the reduction in IL-10^+ T_R with ICOS blockade observed in specific *in vivo* models is likely due to insufficient activation or access to specific environmental cues within tissues rather than an inherent requirement for ICOS signaling to drive IL-10 production.

VAT is a complex tissue, consisting of triglyceride-containing adipocytes and a variety of immune cells which function to maintain metabolic homeostasis. In YF and KO mice, other immune cells in addition to T_R showed evidence of an anti-inflammatory phenotype. Although

ATM and VAT-ILC2 abundance was similar across genotypes at baseline, eosinophil frequency was significantly elevated in YF and KO VAT. In YF and KO mice, VAT-T_{eff} were skewed toward a T_H2 phenotype in a cell-intrinsic manner, with an increased frequency of ST2-expressing and IL-10-producing cells. Therefore, in addition to promoting an anti-inflammatory state by sustaining VAT-T_R, global loss of ICOS signaling supports the abundance and phenotype of other anti-inflammatory adipose-resident immune cells. These combined changes in cellular composition in VAT in the absence of ICOS signaling were maintained in the setting of long-term HFD, and rendered YF and KO mice more resistant to HFD-induced loss of insulin sensitivity.

YF and KO donor T_R preferentially repopulated VAT in mixed bone marrow chimeras, and were able to outcompete both donor and endogenous WT T_R. ST2 is expressed on a large fraction of VAT-T_R (Vasanthakumar et al., 2015), and although we didn't note any differences in the frequency of ST2-expressing VAT-T_R in intact mice, YF and KO VAT-T_R in mixed bone marrow chimeras were comprised of significantly more $ST2^+$ cells compared to WT donor T_R, suggesting that the competitive advantage of YF and KO donor T_R in chimeric VAT is in part due to an enhanced ability to access available IL-33 through increased ST2 expression. The transcriptional regulators BATF and IRF4 cooperate to induce expression of ST2 in T_R, possibly downstream of TCR signals as well as through IL-33 signaling itself (Vasanthakumar et al., 2015). Additionally, IL-2 can work synergistically with IL-33 to upregulate ST2 and specifically expand $ST2^+$ T_R (Guo et al., 2009; Matta et al., 2014). T_R are unable to produce IL-2 themselves due to Foxp3-mediated transcriptional repression at the *Il2* locus (Wu et al., 2006; Ono et al., 2007) and therefore are dependent on paracrine sources of IL-2 produced by, for example, autoreactive T_{eff} (Setoguchi et al., 2005; Stolley and Campbell, 2016). However, KO T_{eff} are defective in production of IL-2 compared to T_{eff} from WT mice (Dong et al., 2001). The absence of an enriched population of ST2-expressing YF and KO VAT-T_R at baseline may be explained

by this lack of IL-2, which is rescued in the presence of WT IL-2 producing cells in mixed bone marrow chimeras.

Seemingly contradictory to our results, Molofsky *et al*. have argued that IL-33 signaling on T_R in VAT is mediated through ICOS/ICOSL interactions with ILC2s and that absence of this interaction results in loss of VAT-T_R (Molofsky et al., 2015). In their system, blockade of ICOS signaling was assessed in *Icosl*$^{-/-}$ mice, where cells are sufficient in ICOS expression though unable to interact with ligand. Consistent with their data in *Icosl*$^{-/-}$ mice, we did not observe any differences in ILC2 frequency or number in VAT of *Icos*$^{-/-}$ mice. However, given that ILC2s express both ICOS and ICOSL, loss of one versus the other could differentially impact ILC2 function, resulting in unique cell extrinsic impacts on T_R. Additionally, recent work investigating the molecular cues downstream of ICOS signaling revealed ligand-independent, constitutive signaling through PI3K-dependent pathways which relies on p85 association with the ICOS cytoplasmic YMFM motif and interactions between the ICOS transmembrane domain and the tyrosine kinase Lck (Feito et al., 2003; Wan et al., 2020). Thus the reported differences observed in our study and Molofsky's may be the result of low level, cell-intrinsic PI3K activation in ICOS-expressing T_R from *Icosl*$^{-/-}$ mice.

Although CCR2 plays an important role in recruitment of T_R to VAT, we did not detect any differences in CCR2 expression in the absence of ICOS signaling. We did, however, observe a significantly increased frequency of CCR3$^+$ T_R in the spleen and VAT of YF and KO mice, which was due to cell-intrinsic loss of ICOS signaling and was enhanced with age. CCR3 is primarily associated with type-2 responses (Danilova et al., 2015; Francis et al., 2007; Humbles et al., 2002; Ma et al., 2002; Nagakubo et al., 2016), and lean, metabolically healthy VAT is maintained in an anti-inflammatory state by the presence of T_H2-associated cells. *In vivo* blockade of CCL11/24 resulted in a modest reduction of T_R in YF VAT with no changes in other tissues analyzed. Parabiosis experiments demonstrate recruitment of circulating parabiont-derived T_R to VAT after months of shared circulation (Kolodin et al., 2015; Vasanthakumar et al.,

2020), indicating that continual, low-level recruitment of T_R to VAT occurs throughout adulthood. Thus, longer-term antibody-mediated blockade may be necessary to observe significant effects on T_R accumulation in our system. Additionally, addressing the role of CCR3 is further complicated by its promiscuity, and whether compensation through other ligands occurs during *in vivo* blockade is unknown. *In vitro*, we found that ICOS stimulation resulted in reduced CCR3 expression in WT VAT-T_R with no changes in YF or KO cultures, suggesting that ICOS-dependent PI3K signaling can inhibit expression of CCR3. Regulation of CCR3 expression in T cells has not been extensively characterized, however there is evidence that the transcription factor GATA3 is able to bind to a regulatory region in the *Ccr3* locus (Kong et al., 2013). Nonlymphoid T_R, including VAT-T_R, express high levels of GATA3 (Cipolletta et al., 2012; Delacher et al., 2020). However, whether ICOS signaling impacts CCR3 expression by modulating GATA3 expression or activity, and whether GATA3 is involved in controlling CCR3 expression in T_R, remains to be explored.

Most studies assessing VAT-T_R biology utilize older male mice due to an increased abundance of canonical VAT-T_R with age (Cipolletta et al., 2015). However, various mediators of tissue inflammation, including IL-6, TNFα, and IL1β, are upregulated in the VAT of aged male mice (older than 24 weeks) (Wu et al., 2007). In our studies, we observed consistent accumulation of VAT-T_R from 5 weeks on in all three genotypes, which was correlated with an increase in $CCR3^+$ T_R up to ~20 weeks of age. CCR2 regulates T cell access to sites of inflammation (Lee et al., 2007), and studies assessing the contribution of CCR2 on T_R migration to VAT utilize mice aged 25-30 weeks, when measures of VAT inflammation are increasing. CCR2 and CCR3 likely both have important roles for promoting recruitment of T_R to VAT, however it will be necessary to evaluate whether these receptors are utilized differentially based on age, sex, and inflammation. For example, CCR3 may be important for early seeding and continuous recruitment of T_R to VAT in comparatively younger mice when VAT inflammation is

more minimal. With increasing age and inflammation (particularly in male mice), a switch to CCL2-CCR2 mediated migration may dominate.

Our work identifies new mechanisms that regulate VAT-T_R biology. Here we describe a surprising, antagonistic role for ICOS-dependent PI3K signaling in the accumulation, prototypical phenotype, and function of T_R specifically in VAT. We suggest that absence of ICOS signaling supports enhanced recruitment of T_R to VAT via increased expression of CCR3. Further studies will be needed to identify the molecular mechanisms by which ICOS inhibits the VAT-T_R phenotype and CCR3 expression. Our work highlights the complexity of tissue-specific T_R development and accumulation and the importance of considering how signals from the immune environment elicit both cell- and tissue-specific effects.

Supplemental Figures

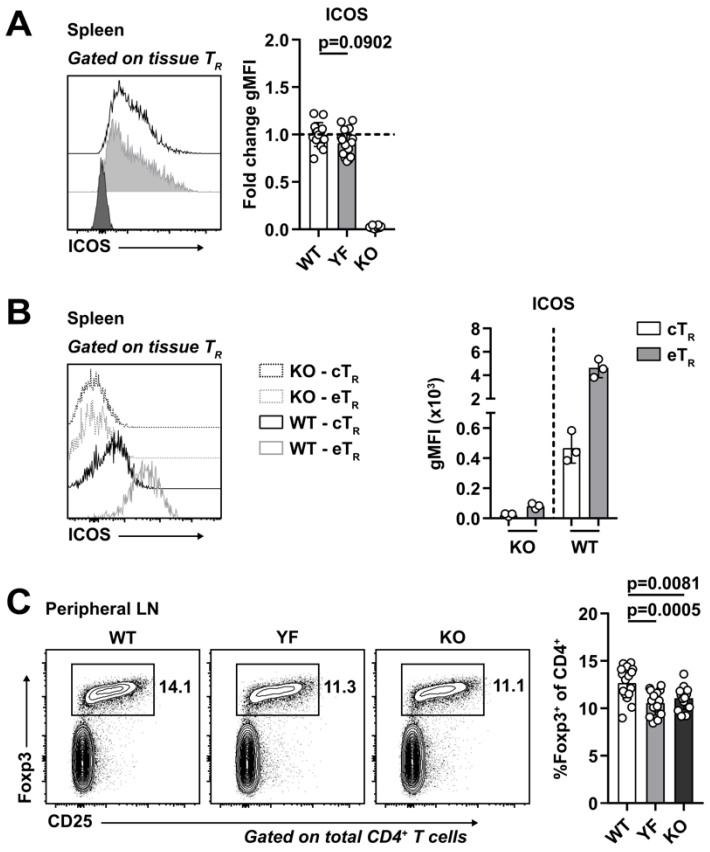

Figure S3.1 (goes with Fig. 3.1): Despite normal surface expression of ICOS, YF mice phenocopy KO with equivalent loss of lymphoid T_R. (A) ICOS expression on gated WT, YF, and KO splenic T_R. Fold change of ICOS geometric MFI is compared to average expression in WT T_R for each individual experiment. **(B)** ICOS expression on gated splenic KO and WT $CD44^{lo}CD62L^{hi}$ cT_R and $CD44^{hi}CD62L^{lo}$ eT_R as measured by flow cytometry. **(C)** T_R frequencies of total $CD4^+$ T cells in peripheral lymph nodes. Flow cytometry plots are representative of data from 3 or more independent experiments. Graphical data are compiled from 3 or more independent experiments with *n* = 3-5 mice per group per experiment. Statistical significance was determined using one-way ANOVA with Tukey's post-test. All data are presented as mean values ± SD.

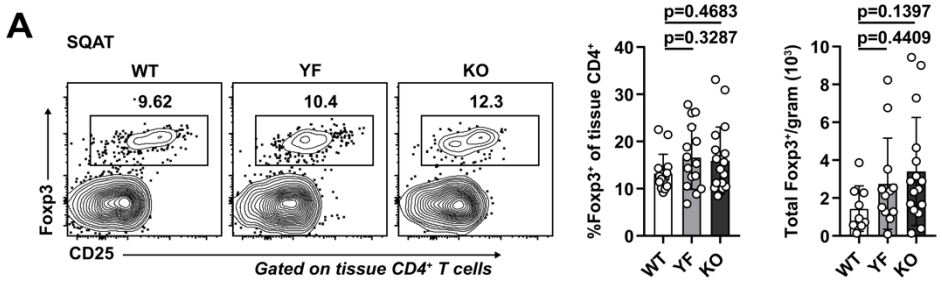

Figure S3.2 (goes with Fig. 3.3): YF and KO mice harbor normal frequencies of SQAT T_R. **(A)** Representative flow cytometry plots showing frequency of tissue-localized T_R in WT, YF, and KO inguinal SQAT. Compiled graphical data from mice aged 8-20 weeks with T_R frequency (left graph) and total T_R number (right graph). Statistical significance was determined using one-way ANOVA with Tukey's post-test with data presented as mean values ± SD.

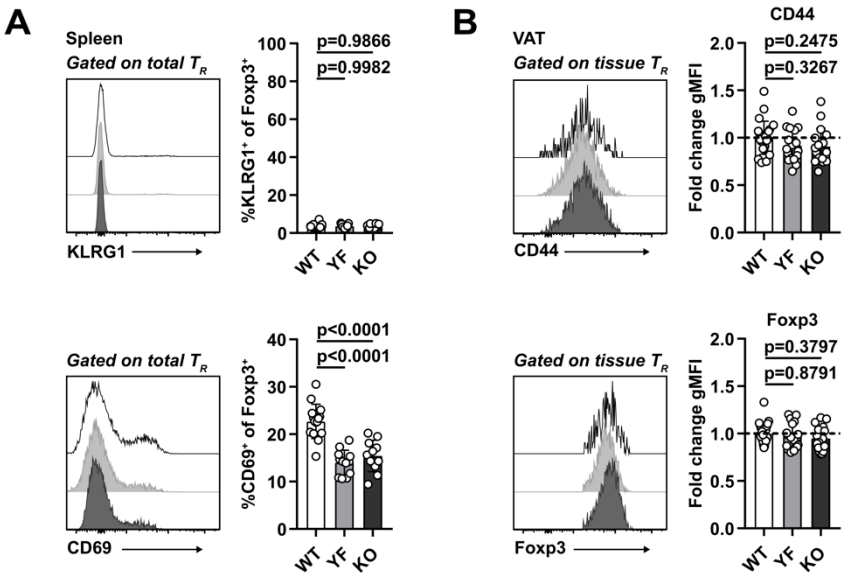

Figure S3.3 (goes with Fig. 3.4): Expression of activation markers on splenic and VAT-T_R. **(A)** KLRG1 (top) and CD69 (bottom) expression in gated WT, YF, and KO splenic T_R. **(B)** CD44 (top) and Foxp3 (bottom) expression in tissue-localized VAT-T_R. Geometric MFI was calculated as fold change compared to average expression in WT T_R for each individual experiment. Flow cytometry plots are representative of data from 3 or more independent experiments. Compiled graphical data are from 3 or more independent experiments with *n* = 3-5 mice per group per experiment. Statistical significance was determined using one-way ANOVA with Tukey's post-test. All data are presented as mean values ± SD.

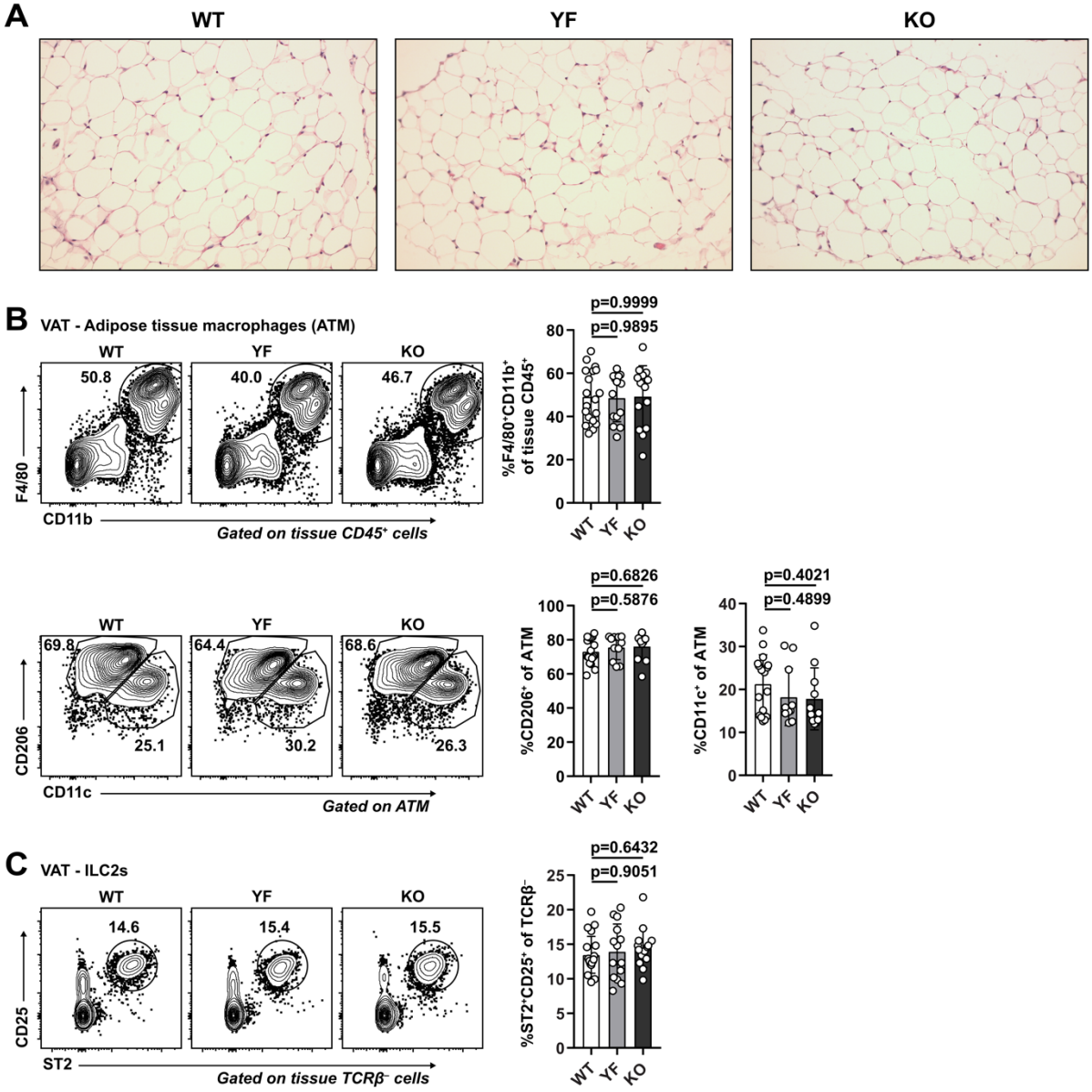

Figure S3.4 (goes with Fig. 3.5): Adipocyte, ATM, and ILC2 populations are unchanged in YF and KO VAT. (A) Hematoxylin and eosin (H&E) staining of VAT from 8 week old mice. Images acquired at 200X magnification. **(B)** Representative flow cytometry plots showing frequencies of tissue-localized ATM in WT, YF, and KO mice and summarized graphical data from mice aged 8-16 weeks (top). Representative gating of ATM on CD11c and CD206 to identify M1-like and M2-like macrophages, respectively, and compiled data from 8-16 week old mice (bottom). **(C)** Frequency of tissue-localized ILC2s in VAT as measured by flow cytometry. Graphical data are compiled from 2 or more independent experiments with *n* = 3-5 mice per group per experiment. Statistical significance was determined using one-way ANOVA with Tukey's post-test. All data are presented as mean values ± SD.

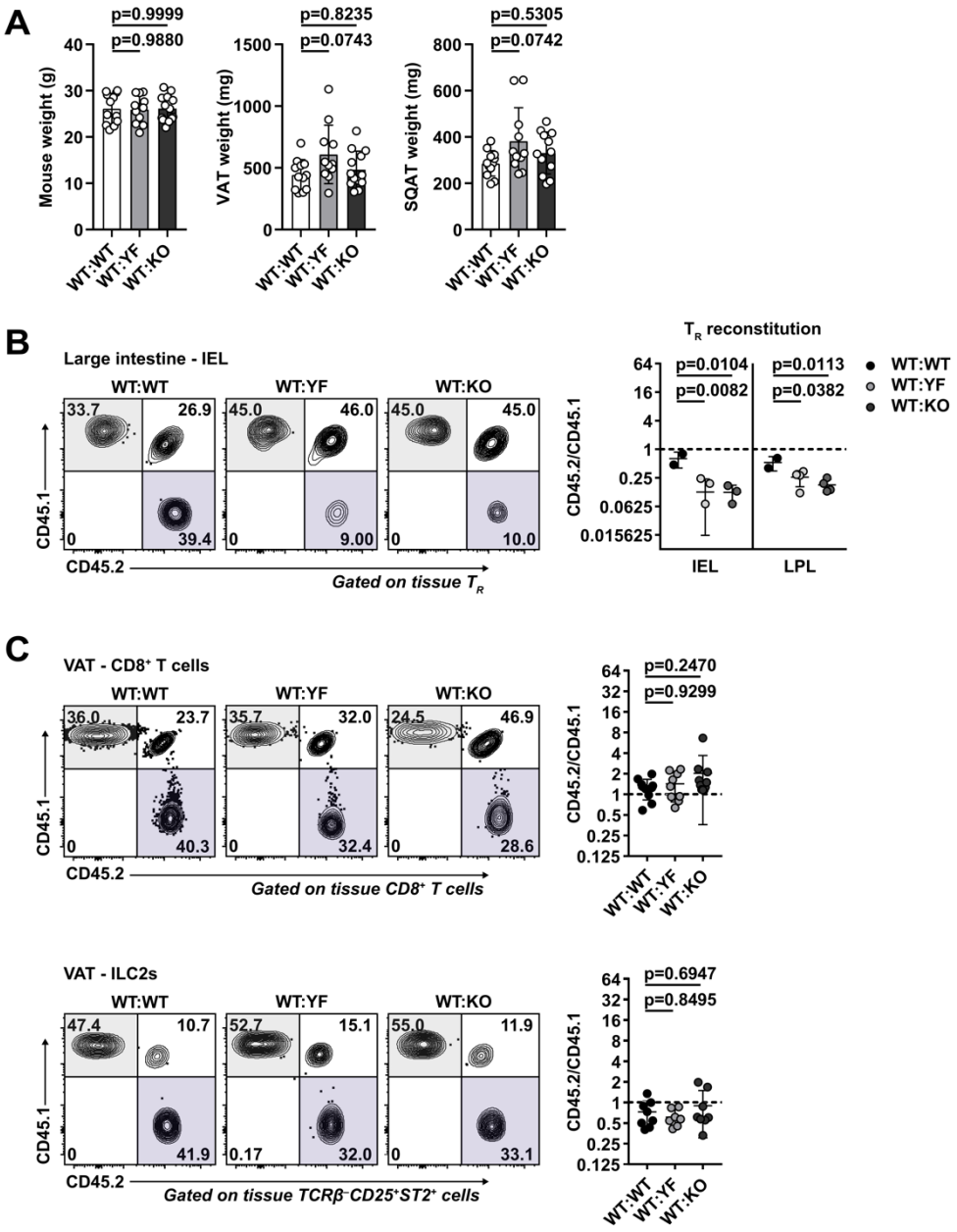

Figure S3.5 (goes with Fig. 3.8): Cell- and tissue-specific changes in reconstitution in ICOS mutant mixed bone marrow chimeras. (A) Summary of total mouse (left panel), VAT (middle panel), and SQAT (right panel) weights in mixed bone marrow chimeras. **(B)** Representative gating of CD45.1 vs. CD45.2 expression on tissue-restricted T_R in intraepithelial lymphocytes (IEL) from the large intestine (LI). Graphs summarize reconstitution of donor T_R of IEL and lamina propria lymphocytes (LPL) in the LI. **(C)** Representative gating of CD45.1 vs. CD45.2 expression in chimeric mice on total $CD8^+$ T cells (top) and ILC2s (bottom) in VAT. Graphs summarize reconstitution of donor $CD8^+$ T cells (top) and ILC2s (bottom) in VAT. Data are representative of 3 independent experiments with *n* = 3-5 mice per group. Statistical significance was determined using one-way ANOVA with Tukey's post-test for each individual tissue. All data are presented as mean values ± SD.

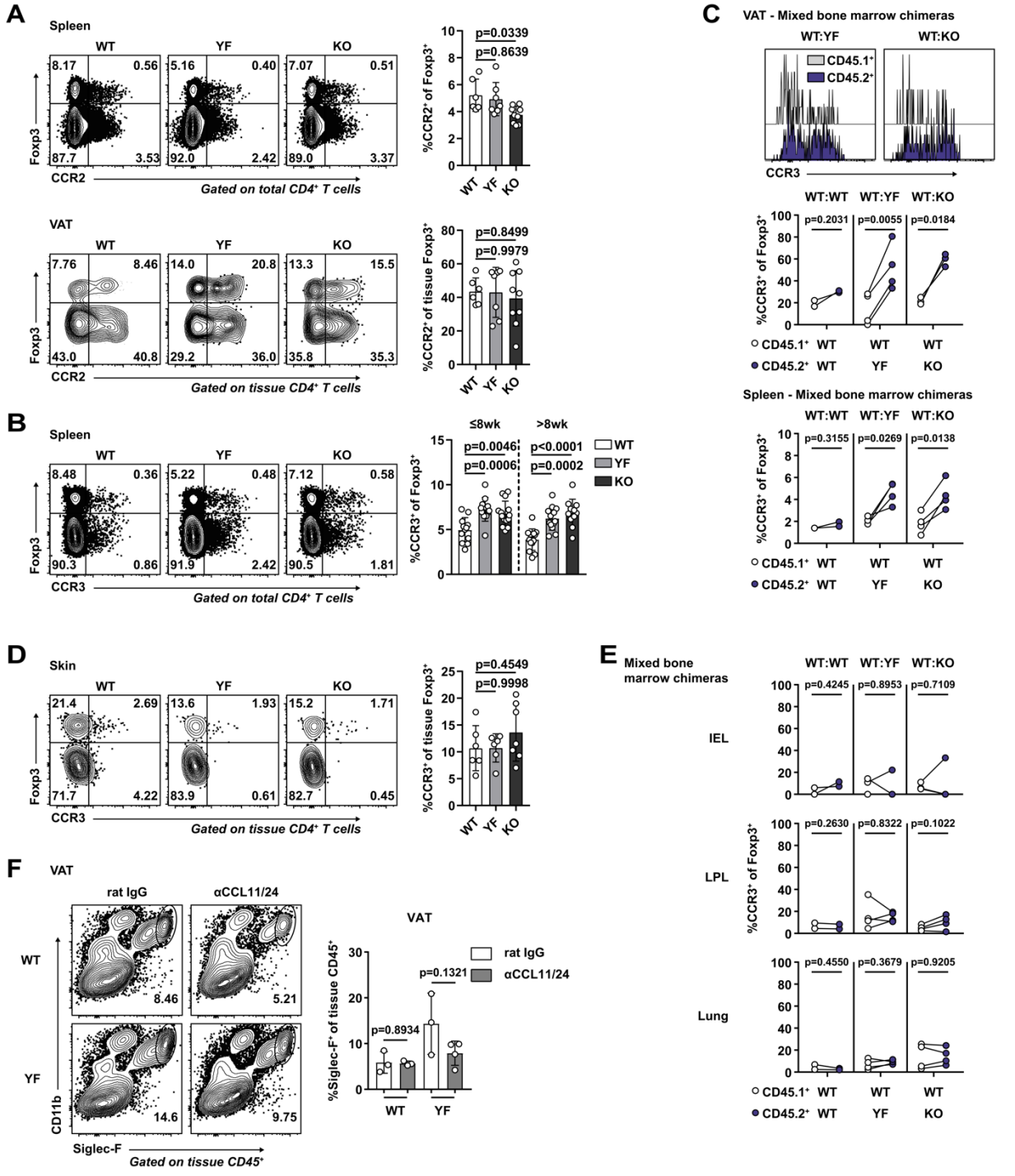
A
Spleen
WT
YF
KO
8.17
0.56
87.7
3.53
5.16
0.40
92.0
2.42
7.07
0.51
89.0
3.37
Foxp3
CCR2
Gated on total CD4+ T cells
p=0.0339
p=0.8639
%CCR2+ of Foxp3+
VAT
7.76
8.46
43.0
40.8
14.0
20.8
29.2
36.0
13.3
15.5
35.8
35.3
Gated on tissue CD4+ T cells
p=0.8499
p=0.9979
%CCR2+ of tissue Foxp3+
B
Spleen
8.48
0.36
90.3
0.86
5.22
0.48
91.9
2.42
7.12
0.58
90.5
1.81
CCR3
Gated on total CD4+ T cells
≤8wk
>8wk
p=0.0046
p=0.0006
p<0.0001
p=0.0002
%CCR3+ of Foxp3+
C
VAT - Mixed bone marrow chimeras
WT:YF
WT:KO
CD45.1+
CD45.2+
CCR3
WT:WT
WT:YF
WT:KO
p=0.2031
p=0.0055
p=0.0184
%CCR3+ of Foxp3+
CD45.1+ WT WT WT
CD45.2+ WT YF KO
Spleen - Mixed bone marrow chimeras
p=0.3155
p=0.0269
p=0.0138
D
Skin
21.4
2.69
71.7
4.22
13.6
1.93
83.9
0.61
15.2
1.71
82.7
0.45
Gated on tissue CD4+ T cells
p=0.4549
p=0.9998
%CCR3+ of tissue Foxp3+
E
Mixed bone marrow chimeras
IEL
LPL
Lung
p=0.4245
p=0.8953
p=0.7109
p=0.2630
p=0.8322
p=0.1022
p=0.4550
p=0.3679
p=0.9205
F
VAT
rat IgG
αCCL11/24
WT
YF
8.46
5.21
14.6
9.75
CD11b
Siglec-F
Gated on tissue CD45+
p=0.8934
p=0.1321
%Siglec-F+ of tissue CD45+

Figure S3.6 (goes with Fig. 3.12, 3.14): Increased accumulation of CCR3$^+$ T_R in the absence of ICOS signaling is specific to VAT. (A) CCR2 expression by splenic (top) and VAT-T_R (bottom) as measured by flow cytometry. **(B)** Expression of CCR3 in splenic T_R in mice ≤8 wk and >8 wk of age. **(C)** Expression of CCR3 by gated CD45.1$^+$ and CD45.2$^+$ donor VAT-T_R in chimeric mice. Graphs summarize CCR3 expression by donor T_R in VAT and spleen. Line connects points representing CD45.1$^+$ and CD45.2$^+$ cells within the same chimeric mouse. **(D)** CCR3 expression by tissue-localized skin T_R as measured by flow cytometry. **(E)** CCR3 expression by CD45.1$^+$ and CD45.2$^+$ donor T_R within the same chimeric mouse in indicated tissues. Line connects CD45.1$^+$ and CD45.2$^+$ cells within the same chimeric mouse. **(F)** Frequency of tissue-restricted VAT-eosinophils with and without *in vivo* CCL11/24 blockade as measured by flow cytometry (from one experiment with n = 3-4 mice per group). All other flow cytometry plots are representative of data from 3 independent experiments. Graphical data are compiled from 3 independent experiments with n = 3-4 mice per group per experiment. Statistical significance was determined using one-way ANOVA with Tukey's post-test **(A, B, D)**, two-tailed, paired Student's *t* test for expression in donor cells within the same chimeric mouse **(C, E)**, and two-tailed Student's *t* test **(F)**. All data are presented as mean values ± SD.

CHAPTER 4: ICOS signaling is required for T_R-mediated resolution of central nervous system autoimmune inflammation

Introduction

Multiple sclerosis (MS) is an inflammatory autoimmune disease which results in the demyelination of neurons in the CNS. It is characterized by the infiltration of inflammatory cells to the CNS, axonal damage, and formation of demyelinated lesions (Dendrou et al., 2015). Experimental autoimmune encephalomyelitis (EAE) is an animal model of CNS autoimmune inflammation and recapitulates many of the clinical and immunopathological features of MS. Induced EAE is achieved either through injection of defined myelin antigens emulsified in complete Freund's adjuvant (CFA) or via transfer of activated myelin-reactive $CD4^+$ T_{eff} followed by permeabilization of the blood-brain barrier (Stromnes and Goverman, 2006a & 2006b). Disease is monophasic and characterized by progressive ataxia and/or ascending paralysis, followed by spontaneous partial recovery. Work has demonstrated pathogenic roles for both T_H1 and T_H17 T_{eff} in these models (Jäger et al., 2009; Fletcher et al., 2010).

Many studies have highlighted a role for T_R in controlling EAE disease progression through suppression of T_{eff}. Indeed, IL-10-producing T_R accumulate in the CNS, peaking at a time correlating with clinical recovery (McGeachy et al., 2005). It is during this recovery phase that CNS-derived T_{eff} become susceptible to T_R-mediated suppression (Korn et al., 2007). Additionally, recruitment of host-derived T_R correlates with recovery in a transfer model of EAE (O'Connor et al., 2007). This underscores a critical role for *in situ* expansion of T_R and suppressive response at effector sites, independent of the T cell priming in lymph nodes and residual antigen deposition that exists in myelin antigen immunization models of EAE.

How ICOS expression impacts T_R maintenance and function in the context of CNS autoimmune inflammation is unknown. Using an induced model of EAE by way of injecting

myelin oligodendrocyte glycoprotein peptide (MOG_{35-55}) into mice on a C57BL/6 background, two studies revealed exacerbated disease in mice deficient in ICOS expression (Dong et al., 2001; Galicia et al., 2009). Enhanced clinical signs were correlated with increased cellular infiltration into the brain and spinal cord and increased *Il17*, *Il6*, and *Ifnγ* transcripts in whole CNS tissue. These results suggest a potential for reduced T_R abundance and/or function in the CNS in the absence of ICOS expression, however this was not addressed. If T_R responses are indeed altered in *Icos*$^{-/-}$ (KO) mice in the context of EAE, it remains to be determined whether insufficient control of T_{eff} takes place during the priming phase in lymphoid organs or within the CNS.

To address these questions, we utilized both immunization and T_{eff} transfer models of induced EAE to assess T_R contributions to disease progression in WT, *Icos*^{Y181F} (YF) and KO mice. Induction by MOG_{35-55} peptide immunization resulted in escalation of disease severity followed by partial recovery in WT mice. Clinical signs in YF and KO mice failed to improve, correlating with a reduction of activated, tissue-localized T_R in the brain. To address the role of host T_R activity specifically in the CNS independent of antigen-presentation and priming in lymphoid tissues, we transferred T_H1-polarized $CD4^+$ cells from 2D2 transgenic mice expressing a MOG_{35-55}-specific TCR (Bettelli et al., 2003) into intact hosts. YF and KO mice exhibited delayed onset of disease compared to WT, but rapidly progressed without improvement of clinical severity, while many WT mice began to recover. This was associated with a reduced ratio of host T_R to 2D2 T_{eff} in the brain and spinal cord of YF and KO mice. These preliminary data suggest that ICOS-dependent PI3K signaling is critical for T_R-mediated control of inflammation within the CNS.

Results

YF and KO mice fail to recover from myelin antigen-induced EAE, correlating with a reduction in activated T_R in the CNS

Subcutaneous immunization with MOG_{35-55} emulsified in CFA, followed by administration of pertussis toxin results in the development of EAE clinical signs starting between day 9 and 14. Classical EAE paralysis begins in the tail and moves caudal to rostral, with most severe disease resulting in forelimb paralysis and failure to thrive (Stromnes and Goverman, 2006a). Onset of disease signs was similar in WT, YF, and KO mice immunized with MOG_{35-55}, and animals reached the same average peak score. However, whereas severity of clinical signs peaked in WT mice and was followed by a recovery phase, both YF and KO mice were unable to resolve disease **[Fig. 4.1A]**. For this initial experiment, we let the disease course carry out for an extended period time. In general, comparisons of populations within the CNS of EAE animals is best achieved closer to peak of disease, when T_R accumulation is at its apex (McGeachy et al., 2005). Despite this caveat, we observed some interesting differences between genotypes that bear further investigation.

We confirmed a modest decrease in the frequency of tissue T_R in the brain with increasing disease severity across genotypes, with no discernable differences in the spinal cord **[Fig. 4.1B]**. Significant differences in T_R abundance between genotypes were not detected at this late timepoint. However, T_R within the brain of YF and KO mice were skewed toward a less activated phenotype, with reduced CD44 expression, a decrease in T_R expressing CD69, and a greater proportion of $CD45RB^+$ T_R **[Fig. 4.1C]**. These changes suggest that YF and KO T_R that accumulate in the CNS could be less suppressive, and decreased expression of CD69 could impact retention of these cells in effector sites. Additionally, we did not note any differences in the frequency of T_{eff} in the brain or spinal cord in WT, YF, and KO mice **[Fig. 4.1D]**. Expression of activation markers, including CD44 and CD69, were similar in T_{eff} across genotypes, suggesting that absence of ICOS signaling is not required for optimal priming of pathogenic

effectors in this model (data not shown). Together, impaired clinical recovery and altered T_R phenotype within the CNS in YF and KO mice suggests that ICOS signaling is important for T_R-mediated resolution of EAE.

Host T_R in mice lacking ICOS signaling are unable to control CNS disease promoted by transfer of encephalitogenic T_{eff}

Initiation of disease by MOG_{35-55} requires proper priming and effector activity of host T_{eff}. ICOS signaling did not appear to impact the ability of YF and KO T_{eff} to induce disease **[Fig. 4.1A]**. However, to better control initiation of disease, we turned to a transfer model of EAE whereby genetically identical, WT 2D2 encephalitogenic T cells are transferred into recipient mice, followed by permeabilization of the blood-brain barrier (Stromnes and Goverman, 2006b). *In vitro* culture of 2D2 lymphoid $CD4^+$ T cells in T_H1-polarizing conditions resulted in ~75-80% $IFN\gamma^+$ cells **[Fig. 4.2A]**. These polarized cells were injected into WT, YF, and KO mice to produce a similar clinical progression as myelin-antigen immunization. We observed a slight delay in onset of clinical signs in YF and KO mice compared to WT mice **[Fig. 4.2B]**. However, whereas disease in WT mice started to resolve at day 22, YF and KO mice continued to progress in clinical disease severity and many had to be sacrificed due to dramatic weight loss **[Fig. 4.2B]**. Though not statistically significant, enhanced disease in YF and KO mice was associated with a reduced abundance of T_R in the CNS and reciprocally more 2D2 T_{eff} **[Fig. 4.2C]**, therefore suggesting that defects in host T_R precipitate impaired recovery in the absence of ICOS signaling.

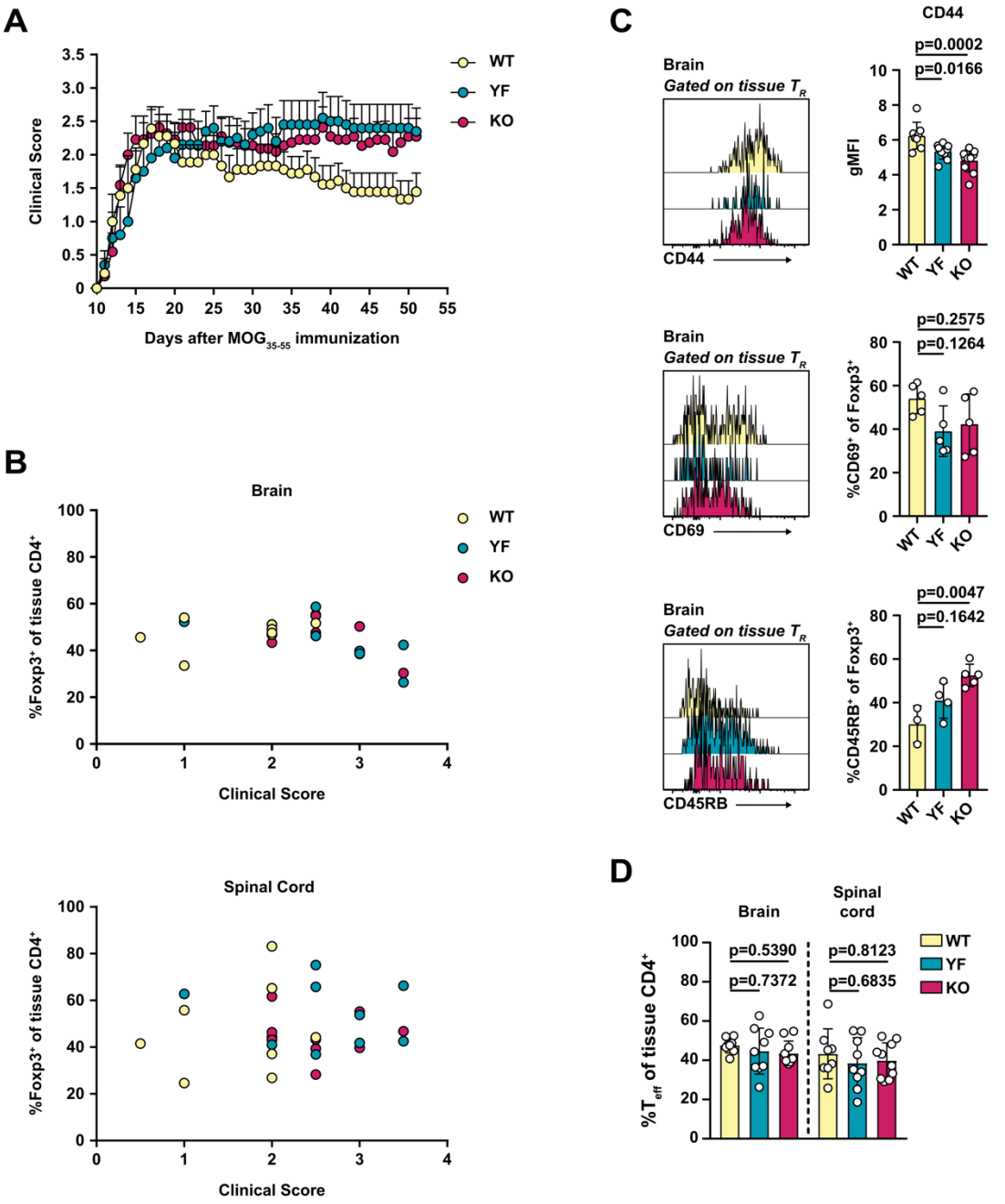

Figure 4.1: YF and KO mice fail to recover from MOG_{35-55}-induced EAE, correlating with reduced activation of T_R in the CNS. EAE was induced in WT (yellow), YF (teal), and KO (magenta) mice by immunization with MOG_{35-55} in CFA. **(A)** Mean clinical score for each group over time (*n* = 8-9, ±SEM). **(B)** T_R frequencies in brain (top) and spinal cord (bottom) at indicated clinical scores. Each point represents data from one mouse. **(C)** CNS mononuclear cells were collected at the end of the disease time course. Representative flow cytometry plots with expression of CD44, CD69, and CD45RB in tissue-localized brain T_R. **(D)** Frequency of CNS-infiltrating T_{eff} as measured by flow cytometry. Statistical significance was determined using one-way ANOVA with Tukey's post-test. Flow cytometry data are presented as mean values ± SD.

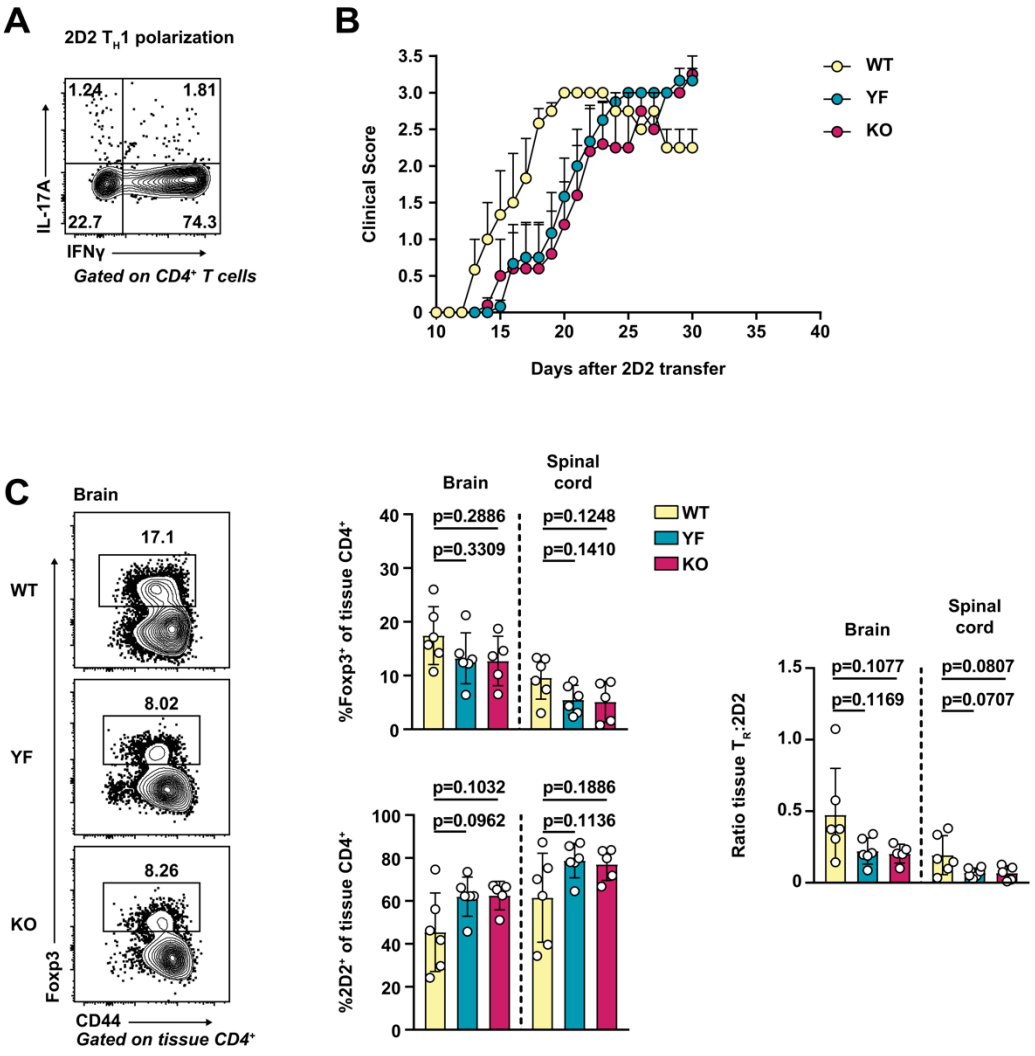

Figure 4.2: EAE by 2D2 transfer is exacerbated in the absence of ICOS signaling, corresponding with reduced CNS-localized T_R. EAE was induced in WT (yellow), YF (teal), and KO (magenta) mice by transfer of T_H1-polarizied 2D2 T_{eff}. **(A)** IFNγ and IL-17A production in 2D2 lymphoid CD4$^+$ T cells cultured in T_H1 polarizing conditions. Cells were stimulated for 4h with PMA/I+monensin and stained for intracellular cytokines for flow cytometry. **(B)** Mean clinical score for each group over time (n = 6, ±SEM). **(C)** CNS mononuclear cells were collected at the end of the disease time course. (Left) representative flow cytometry plots of tissue-localized T_R frequency in the brain. (Middle) summarized graphical data with frequencies of tissue-T_R and -2D2 T_{eff} in brain and spinal cord. (Right) ratio of tissue T_R frequency to 2D2 T_{eff} frequency in the CNS. Statistical significance was determined using one-way ANOVA with Tukey's post-test. Flow cytometry data are presented as mean values ± SD.

Discussion

Although these are preliminary studies, our results from both antigen-induced EAE and 2D2 transfer of disease point toward defects in T_R accumulation and/or function when ICOS signaling is not intact. We have two working models for CNS autoimmune inflammation which allow us to assess activity of T_R both during priming in lymph nodes and effector responses in the CNS. Because ICOS signaling can impact different T cell subsets, we were concerned that altered T_{eff} functions might drive T_R cell-extrinsic changes in disease course. However, YF and KO T_{eff} were capable of inducing disease in the MOG_{35-55} immunization model. Additionally, using a transfer model of disease, we were able to minimize possible differences in T_{eff} activation and differentiation by transferring genetically identical 2D2 disease-inducing cells.

Future studies are needed to understand the mechanisms behind enhanced disease severity in YF and KO mice. We allowed the disease to run its course through to recovery for these initial experiments. Thus the lack of significant differences we detected in CNS cell populations could be in part due to timing. Future studies will require extensive characterization of CNS-infiltrating cells along the disease curve in both T_H1- and T_H17-mediated disease, including at peak of disease when recruitment of T_R is maximized. Whether absence of ICOS signaling in T_R results in functional differences in EAE remains to be addressed. *Ex vivo* cytokine staining in both CNS-T_R and -T_{eff}, as well as *in vitro* suppression assays will shed light on this. Interestingly, we observed later onset of disease in YF and KO mice in the transfer mode of EAE, suggesting potential differences in suppression of circulating 2D2 cells prior to disease onset. Evaluating T_R abundance and suppressive capacity in lymphoid tissues during early priming will be necessary to establish contributions of ICOS signaling to T_R function in lymphoid and effectors sites.

CHAPTER 5: Closing remarks

Although ICOS is a marker associated with highly suppressive eT_R, the signaling pathways activated, and the impacts of this signaling, in T_R from different nonlymphoid tissues has not been well-characterized. We demonstrate that PI3K signaling activated downstream of ICOS exerts unique impacts on T_R maintenance and function in a tissue-dependent manner. ICOS-dependent PI3K signaling limited the accumulation, activated phenotype, and function of T_R in VAT. Conversely, preliminary work identified a critical role for ICOS signaling in the maintenance and function of T_R in the CNS in the context of autoimmune inflammation.

Future studies are needed to unravel the intricacies of how ICOS exerts such contrasting tissue-specific effects. VAT is a unique tissue in that it is maintained in an overwhelmingly type 2 immune environment in the healthy state. Eosinophils, anti-inflammatory macrophages, ILC2s, and T_H2 T_{eff} dominate the immune environment in VAT. T_R residing in VAT exhibit a T_H2-like phenotype, with high expression of ST2 and GATA3. This is in contrast to other tissues we assessed, like the brain and spinal cord during CNS inflammation, which is driven primarily by T_H1 or T_H17 inflammatory processes. Unlike barrier tissues such as skin, lung, and gut, VAT is not chronically challenged by pathogenic and/or commensal microbiota. Therefore, ICOS signaling may play divergent roles in maintaining T_R depending on the type of immune response elicited or whether inflammation is initiated by microbes or within a sterile environment.

Studies will continue to unveil the heterogeneity of T_R across and within different tissues and inflammatory settings down to a single-cell level. In addition to their classic immunosuppressive function, T_R are being recognized for their vital roles in tissue repair and regeneration and maintenance of organismal metabolism. With this growing diversity, it will become increasingly important to parse apart the environmental signals that support or restrict specific T_R populations in order to harness their therapeutic potential.

REFERENCES

Ahnstedt, H., M. Roy-O'Reilly, M. S. Spychala, A. S. Mobley, J. Bravo-Alegria, A. Chauhan, J. Aronowski, S. P. Marrelli, and L. D. McCullough. 2018. Sex differences in adipose tissue CD8+ T cells and regulatory T cells in middle-aged mice. *Front. Immunol.* 9:659.

Ali, N., B. Zirak, R. Rodriguez, M. Pauli, H.-A. Truong, K. Lai, R. Ahn, K. Corbin, M. Lowe, T. Scharschmidt, K. Taravati, M. Tan, R. Ricardo-Gonzalez, A. Nosbaum, M. Bertolini, W. Liao, F. Nestle, R. Paus, G. Cotsarelis, A. Abbas, and M. Rosenblum. 2017. Regulatory T cells in skin facilitate epithelial stem cell differentiation. *Cell*. 169:1119–1129.

Anderson, K., K. Mayer-Barber, H. Sung, L. Beura, B. James, J. Taylor, L. Qunaj, T. Griffith, V. Vezys, D. Barber, and D. Masopust. 2014. Intravascular staining for discrimination of vascular and tissue leukocytes. *Nat. Protoc.* 9:209–222.

Arimura, Y., H. Kato, U. Dianzani, T. Okamoto, S. Kamekura, D. Buonfiglio, T. Miyoshi-Akiyama, T. Uchiyama, and J. Yagi. 2002. A co-stimulatory molecule on activated T cells, H4/ICOS, delivers specific signals in T(h) cells and regulates their responses. *Int. Immunol.* 14:555–566.

Arpaia, N., J. A. Green, B. Moltedo, A. Arvey, S. Hemmers, S. Yuan, P. M. Treuting, and A. Y. Rudensky. 2015. A distinct function of regulatory T cells in tissue protection. *Cell*. 162:1078–1089.

Bennett, C. L., J. Christie, F. Ramsdell, M. E. Brunkow, P. J. Ferguson, L. Whitesell, T. E. Kelly, F. T. Saulsbury, P. F. Chance, and H. D. Ochs. 2001. The immune dysregulation, polyendocrinopathy, enteropathy, X-linked syndrome (IPEX) is caused by mutations of FOXP3. *Nat. Genet.* 27:20–21.

Bensinger, S. J., P. T. Walsh, J. Zhang, M. Carrol, R. Parsons, J. C. Rathmell, C. B. Thompson, M. A. Burchill, M. A. Farrar, and L. A. Turka. 2004. Distinct IL-2 receptor signaling pattern in $CD4^{+}CD25^{+}$ regulatory T cells. *J. Immunol.* 172:5287–5296.

Bettelli, E., M. Pagany, H. L. Weiner, C. Linington, R. A. Sobel, and V. J. Kuchroo. 2003. Myelin oligodendrocyte glycoprotein-specific T cell receptor transgenic mice develop spontaneous autoimmune optic neuritis. *J. Exp. Med*. 197:1073–1081.

Bhaskar, P. T., and N. Hay. 2007. The two TORCs and Akt. *Dev. Cell*. 12:487–502.

Brunkow, M. E., E. W. Jefferey, K. A. Hjerrlid, B. Paeper, L. B. Clark, S.-A. Yasayko, J. E. Wilkinson, D. Galas, S. F. Ziegler, and F. Ramsdell. 2001. Disruption of a new forkhead/winged-helix protein, scurfin, results in the fatal lymphoproliferative disorder of the scurfy mouse. *Nat. Genet.* 27:68–73.

Burhans, M. S., D. K. Hagman, J. N. Kuzma, K. A. Schmidt, and M. Kratz. 2018. Contribution of adipose tissue inflammation to the development of type 2 diabetes mellitus. *Compr. Physiol.* 9:1–58.

Burmeister, Y., T. Lischke, A. C. Dahler, H. W. Mages, K.-P. P. Lam, A. J. Coyle, R. A. Kroczek, and A. Hutloff. 2008. ICOS controls the pool size of effector-memory and regulatory T cells. *J. Immunol.* 180:774–782.

Burzyn, D., W. Kuswanto, D. Kolodin, J. L. Shadrach, M. Cerletti, Y. Jang, E. Sefik, T. G. Tan, A. J. Wagers, C. Benoist, and D. Mathis. 2013. A special population of regulatory T cells potentiates muscle repair. *Cell*. 155:1282–1295.

Busse, M., M. Krech, A. Meyer-Bahlburg, C. Hennig, and G. Hansen. 2012. ICOS mediates the generation and function of CD4+CD25+Foxp3+ regulatory T cells conveying respiratory tolerance. *J. Immunol.* 189:1975–1982.

Campbell, D. J. 2015. Control of regulatory T cell migration, function, and homeostasis. *J. Immunol.* 195:2507–2513.

Campbell, D. J., and M. A. Koch. 2011. Phenotypical and functional specialization of Foxp3^{+} regulatory T cells. *Nat. Rev. Immunol.* 11:119–130.

Cipolletta, D. P. Cohen, B. M. Spiegelman, C. Benoist, and D. Mathis. 2015. Appearance and disappearance of the mRNA signature characteristic of Treg cells in visceral adipose tissue: age, diet, and PPARγ effects. *Proc. Natl. Acad. Sci. U.S.A.* 112:482–487.

Cipolletta, D. M. Feuerer, A. Li, N. Kamei, J. Lee, S. E. Shoelson, C. Benoist, and D. Mathis. 2012. PPAR-γ is a major driver of the accumulation and phenotype of adipose tissue Treg cells. *Nature*. 486:549–553.

Cretney, E., A. Xin, W. Shi, M. Minnich, F. Masson, M. Miasari, G. T. Belz, G. K. Smyth, M. Busslinger, S. L. Nutt, and A. Kallies. 2011. The transcription factors Blimp-1 and IRF4 jointly control the differentiation and function of effector regulatory T cells. *Nat. Immunol.* 12:304–311.

Danilova, E., I. Skrindo, E. Gran, B. J. Hales, W. A. Smith, J. Jahnsen, F. E. Johansen, F. L. Jahnsen, and E. S. Baekkevold. 2015. A role for CCL28–CCR3 in T-cell homing to the human upper airway mucosa. *Nat. Mucosal Immunol*. 8:107–114.

Deaglio, S., K. M. Dwyer, W. Gao, D. Friedman, A. Usheva, A. Erat, J.-F. Chen, K. Enjyoji, J. Linden, M. Oukka, V. K. Kuchroo, T. B. Strom, and S. C. Robson. 2007. Adenosine generation catalyzed by CD39 and CD73 expressed on regulatory T cells mediates immune suppression. *J. Exp. Med.* 204:1257–1265.

Deiuliis, J., Z. Shah, N. Shah, B. Needleman, D. Mikami, V. Narula, K. Perry, J. Hazey, T. Kampfrath, M. Kollengode, Q. Sun, A. R. Satoskar, C. Lumeng, S. Moffatt-Bruce, and S. Rajagopalan. 2011. Visceral adipose inflammation in obesity is associated with critical alterations in Tregulatory cell numbers. *PLoS One*. 6:e16376.

Delacher, M., C. Imbusch, A. Hotz-Wagenblatt, J.-P. Mallm, K. Bauer, M. Simon, D. Riegel, A. Rendeiro, S. Bittner, L. Sanderink, A. Pant, L. Schmidleithner, K. Braband, B. Echtenachter, A. Fischer, V. Giunchiglia, P. Hoffmann, M. Edinger, C. Bock, M. Rehli, B. Brors, C. Schmidl, and M. Feuerer. 2020. Precursors for nonlymphoid-tissue Treg cells reside in secondary lymphoid organs and are programmed by the transcription factor BATF. *Immunity*. 52:1–18.

Delacher, M., C. Imbusch, D. Weichenhan, A. Breiling, A. Hotz-Wagenblatt, U. Träger, A.-C. Hofer, D. Kägebein, Q. Wang, F. Frauhammer, J.-P. Mallm, K. Bauer, C. Herrmann, P. Lang, B. Brors, C. Plass, and M. Feuerer. 2017. Genome-wide DNA-methylation landscape defines specialization of regulatory T cells in tissues. *Nat. Immunol.* 18:1160–1172.

Dendrou, C. A., L. Fugger, and M. A. Friese. 2015. Immunopathology of multiple sclerosis. *Nat. Rev. Immunol.* 15:545–558.

DiSpirito, J. R., D. Zemmour, D. Ramanan, J. Cho, R. Zilionis, A. M. Klein, C. Benoist, and D. Mathis. 2018. Molecular diversification of regulatory T cells in non-lymphoid tissues. *Sci. Immunol.* 3:eaat5861.

Dombrowski, Y., T. O'Hagan, M. Dittmer, R. Penalva, S. R. Mayoral, P. Bankhead, S. Fleville, G. Eleftheriadis, C. Zhoa, M. Naughton, R. Hassan, J. Moffat, J. Falconer, A. Boyd, P. Hamilton, I. V. Allen, A. Kissenpfennig, P. N. Moynagh, E. Evergren, B. Perbal, A. C. Williams, R. J. Ingram, J. R. Chan, R. J. M. Franklin, and D. C. Fitzgerald. 2017. Regulatory T cells promote myelin regeneration in the central nervous system. *Nat. Neurosci.* 20:674–680.

Dominguez-Villar, M., and D. A. Hafler. 2018. Regulatory T cells in autoimmune disease. *Nat. Immunol.* 19:665–675.

Dong, C., A. E. Juedes, U. A. Temann, S. Shresta, J. P. Allison, N. H. Ruddle, and R. A. Flavell. 2001. ICOS co-stimulatory receptor is essential for T-cell activation and function. *Nature*. 409:97–101.

Eller, K., A. Kirsch, A. M. Wolf, S. Sopper, A. Tagwerker, U. Stanzl, D. Wolf, W. Patsch, A. R. Rosenkranz, and P. Eller. 2011. Potential role of regulatory T cells in reversing obesity-linked insulin resistance and diabetic nephropathy. *Diabetes*. 60:2954–2962.

Fasshauer, M., and M. Blüher. 2015. Adipokines in health and disease. *Trends Pharmacol. Sci.* 36:461–470.

Feito, M., R. Vaschetto, G. Criado, A. Sánchez, A. Chiocchetti, A. Jiménez-Periáñez, U. Dianzani, P. Portoles, and J. Rojo. 2003. Mechanisms of H4/ICOS costimulation: effects on proximal TCR signals and MAP kinase pathways. *Eur. J. Immunol*. 33:204–214.

Feuerer, M., L. Herrero, D. Cipolletta, A. Naaz, J. Wong, A. Nayer, J. Lee, A. Goldfine, C. Benoist, S. Shoelson, and D. Mathis. 2009. Lean, but not obese, fat is enriched for a unique population of regulatory T cells that affect metabolic parameters. *Nat. Med.* 15:930–939.

Fisson, S., G. Darrasse-Jèze, E. Litvinova, F. Septier, D. Klatzmann, R. Liblau, and B. L. Salomon. 2003. Continuous activation of autoreactive $CD4^+CD25^+$ regulatory T cells in the steady state. *J. Exp. Med.* 198:737–746.

Fletcher, J. M., S. J. Lalor, C. M. Sweeney, N. Tubridy, and K. H. G. Mills. 2010. T cells in multiple sclerosis and experimental autoimmune encephalomyelitis. *Clin. Exp. Immunol.* 162:1–11.

Fontenot, J., M. Gavin, and A. Rudensky. 2003. Foxp3 programs the development and function of $CD4^+CD25^+$ regulatory T cells. *Nat. Immunol*. 4:330–336.

Fontenot, J. D., J. P. Rasmussen, M. A. Gavin, and A. Y. Rudensky. 2005. A function for interleukin 2 in Foxp3-expressing regulatory T cells. *Nat. Immunol*. 6:1142–1151.

Fos, C., A. Salles, V. Lang, F. Carrette, S. Audebert, S. Pastor, M. Ghiotto, D. Olive, G. Bismuth, and J. A. Nunès. 2008. ICOS ligation recruits the p50alpha PI3K regulatory subunit to the immunological synapse. *J. Immunol.* 181:1969–1977.

Francis, J. N., C. M. Lloyd, I. Sabroe, S. R. Durham, and S. J. Till. 2007. T lymphocytes expressing CCR3 are increased in allergic rhinitis compared with non-allergic controls and following allergen immunotherapy. *Allergy*. 62:59–65.

Galicia, G., A. Kasran, C. Uyttenhove, K. De Swert, J. Van Snick, and J. L. Ceuppens. 2009. ICOS deficiency results in exacerbated IL-17 mediated experimental autoimmune encephalomyelitis. *J. Clin. Immunol*. 29:426–433.

Gao, T., F. Furnari, and A. C. Newton. 2005. PHLPP: a phosphatase that directly dephosphorylates Akt, promotes apoptosis, and suppresses tumor growth. *Mol. Cell*. 18:13–24.

Gigoux, M., J. Shang, Y. Pak, M. Xu, J. Choe, T. W. Mak, and W.-K. K. Suh. 2009. Inducible costimulator promotes helper T-cell differentiation through phosphoinositide 3-kinase. *Proc. Natl. Acad. Sci. U.S.A.* 106:20371–20376.

Gondek, D. C., L.-F. Lu, S. A. Quezada, S. Sakaguchi, and R. J. Noelle. 2005. Cutting edge: contact-mediated suppression by $CD4^+CD25^+$ regulatory T cells involves a granzyme B-dependent, perforin-independent mechanism. *J. Immunol*. 174:1783–1786.

Guo, L., G. Wei, J. Zhu, W. Liao, W. J. Leonard, K. Zhao, and W. Paul. 2009 IL-1 family members and STAT activators induce cytokine production by Th2, Th17, and Th1 cells. *Proc. Natl. Acad. Sci. U.S.A.* 106:13463–13468.

Han, J. M., D. Wu, H. C. Denroche, Y. Yao, C. B. Verchere, and M. K. Levings. 2015. IL-33 reverses an obesity-induced deficit in visceral adipose tissue ST2+ T regulatory cells and ameliorates adipose tissue inflammation and insulin resistance. *J. Immunol.* 194:4777–4783.

Harris, S. J., R. V. Parry, J. Westwick, and S. G. Ward. 2008. Phosphoinositide lipid phosphatases: natural regulators of phosphoinositide 3-kinase signaling in T lymphocytes. *J. Biol. Chem.* 283:2465–2469.

Herman, A., G. Freeman, D. Mathis, and C. Benoist. 2004. CD4+CD25+ T regulatory cells dependent on ICOS promote regulation of effector cells in the prediabetic lesion. *J. Exp. Med.* 199:1479–1489.

Hori, S., T. Nomura, and S. Sakaguchi. 2003. Control of regulatory T cell development by the transcription factor Foxp3. *Science*. 299:1057–1061.

Hsieh, C.-S., H.-M. Lee, and C.-W. Lio. 2012. Selection of regulatory T cells in the thymus. *Nat. Rev. Immunol.* 12:157–167.

Hsieh, C.-S., Y. Liang, A. J. Tyznik, S. G. Self, D. Liggitt, and A. Y. Rudensky. 2004. Recognition of the peripheral self by naturally arising CD25+ CD4+ T cell receptors. *Immunity*. 21:267–277.

Huang, Y. H., and K. Sauer. 2010. Lipid signaling in T-cell development and function, *Cold Spring Harb. Perspect. Biol.* 2:a002428.

Humbles, A. A., B. Lu, D. S. Friend, S. Okinaga, J. Lora, A. Algarawi, T. R. Martin, N. P. Gerard, and C. Gerard. 2002. The murine CCR3 receptor regulates both the role of eosinophils and mast cells in allergen-induced airway inflammation and hyperresponsiveness. *Proc. Natl. Acad. Sci. U.S.A.* 99:1479–1484.

Hutloff, A., A. Dittrich, K. Beier, B. Eljaschewitsch, R. Kraft, I. Anagnostopoulos, and R. Kroczek. 1999. ICOS is an inducible T-cell co-stimulator structurally and functionally related to CD28. *Nature*. 397:263–266.

Ilan, Y., R. Maron, A.-M. Tukpah, T. Maioli, G. Murugaiyan, K. Yang, H. Wu, and H. Weiner. 2010. Induction of regulatory T cells decreases adipose inflammation and alleviates insulin resistance in ob/ob mice. *Proc. Nat. Acad. Sci.* 107:9765–9770.

Ito, M., K. Komai, S. Mise-Omata, M. Iizuka-Koga, Y. Noguchi, T. Kondo, R. Sakai, K. Matsuo, T. Nakayama, O. Yoshie, H. Nakatsukasa, S. Chikuma, T. Shichita, and A. Yoshimura. 2019. Brain regulatory T cells suppress astrogliosis and potentiate neurological recovery. *Nature*. 565:246–250.

Jäger, A., V. Dardalhon, R. A. Sobel, E. Bettelli, and V. K. Kuchroo. 2009. Th1, Th17, and Th9 effector cells induce experimental autoimmune encephalomyelitis with different pathological phenotypes. *J. Immunol*. 183:7169–7177.

Jordan, M. S., A. Boesteanu, A. J. Reed, A. L. Petron, A. E. Holenbeck, M. A. Lerman, A. Naji, and A. J. Caton. 2001. Thymic selection of $CD4^+CD25^+$ regulatory T cells induced by an agonist self-peptide. *Nat. Immunol*. 2:301–306.

Josefowicz, S. Z., L.-F. Lu, and A. Y. Rudensky. 2012. Regulatory T cells: mechanisms of differentiation and function. *Annu. Rev. Immunol*. 30:531–564.

Kalekar, L. A., J. N. Cohen, N. Prevel, P. M. Sandoval, A. N. Mathur, J. M. Moreau, M. M. Lowe, A. Nosbaum, P. J. Wolters, A. Haemel, F. Boin, and M. D. Rosenblum. 2019. Regulatory T cells in skin are uniquely poised to suppress profibrotic immune responses. *Sci. Immunol*. 4:eaaw2910.

Kerdiles, Y. M., D. R. Beisner, R. Tinoco, A. S. Dejean, D. H. Castrillon, R. A. DePinho, and S. M. Hedrick. 2009. Foxo1 links homing and survival of naive T cells by regulating L-selectin, CCR7 and interleukin 7 receptor. *Nat. Immunol.* 10:176–184.

Khattri, R., T. Cox, S.-A. Yasayko, and F. Ramsdell. 2003. An essential role for scurfin in $CD4^+CD25^+$ T regulatory cells. *Nat. Immunol.* 4:337–342.

Killebrew, J. R., N. Perdue, A. Kwan, A. M. Thornton, E. M. Shevach, and D. J. Campbell. 2011. A self-reactive TCR drives the development of $Foxp3^+$ regulatory T cells that prevent autoimmune disease. *J. Immunol*. 187:861–869.

Koch, M. A., G. Tucker-Heard, N. R. Perdue, J. R. Killebrew, K. B. Urdahl, and D. J. Campbell. 2009. T-bet controls regulatory T cell homeostasis and function during type-1 inflammation. *Nat. Immunol.* 10:595–602.

Kohyama, M., D. Sugahara, S. Sugiyama, H. Yagita, K. Okumura, and N. Hozumi. 2004. Inducible costimulator-dependent IL-10 production by regulatory T cells specific for self-antigen. *Proc. Natl. Acad. Sci. U.S.A.* 101:4192–4197.

Kolodin, D., N. van Panhuys, C. Li, A. M. Magnuson, D. Cipolletta, C. M. Miller, A. Wagers, R. N. Germain, C. Benoist, and D. Mathis. 2015. Antigen- and cytokine-driven accumulation of regulatory T cells in visceral adipose tissue of lean mice. *Cell. Metab.* 21:543–557.

Komatsu N., and S. Hori. 2007. Full restoration of peripheral Foxp3+ regulatory T cell pool by radioresistant host cells in scurfy bone marrow chimeras. *Proc. Natl. Acad. Sci. U.S.A.* 104:8959–8964.

Kong, S.-K. K., B. S. Kim, T. G. Uhm, W. Lee, G. R. Lee, C.-S. S. Park, C.-H. H. Lee, and I. Y. Chung. 2013. Different GATA factors dictate CCR3 transcription in allergic inflammatory cells in a cell type-specific manner. *J. Immunol.* 190:5747–5756.

Korn, T., J. Reddy, W. Gao, E. Bettelli, A. Awasthi, T. R. Petersen, B. T. Bäckström, R. A. Sobel, K. W. Wucherpfennig, T. B. Strom, M. Oukka, and V. K. Kuchroo. 2007. Myelin-specific regulatory T cells accumulate in the CNS but fail to control autoimmune inflammation. *Nat. Med*. 13:423–431.

Kornete, M., E. Sgouroudis, and C. A. Piccirillo. 2012. ICOS-dependent homeostasis and function of Foxp3+ regulatory T cells in islets of nonobese diabetic mice. *J. Immunol.* 188:1064–1074.

Landuyt, A., B. Klocke, T. Colvin, T. Schoeb, and C. Maynard. 2019. Cutting Edge: ICOS-deficient regulatory T cells display normal induction of Il10 but readily downregulate expression of Foxp3. *J. Immunol.* 202:1039–1044.

Lee, J. H., S. G. Kang, and C. H. Kim. 2007. FoxP3+ T cells undergo conventional first switch to lymphoid tissue homing receptors in thymus but accelerated second switch to nonlymphoid tissue homing receptors in secondary lymphoid tissues. *J. Immunol.* 178:301–311.

Levine, A. G., A. Arvey, W. Jin, and A. Y. Rudensky. 2014. Continuous requirement for the TCR in regulatory T cell function. *Nat. Immunol.* 15:1070–1078.

Li, C., J. R. DiSpirito, D. Zemmour, R. G. Spallanzani, W. Kuswanto, C. Benoist, and D. Mathis. 2018. TCR transgenic mice reveal stepwise, multi-site acquisition of the distinctive fat-Treg phenotype. *Cell*. 174:285–299.

Liu, Z., M. Y. Gerner, N. Van Panhuys, A. G. Levine, A. Y. Rudensky, and R. N. Germain. 2015. Immune homeostasis enforced by co-localized effector and regulatory T cells. *Nature*. 528:225–230.

Lumeng, C. N., J. L. Bodzin, and A. R. Saltiel. 2007. Obesity induces a phenotypic switch in adipose tissue macrophage polarization. *J. Clin. Invest*. 117:175–184.

Luo, C. T., W. Liao, S. Dadi, A. Toure, and M. O. Li. 2016. Graded Foxo1 activity in Treg cells differentiates tumour immunity from spontaneous autoimmunity. *Nature*. 529:532–536.

Ma, W., P. J. Bryce, A. A. Humbles, D. Laouini, A. Yalcindag, H. Alenius, D. S. Friend, H. C. Oettgen, C. Gerard, and R. S. Geha. 2002. CCR3 is essential for skin eosinophilia and airway hyperresponsiveness in a murine model of allergic skin inflammation. *J. Clin. Invest.* 109:621–628.

Mahlakõiv, T., A.-L. Flamar, L. K. Johnston, S. Moriyama, G. G. Putzel, P. J. Bryce, and D. Artis. 2019. Stromal cells maintain immune cell homeostasis in adipose tissue via production of interleukin-33. *Sci. Immunol*. 4:eaax0416.

Matta, B. M., J. M. Lott, L. R. Mathews, Q. Liu, B. R. Rosborough, B. R. Blazar, and H. R. Turnquist. 2014. IL-33 is an unconventional alarmin that stimulates IL-2 secretion by dendritic cells to selectively expand IL-33R/ST2+ regulatory T cells. *J. Immunol.* 193:4010–4020. doi:10.4049/jimmunol.1400481

McGeachy, M. J., L. A. Stephens, and S. M. Anderton. 2005. Natural recovery and protection from autoimmune encephalomyelitis: contribution of $CD4^+CD25^+$ regulatory cells within the central nervous system. *J. Immunol*. 175:3025–3032.

Miyamoto, K., C. Kingsley, X. Zhang, C. Jabs, L. Izikson, R. Sobel, H. Weiner, V. Kuchroo, and A. Sharpe. 2005. ICOS molecule plays a crucial role in the development of mucosal tolerance. *J. Immunol.* 175:7341–7347.

Molofsky, A., J. Nussbaum, H.-E. Liang, S. Dyken, L. Cheng, A. Mohapatra, A. Chawla, and R. Locksley. 2013. Innate lymphoid type 2 cells sustain visceral adipose tissue eosinophils and alternatively activated macrophages. *J. Exp. Med.* 210:535–549.

Molofsky, A. B., F. Van Gool, H.-E. E. Liang, S. J. Van Dyken, J. C. Nussbaum, J. Lee, J. A. Bluestone, and R. M. Locksley. 2015. Interleukin-33 and Interferon-γ counter-regulate group 2 innate lymphoid cell activation during immune perturbation. *Immunity* 43:161–174.

Nagakubo, D., O. Yoshie, and T. Hirata. 2016. Upregulated CCL28 expression in the nasal mucosa in experimental allergic rhinitis: Implication for CD4+ memory T cell recruitment. *Cell. Immunol.* 302:58–62.

Nishioka, T., J. Shimizu, R. Iida, S. Yamazaki, and S. Sakaguchi. 2006. CD4+ CD25+ Foxp3+ T cells and CD4+ CD25− Foxp3+ T cells in aged mice. *J. Immunol.* 176:6586–6593.

Nosbaum, A., N. Prevel, H.-A. Truong, P. Mehta, M. Ettinger, T. C. Scharschmidt, N. H. Ali, M. L. Pauli, A. K. Abbas, and M. D. Rosenblum. 2016. Regulatory T cells facilitate cutaneous wound healing. *J. Immunol*. 196:2010–2014.

O'Brien, C. A., S. J. Batista, K. M. Still, and T. H. Harris. 2019. IL-10 and ICOS differentially regulate T cell responses in the brain during chronic *Toxoplasma gondii* infection. *J. Immunol*. 202:1755–1766.

O'Connor, R. A., K. H. Malpass, and S. M. Anderton. 2007. The inflamed central nervous system drives the activation and rapid proliferation of $Foxp3^+$ regulatory T cells. *J. Immunol*. 179:958–966.

Okamoto, N., K. Tezuka, M. Kato, R. Abe, and T. Tsuji. 2003. PI3-kinase and MAP-kinase signaling cascades in AILIM/ICOS- and CD28-costimulated T-cells have distinct functions

between cell proliferation and IL-10 production. *Biochem. Biophys. Res. Commun.* 310:691–702.

Ono, M., H. Yaguchi, N. Ohkura, I. Kitabayashi, Y. Nagamura, T. Nomura, Y. Miyachi, T. Tsukada, and S. Sakaguchi. 2007. Foxp3 controls regulatory T-cell function by interacting with AML1/Runx1. *Nature.* 446:685–689.

Ouyang, W., W. Liao, C. T. Luo, N. Yin, M. Huse, M. V. Kim, M. Peng, P. Chan, Q. Ma, Y. Mo, D. Meijer, K. Zhao, A. Y. Rudensky, G. Atwal, M. Q. Zhang, and M. O. Li. 2012. Novel Foxo1-dependent transcriptional programs control T_{reg} cell function. *Nature*. 491:554–561.

Panneton, V., J. Chang, M. Witalis, J. Li, and W.-K. Suh. 2019. Inducible T-cell co-stimulator : signaling mechanisms in T follicular helper cells and beyond. *Immunol. Rev.* 291:91–103.

Patton, D. T., O. A. Garden, W. P. Pearce, L. E. Clough, C. R. Monk, E. Leung, W. C. Rowan, S. Sancho, L. S. K. Walker, B. Vanhaesebroeck, and K. Okkenhaug. 2006. Cutting edge: the phosphoinositide 3-kinase p110 delta is critical for the function of $CD4^+CD25^+Foxp3^+$ regulatory T cells. *J. Immunol.* 177:6598–6602.

Pettersson, U., T. Waldén, P.-O. Carlsson, L. Jansson, and M. Phillipson. 2012. Female mice are protected against high-fat diet induced metabolic syndrome and increase the regulatory T cell population in adipose tissue. *PLoS One*. 7:e46057.

Qureshi, O. S., Y. Zheng, K. Nakamura, K. Attridge, and C. Manzotti. 2011. Trans-endocytosis of CD80 and CD86: a molecular basis for the cell-extrinsic function of CTLA-4. *Science*. 332: 600–603.

Redpath, S., N. van der Werf, A. Cervera, A. MacDonald, D. Gray, R. Maizels, and M. Taylor. 2013. ICOS controls Foxp3(+) regulatory T-cell expansion, maintenance and IL-10 production during helminth infection. *Eur. J. Immunol*. 43:705–715.

Rivas, M. N., and T. A. Chatila. 2016. Regulatory T cells in allergic diseases. *J. Allergy Clin. Immunol.* 138:639–652.

Sakaguchi, S., N. Sakaguchi, M. Asano, M. Itoh, and M. Toda. 1995. Immunologic self-tolerance maintained by activated T cells expressing IL-2 receptor alpha-chains (CD25). Breakdown of a single mechanism of self-tolerance causes various autoimmune diseases. *J. Immunol*. 155:1151–1164.

Sather, B. D., P. Treuting, N. Perdue, M. Miazgowicz, J. D. Fontenot, A. Y. Rudensky, and D. J. Campbell. 2007. Altering the distribution of Foxp3(+) regulatory T cells results in tissue-specific inflammatory disease. *J. Exp. Med.* 204:1335–1347.

Schmidleithner, L., Y. Thabet, E. Schönfeld, M. Köhne, D. Sommer, Z. Abdullah, T. Sadlon, C. Osei-Sarpong, K. Subbaramaiah, Fr. Copperi, Kr. Haendler, T. Varga, O. Schanz, S. Bourry, K. Bassler, W. Krebs, A. E. Peters, A.-K. Baumgart, M. Schneeweiss, K. Klee, S. V. Schmidt, S. Nüssing, J. Sander, N. Ohkura, A. Waha, T. Sparwasser, F. T. Wunderlich, I. Förster, T. Ulas, H. Weighardt, S. Sakaguchi, A. Pfeifer, M. Blüher, A. J. Dannenberg, N. Ferreirós, L. J. Muglia, C. Wickenhauser, S. C. Barry, J. L. Schultze, and M. Beyer. 2019. Enzymatic activity of HPGD in Treg cells suppresses Tconv cells to maintain adipose tissue homeostasis and prevent metabolic dysfunction. *Immunity*. 50:1232–1248.

Schmidt, A., N. Oberle, and P. H. Krammer. 2012. Molecular mechanisms of Treg-mediated T cell suppression. *Front. Immunol.* 3:51.
Schmitz, J., A. Owyang, E. Oldham, Y. Song, E. Murphy, T. K. McClanahan, G. Zurawski, M. Moshrefi, J. Qin, X. Li, D. M. Gorman, J. F. Bazan, and R. A. Kastelein. 2005. IL-33, an interleukin-1-like cytokine that signals via the IL-1 receptor-related protein ST2 and induces T helper type 2-associated cytokines. *Immunity*. 23:479–490.

Seddon, B., and D. Mason. 1999. Peripheral autoantigen induces regulatory T cells that prevent autoimmunity. *J. Exp. Med*. 189:877–881.

Setoguchi, R., S. Hori, T. Takahashi, and S. Sakaguchi. 2005. Homeostatic maintenance of natural Foxp3(+) CD25(+) CD4(+) regulatory T cells by interleukin (IL)-2 and induction of autoimmune disease by IL-2 neutralization. *J. Exp. Med.* 201:723–735.

Smigiel, K. S., E. Richards, S. Srivastava, K. R. Thomas, J. C. Dudda, K. D. Klonowski, and D. J. Campbell. 2014a. CCR7 provides localized access to IL-2 and defines homeostatically distinct regulatory T cell subsets. *J. Exp. Med*. 211:121–136.

Smigiel, K. S., S. Srivastava, J. M. Stolley, and D. J. Campbell. 2014b. Regulatory T-cell homeostasis: steady-state maintenance and modulation during inflammation. *Immunol. Rev.* 259:40–59.

So, L., and D. A. Fruman. 2012. PI3K signalling in B- and T-lymphocytes: new developments and therapeutic advances. *Biochem. J.* 442:465–481.

Spallanzani, R. G., D. Zemmour, T. Xiao, T. Jayewickreme, C. Li, P. J. Bryce, C. Benoist, and D. Mathis. 2019. Distinct immunocyte-promoting and adipocyte-generating stromal components coordinate adipose tissue immune and metabolic tenors. *Sci. Immunol*. 4:eaaw3658.

Stolley, J. M., and D. J. Campbell. 2016. A 33D1+ dendritic cell/autoreactive CD4+ T cell circuit maintains IL-2-dependent regulatory T cells in the spleen. *J. Immunol.* 197:2635–2645.

Stromnes, I. M., and J. M. Goverman. 2006a. Active induction of experimental autoimmune encephalomyelitis. *Nat. Protoc*. 1:1810–1819.

Stromnes, I. M., and J. M. Goverman. 2006b. Passive induction of experimental autoimmune encephalomyelitis. *Nat. Protoc*. 1:1952–1960.

Sullivan, J. M., B. Höllbacher, and D. J. Campbell. 2019. Cutting edge: dynamic expression of Id3 defines the stepwise differentiation of tissue-resident regulatory T cells. *J. Immunol*. 202:31–36.

Tang, Q., K. J. Henriksen, E. K. Boden, A. J. Tooley, J. Ye, S. K. Subudhi, X. X. Zheng, T. B. Strom, and J. A. Bluestone. 2003. Cutting edge: CD28 controls peripheral homeostasis of CD4+CD25+ regulatory T cells. *J. Immunol.* 171:3348–3352.

Vasanthakumar, A., D. Chisanga, J. Blume, R. Gloury, K. Britt, D. C. Henstridge, Y. Zhan, S. V. Torres, S. Liene, N. Collins, E. Cao, T. Sidwell, C. Li, R. G. Spallanzani, Y. Liao, P. A. Beavis, T. Gebhardt, N. Trevaskis, S. L. Nutt, J. D. Zajac, R. A. Davey, M. A. Febbraio, D. Mathis, W. Shi, and A. Kallies. 2020. Sex-specific adipose tissue imprinting of regulatory T cells. *Nature*. 579:581–585.

Vasanthakumar, A., K. Moro, A. Xin, Y. Liao, R. Gloury, S. Kawamoto, S. Fagarasan, L. Mielke, S. Afshar-Sterle, S. Masters, S. Nakae, H. Saito, J. Wentworth, P. Li, W. Liao, W. Leonard, G. Smyth, W. Shi, S. Nutt, S. Koyasu, and A. Kallies. 2015. The transcriptional regulators IRF4, BATF and IL-33 orchestrate development and maintenance of adipose tissue-resident regulatory T cells. *Nat. Immunol.* 16:276–285.

Wan, Y. Y., and R. A. Flavell. 2005. Identifying Foxp3-expressing suppressor T cells with a bicistronic reporter. *Proc. Natl. Acad. Sci. U.S.A.* 102:5126–5131.

Wan, Z., X. Shao, X. Ji, L. Dong, J. Wei, Z. Xiong, W. Liu, and H. Qi. 2020. Transmembrane domain-mediated Lck association underlies bystander and costimulatory ICOS signaling. *Cell & Mol. Immunol.* 17:143–152.

Wikenheiser, D. J., and J. S. Stumhofer. 2016. ICOS co-stimulation: friend or foe? *Front. Immunol.* 7:304.

Wu, D., A. B. Molofsky, H.-E. E. Liang, R. R. Ricardo-Gonzalez, H. A. Jouihan, J. K. Bando, A. Chawla, and R. M. Locksley. 2011. Eosinophils sustain adipose alternatively activated macrophages associated with glucose homeostasis. *Science*. 332:243–247.

Wu, D., Z. Ren, M. Pae, W. Guo, X. Cui, A. H. Merrill, and S. N. Meydani. 2007. Aging up-regulates expression of inflammatory mediators in mouse adipose tissue. *J. Immunol.* 179:4829–4839.

Wu, Y. M. Borde, V. Heissmeyer, M. Feuerer, A. Lapan, J. Stroud, D. Bates, L. Guo, A. Han, S. Ziegler, D. Mathis, C. Benoist, L. Chen, and A. Rao. 2006. FOXP3 controls regulatory T cell function through cooperation with NFAT. *Cell*. 126:375–387.

Xing, Y., and K. A. Hogquist. 2012. T-cell tolerance: central and peripheral. *Cold Spring Harb. Perspect. Biol.* 4:a006957.

Yadav, M., S. Stephan, and J. A. Bluestone. 2013. Peripherally induced Tregs – role in immune homeostasis and autoimmunity. *Front. Immunol*. 4:232.

Yamaguchi, T., J. B. Wing, and S. Sakaguchi. 2011. Two modes of immune suppression by Foxp3^{+} regulatory T cells under inflammatory or non-inflammatory conditions. *Sem. Immunol.* 23:424–430.

Zhang, R., A. Huynh, G. Whitcher, J. Chang, J. S. Maltzman, and L. A. Turka. 2013. An obligate cell-intrinsic function for CD28 in Tregs. *J. Clin. Invest*. 123:580–593.

Zheng, Y., A. Chaudhry, A. Kas, P. deRoos, J. M. Kim, T.-T. Chu, L. Corcoran, P. Treuting, U. Klein, and A. Y. Rudensky. 2009. Regulatory T-cell suppressor program co-opts transcription factor IRF4 to control T(H)2 responses. *Nature*. 458:351–356.